Università degli Studi di Catania
Dipartimento di Matematica e Informatica
Dottorato di Ricerca in Matematica
Applicata all'Ingegneria

Carmen Mineo

Mathematical Models for Geophysical Mass Flows

Tesi di Dottorato

XXII CICLO

Tutor
Prof. Mariano Torrisi

Coordinatore
Prof. Mariano Torrisi

Anno Accademico 2009/2010

Contents

Introduction

The increase, in the past few decades, of the phenomena of intense transport of geophysical mass flows, pushed the technical and scientific community in face of the heavy responsibility to effectively protect people, man-made structures, and the economic activities of affected areas. Typical examples of these dangerous and destructive natural phenomena are landslides, snow avalanches, pyroclastic flows, debris flows that are driven down a slope under the action of gravity ([1]-[13]).

These gravity-driven flows, characterized by a mixture of soil, rocks and water, are often originated by sediments of natural deposits, mobilized of a considerable quantity of fluid and resulting in the formation of huge floods of sediments that are propagated with elevated speed. The characteristics of the flow depend on the rheology of dry granular flows and of the amount of fluid that is added, characterizing the mechanism of initiation along the streams listed first ([14]-[28].

Following the celebrated paper of Savage and Hutter [29], in the last two decades great progresses have been made in the mathematical and numerical modeling of granular geophysical flows by means of *depth-averaged* or *thin layer models*, which are based on the small aspect ratio of typical flows (small characteristic flow depth H compared to the characteristic flow length L). The study of Savage and Hutter was concerned with the one-dimensional motion of a relatively thin layer of a dry granular material along a slope. They started from the classical Saint-Venant system [30]:

$$\begin{aligned} &\partial_t h + \partial_x(hu) = 0, \\ &\partial_t(hu) + \partial_x(hu^2 + \tfrac{1}{2}gh^2) + hg\partial_x z(x) = 0 \end{aligned} \tag{1}$$

that has been widely used to model single-phase flows in one space dimension. In (1) h denotes the height of the material, u the velocity in the direction parallel to the bed, g the gravity constant. The influence of the topography enters through the function $z(x)$ which is the altitude of the relief and it is assumed that $\partial_x z$ is small.

Savage and Hutter, modifying the Saint Venant equations, introduced a model which is still one-dimensional but take into account the curvature of the terrain at least when small. Both systems are hyperbolic and posses a convex entropy.

Eventually their approach has been followed and generalized by several authors which studied a bidimensional model but began to consider a complex basal topography ([31]-[38]). Even the extension to multidimensions of the Saint-Venant system is obvious, however it is valid only for almost flat topography, thus not relevant for debris avalanches in particular. Unfortunately the extension to several dimensions of the Savage-Hutter model appears to be far from trivial. The first attempt has been made by Gray, Wieland and Hutter [34], they assumed that the topography has large variation only in one direction, while it is essentially flat in the other direction. Later, see [39] and [40], Hutter and Pudasaini introduced a model for avalanches in arbitrarily curved channels.

It is worthwhile stressing that a considerable part of the literature on debris flow modeling, from the early studies to the most recent ones is devoted to single-phase dry granular masses. Single-phase models are, however, limited in the simulation of the complex behavior of debris flows. As Hutter points out in [41] this is mainly due to neglecting the effects of the interstitial fluid. The effects of pore pressure on the fluidization of a solid-fluid mixture is often necessary for an accurate description of debris flows mechanics. In fact the interaction forces between solid grains and interstitial fluid influence not only the rheological behavior of the moving mass but also may play an important role in deformation processes, flow mobility and run-out. It is possible to find examples going from dry rock avalanches, in which pore fluid influence may be negligible, to liquid-saturated debris flows and gas-charged pyroclastic flows, in which fluids may enhance bulk mobility.

In order to take into account intergranular fluid effects in the flowing material Iverson [42] and Iverson and Denlinger [35], [43] suggested a new model by developing a depth averaged solid-fluid mixture theory based on the simplifying assumptions of constant porosity (fluid volume fraction) and equality of fluid velocity to solid velocity. In these models the flow is described by a set of balance equations for the mass and for the momentum of the mixture, which formally appears as a single-phase model with a stress term accounting for contributions from the two constituents. This mixture formulation lacks an inherent description of the pore fluid motion and the model needs to be supplemented with some specification of the pore fluid pressure evolution. In particular, the Iverson and Denlinger model extended the modeling to two dimensions, and included several refinements to the equations. Moreover, they postulate an advection-diffusion equation for the

fluid pressure, allowing for changes in the pressure in response to the movement of solid. Numerical applications of this model to laboratory avalanches and debris flume experiments are reported in [43].

The models of Savage and Hutter [29] and Iverson [42] have a very similar structure, this fact allows to formulate with appropriate positions a single model for two flows classes [44]. This particular model is hyperbolic, so for some experimental data, it is possible to write weak discontinuity evolution equation [45] and to evaluate the critical time, that is the instant when discontinuity amplitude becomes unbounded.

Making a significant progress with respect to the previous models, Pitman and Le [90] have recently introduced a novel depth-averaged two-phase model for debris flows and avalanches that contains mass and momentum balance equations for both the solid and fluid component. This implicitly provides equations for the velocities of both phases and for porosity. This model is tractable to describe unsteady and non uniform configurations encountered in real geophysical flows. In their work, the granular phase is described as a Coulomb material, and again, no dilatancy is present.

Moreover, in this thesis taking in consideration the Pitman and Le model and we study the partial differential equation system that tries to approach the range of scales and the complexity of the rheology for geological materials ([46], [47]). This system is a first order quasilinear system and we wonder if it is hyperbolic or not in order to look for propagation of weak discontinuities [45] and for further developments. Being the characteristic polynomial, in one space dimension, of degree four it is not trivial task to discuss about the reality of its zeros. Because of our interest are the application of this model to gravitational geophysical flows such as avalanches and debris flows, some experimental data are considered in order to compute the zeros of characteristic polynomial, to write weak discontinuity evolution equations and to evaluate the critical time.

The thesis is organized as follows. In section 1 the phenomenology of the geophysical mass flows is described. In section 2, the single-phase model of Savage and Hutter are shown. In section 3 the classical theory of mixtures are recalled, the derivation of a simple model for a Debris Flow Surges is shown and finally the "hydraulic" model of Iverson is described. In section 4 the bi-phase model of Iverson and Denlinger is shown. In section 5 "a model for two flows classes" is formulated and the propagation of weak discontinuities is studied. Finally, in section 6 the derivation of the two fluid model of Pitman and Le is shown, the hyperbolicity is discussed and the propagation of weak discontinuities is studied. In the last section conclusion are given.

Chapter 1

Phenomenology

1.1 Classification of the phenomena of mass flows

The phenomena of instability of a slope are mainly due to factors directly related to the geometric shape of the slope, to the geological and geotechnical properties of earth and rocks involved in the process, and finally to the hydraulic characteristic of the site. These factors are extremely variable in time and space determine how the kinematics of breaking.

The apparent complexity of the phenomena has given rise to a large number of classifications, in which we tried to group events according to the seemingly common material, the morphology of the deposit and the type of motion. However, as regards the casting of both land, both detritus, fast or slow with fluid consisting of water alone, alone by air or air-water mixture, were considered more significant that proposed by Varnes [48] on the phenomena of flow within mass motion, and descriptions of different types of motion of debris seconds Hutchinson ([49]-[51]).

The classification of Varnes [48] is the most complete and has become, especially from the engineering point of view, the most widely used reference for the terminology of mass motions. It uses as discriminatory elements, the type of motion derived from geometric and kinematic characteristics, and the type of material involved in the movement itself:

- type motion: collapse, overturning, rotational and passed slips, expanding side, castings and complex motions.
- type material: the rock in place, coarse detritus, fine-grained soils.

Varnes introduces the cast, starting from the observation that many examples of motions of slopes can not be classified as structural collapse, overturning or

slipping, and that in many cases the speed of distribution of mass in motion seems that of a viscous fluid. He considers two main types of flows: the flows in the rocks and streams of debris and soil.

The classification of Hutchinson [51] divides the movement of debris that looked like a stream into 4 types, showing that essentially differ in their mechanism of propagation ([52]-[64]).

- **Mudslide**. Are characterized by slow motions of debris accumulated in a clay matrix, mainly consisting of slips rather than flow.

- **Debris flows**. These flows fast or very fast debris and mixed with water are characteristic phenomena of instability of the mountain slopes, where water leakage sudden supplied by rain or melting snow, can mobilize coperture detrital.

- **Flowslides**. Are characterized by a sudden collapse and from the wide one and rapids propagation of a mass of granular material or detrital after an external cause. Having the material a loose structure or high porosity, following the trouble, the collapse is had with partial total transfer of the overload on the fluid of porosity and therefore the generation of an excess of pressure is had. The pore fluid usually consists of water, but in some cases it may be gas.

- **Sturzstrom**. This is true "pattern of debris" that affect large volumes, with values of high-speed. The movement of sturzstrom depends on the turbolent granular flow, with a necessary tension dispersive in normal direction to the flow furnished by the transfer of momentum between the grains that collide and not by the presence of a liquid or gaseous fluid. There is therefore a fundamental difference between the behavior of sturzstrom and flowslides because, in addition to the different volumes involved, in the first ones the physical trial is tied up to the quantity of motion transferred through the collisions among wheats, while in the seconds it is essentially a phenomenon of impact liquefaction.

1.2 Physical characteristics of mass flows

The mass flows consists of detritus from mixtures consisting of air, water, colloidal suspensions of clay minerals, solid grains of various sizes (from sand to the blocks) in different proportions.

These phenomena of instability, typical of mountain slopes, are mobilized in connection with flooding and propagate downstream with speeds that can reach a few tens of meters per second. Flash floods gravitated in which the material undergoes a state of tension ring is unable to resist distortion and flows like a viscous fluid.

The main physical characteristics of the mass flows are: granulometry, speed and gradient.

1.2.1 Granulometry

The geological deposits which arise from the mass flows are not usually stratified and multi-class grain. The examination of the grading curve of some debris that have been casting motions [51] allows to put in evidence a breakdown of the material that extends from the clay, the pebbles, the blocks. The percentage of each class may vary from one deposit to another and within a deposit.

The mass flows are, in fact, characterized by several phases of movement: a flow of material consists of mainly coarse elements are generally followed phases of fluidder flow.

1.2.2 Speed

The danger of Geophysical mass flows is closely linked to high speed with which these phenomena occur, since the speed between 0,5 m/s and 10 m/s. The differences between the values of velocity may be due to granulomatry material affected, to the geometry of the channel and therefore to the inclination, the size and morphology of the area concerned.

1.2.3 Slopes

Although the mass flows originate on very inclined slopes, however, are characterized by the ability to move up inclines very weak. The ranges of observed slopes vary between 2% and 32%.

1.3 Mechanisms of initiation, propagation and arrest of mass flows

A comprehensive study of physical processes in question should also consider the phase of initiation, as well as the maintenance of the phenomenon.

The formation of mass flow can in general due to the simultaneous occurrence of the following three conditions:

1. the presence of detrital material (storage, layer, etc.);
2. intake of fluid (water, mud, etc..) sufficient for the mobilization of the material;
3. a slope of adequate fund.

In a mass flow can refer to two typical sources of material constituent, in percentage as:

- material accumulated and deposited in streams, from the sides, by the erosive action on the rocks, etc..
- material originated from erosive events concurrent with the occurrence of detrital casting.

The flow are mainly caused by events of particularly intense rainfall or sudden dissolution of the phenomena of glaciers due to sudden variations. Sometimes there may be a result of volcanic phenomena or as a result of landslides caused by earthquakes accompanied by surface water.

In such cases, the shear direction parallel to the slope increases with the degree of saturation, while the shear strength decreases with the increase in interstitial pression. The rupture occurs when cutting the shear active reaches the shear strength available. After the break, the unstable mass is moving, in some cases, very slowly and travels short distances, in other cases, however, is transformed into flow of detritus, reaching very high speeds and driving long distances.

Tubino and Seminara [65] have identified 4 different types of ignition of mass flows:

1. flow generated by the mobilization of debris deposited in the bed of streams, following the surface currents produced by heavy rainfall or thawing;
2. flow originated from the collapse of a slope, with subsequent transformation of the landslide in detrital casting;

3. flow originated from the collapse of a natural dam, produced by the occlusion of a stream following a landslide the previous event;

4. flow produced by the fluidized immediate constituent of the material a landslide, due to the presence of an abundant surface current.

The mechanisms for generation of type 1, 3 and 4 are characterized, although with different modalities, from a flow of water in the form of tracking that is the cause of the phenomenon of instability. The mechanism of type 2 is, however, fundamentally different in that, to produce the phenomenon of instability, it is necessary that it is delivering the interstitial overpressure inside the material, leading to liquefazio with.

The classification proposed by Seminara and Tubino [65] reflects, besides, substantial differences in response times of the phenomenon: the time interval between the phenomenon and not trigger the occurrence of debris flow shows the hour-days in the case castings caused by landslides or slope failure, and stroke is reduced to the order of minutes-hours in the case of castings produced by the mobilization of deposits in the streams. In particular movement is very rapid in the case of non-saturated layers on high slopes.

The main characteristics of the debris on the move are:

- erosive capacity is particularly high during the initiation and development, during which the front of material thickens incorporating large, but much reduced in the subsequent propagation phase, during which the casting is characterized by a front face, where the sediments of greater dimensions are assembled, and an opposite rear end of the matrix;

- impact strength: due to the size of the granules of the front face (causing major damage).

I can stop debris flows naturally and the effect of artificially drawn structures suitable for this purpose.

Experimentally it was observed that the debris flows deposited in plains or mountain gorges where the slope of the fund is reduced to values which can not exceed 3^o. Generally, however, arrested at the mouth of a river or at the apex of a cone.

In cases of non-stop the width of the current debris flow increases slightly and it has side storage with the formation of natural levees on both sides.

Chapter 2

The Savage-Hutter model

The Savage-Hutter model is a depth averaged dynamical model of a finite volume of cohesionless granular material in two dimensions released from rest on rough inclines. It takes into account the assumptions of density preserving (incompressibility), of a dry Coulomb-like friction law with bed friction angle σ, of shallowness of the flow with small topographic curvatures and finally the assumption of nearly uniform velocity profile through the flow depth.

Depth averaging the equations of conservation of mass and momentum yielding a tractable model of hyperbolic equations, reminiscent of the non-linear shallow-water equations. The granular mass is treated as a continuum along a slowly varying bottom profile with thickness, in which consider free surface flow and density not variable.

Mass and momentum balance equations for the incompressible model are written as

$$\begin{cases} \nabla \cdot (\rho^s \mathbf{v}) = 0, \\ \\ \rho^s(\partial_t \mathbf{v} + (\mathbf{v} \cdot \nabla)\mathbf{v}) = -\nabla \cdot \mathbf{T^s} + \rho^s \mathbf{g}, \end{cases} \tag{2.1}$$

where ρ^s is the constant density, $\mathbf{v}$ is the velocity vector, $\mathbf{T^s}$ is the solid stress tensor and $\mathbf{g}$ the gravity acceleration.

The flow considered is represented in two-dimensional Cartesian coordinate system with x is the downslope direction and z the normal direction (see figure 2.1).

The equations of the system (2.1) in these coordinates system become:

$$\begin{cases} v_x^x + v_z^z = 0, \\ \\ \rho^s(g v_t^x + v^x v_x^x + v^z v_z^x) = \rho^s g sin(\theta) - T_x^{sxx} - T_z^{sxz} +, \\ \\ \rho^s(v_t^z + v^x v_x^z + v^z v_z^z) = -\rho^s g cos(\theta) - T_x^{sxz} - T_z^{szz}, \end{cases} \tag{2.2}$$

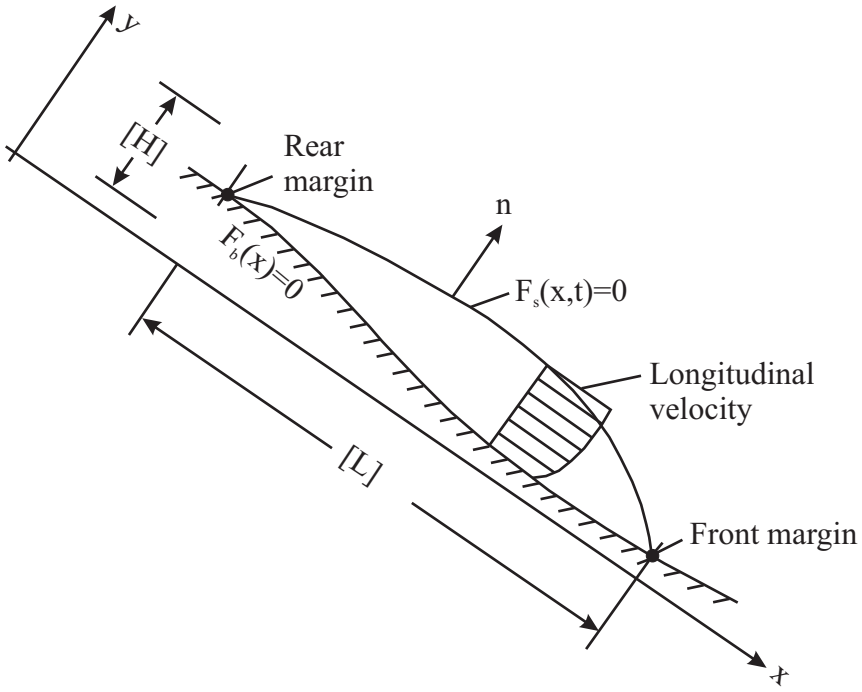

Fig. 2.1: Sketch of the geometry of a finite mass of granular material moving along a curved rigid bed showing definitions of the free surface given by $F^h(x,z,t) = 0$ and the equation of the bed $F^b(x,z,t) = 0$. Also indicated are the scales [L] and [H] for the spread and maximum height.

where θ is the angle that the base of the mass flow makes with the horizontal, consequently $sin(\theta)$ and $cos(\theta)$ are the local components of gravity.

Boundary conditions at the upper free surface are two. First is the following stress free condition:

$$\mathbf{T^s} \cdot \mathbf{n} = 0, \tag{2.3}$$

where $\mathbf{n}$ is the exterior unit normal vector. The second boundary condition that in water wave problem is known as kinematic condition, is expressed by a function F, which is $F^h(x,z,t) = 0$ to indicate the position of the free surface, then the further condition becomes:

$$F^h_t + \nabla F^h \cdot \mathbf{v} = 0, \tag{2.4}$$

where the subscript t denotes the derivative with respect to the time. Instead, at the base the expression $F^b(x,z) = 0$ indicates the tangency of the flow,

that must satisfy the following condition:

$$\mathbf{v} \cdot \mathbf{n} = 0. \tag{2.5}$$

Furthermore, the boundary condition at the base satisfy the a sliding friction law, which expresses the proportionality between the shear traction S and the normal stress N as follows:

$$S = \pm N tang(\phi_{bed}), \tag{2.6}$$

where ϕ_{bed} is the basal friction angle and the sign is given by the direction of the sliding velocity.

With

$$S = \mathbf{n} \cdot \mathbf{T^s} - \mathbf{n}(\mathbf{n} \cdot \mathbf{T^s} \cdot \mathbf{n}), \tag{2.7}$$

and

$$N = \mathbf{n} \cdot \mathbf{T^s} \cdot \mathbf{n}, \tag{2.8}$$

the two boundary conditions at the base ($F_b(x, z) = 0$) becomes:

$$\begin{cases} \mathbf{v} \cdot \mathbf{n} = 0, \\ \\ \mathbf{n} \cdot \mathbf{T^s} - \mathbf{n}(\mathbf{n} \cdot \mathbf{T^s} \cdot \mathbf{n}) = -\left(\dfrac{v_s}{|v_s|}\right)(\mathbf{n} \cdot \mathbf{T^s} \cdot \mathbf{n}) tang(\phi_{bed}), \end{cases} \tag{2.9}$$

where v_s is the sliding velocity relative to the stationary bed.

The system of equations (2.1) is put in a non dimensional form by using the following scaling transformation:

$$\begin{cases} (x, z, t) = L\left[\tilde{x}, \dfrac{H}{L}\tilde{z}, \left(\dfrac{L}{g}\right)^{\frac{1}{2}}\tilde{t}\right], \\ \\ (v^x, \mathbf{u^z}) = (gL)^{\frac{1}{2}}\left(\tilde{v^x}, \dfrac{H}{L}\tilde{v^z}\right), \\ \\ \mathbf{T}^s = \rho^s g H \tilde{\mathbf{T}}^s, \end{cases} \tag{2.10}$$

where H is the characteristic thickness in the z-direction and L is the characteristic flow length in the x direction. Moreover, are specialized the free surface and the bed by $z = h(x, t)$ and $z = b(x)$, so that when h and b are scaled by H obtained:

$$\begin{cases} h(x, t) = H[\tilde{h}(\tilde{x}, \tilde{t})], \\ \\ b(x) = H[\tilde{b}(\tilde{x})]. \end{cases} \tag{2.11}$$

Consistent with the assumption of slow variation of the bed and the free surface, take $\tilde{h}$ and $\tilde{b}$, as well as $\dfrac{\partial \tilde{h}}{\partial \tilde{x}}$ and $\dfrac{\partial \tilde{b}}{\partial \tilde{x}}$ to be order-unity functions. Moreover, introducing the term $\epsilon = \dfrac{H}{L} << 1$, we can assert that the functions listed above are of order ϵ.

From eqn. (2.1) with scaling transformation (2.10), by dropping tilde and dividing each term by $\rho^s g$, we get the following three scalar equations written in component form:

$$\begin{cases} v_x^x + v_z^z = 0, \\ v_t^x + v^x v_x^x + v^z v_z^x = -\epsilon T_x^{sxx} - T_z^{sxz} + sin(\theta), \\ \epsilon(v_t^z + v^x v_x^z + v^z v_z^z) = -\epsilon T_x^{sxz} - T_z^{szz} - cos(\theta), \end{cases} \tag{2.12}$$

Putting $\epsilon = 0$ in the z-momentum equation we obtain the following lithostatic equilibrium equation:

$$T_z^{szz} = -cos(\theta). \tag{2.13}$$

Instead, taking $\epsilon = 0$ in the x-momentum equation, should neglect the longitudinal stress tensor ϵT_x^{sxx}, but unlike of the transverse stress tensor ϵT_x^{sxz}, is sufficiently large to be retained.

The final procedure to simplify the x-momentum equation is the depth-average, which is integration in z, from the basal surface $z = b(x)$ to the upper free surface $z = h(x,t)$. Moreover, using the continuity equation and the Leibnitz's rule, interchanging integrations and differentiations, the equation becomes:

$$\begin{aligned} &\frac{\partial}{\partial t}\int_b^h v^x dz + \frac{\partial}{\partial x}\int_b^h v^{x^2} dz - \left[v^x\left(\frac{\partial h}{\partial t} + v^x\frac{\partial}{\partial t} - v^z\right)\right]_{z=h(x,t)} + \\ &+\left[v^x\left(v^x\frac{\partial b}{\partial x} - v^z\right)\right]_{z=b(x)} = sin(\theta)(h-b) - T^{sxz}_{|z=h(x,t)} + T^{sxz}_{|z=b(x)} + \\ &\qquad -\epsilon\left[\frac{\partial}{\partial x}\int_b^h T^{szz} dy - T^{szz}_{|z=h(x,t)}\frac{\partial h}{\partial x} + T^{szz}_{|z=b(x)}\frac{\partial b}{\partial x}\right] \end{aligned} \tag{2.14}$$

Applying the boundary conditions at the free surface and the base, in the latter equation many terms are simplified. Moreover, the equation (2.14)

incorporates the following kinematic boundary conditions:

$$\begin{cases} \dfrac{\partial h}{\partial t} + v^x \dfrac{\partial}{\partial t} - v^z \quad at \quad z = h(x,t), \\ \\ v^x \dfrac{\partial b}{\partial x} - v^z \qquad\quad at \quad z = b(x), \end{cases} \tag{2.15}$$

These conditions include the assumption that the surface of the flow of material is free of the stress, then consider:

$$T^{sxz} = T^{sxx} = T^{szz} = 0 \quad at \quad z = h(x,t), \tag{2.16}$$

The equation (2.14) with the use of (2.15) and (2.16) simplifies and becomes:

$$\frac{\partial}{\partial t}\int_b^h v^x dz + \frac{\partial}{\partial x}\int_b^h v^{x^2} dz = sin(\theta)(h-b) + sin(\theta) T^{sxz}_{|z=b(x)} + \\ -\epsilon cos(\theta)\left[\frac{\partial}{\partial x}\int_b^h T^{szz} dy + T^{szz}_{|z=b(x)}\frac{\partial b}{\partial x}\right]. \tag{2.17}$$

Moreover, the depth-averaged velocities and normal stresses are defined as follows:

$$\overline{v^x} = \frac{1}{h-b}\int_b^h v^x dz, \tag{2.18}$$

$$\overline{T^{sxx}} = \frac{1}{h-b}\int_b^h T^{sxx} dz, \tag{2.19}$$

$$\overline{T^{szz}} = \frac{1}{h-b}\int_b^h T^{szz} dz, \tag{2.20}$$

$$\overline{v^{x^2}} = \frac{1}{h-b}\int_b^h \alpha v^{x^2}(h-b) dz, \tag{2.21}$$

The term α in (2.21) indicates that if its value differs from unit, the velocity profile deviates from uniformity. Then, a value of $\alpha = 1$ indicates a uniform profile and that the mass flow moves slipping on the base, with no differential shear. In this case the active shear zone is confined to a thin basal layer and the velocity profile is blunt [66].

Instead, if you do not slip on the base and the shear is all differential, the speed profile is parabolic and takes $\alpha = \frac{6}{5}$.

Therefore assume a value of $\alpha \approx 1$ represents a good approximation, since it does not introduce a large errors.

With the shallowness assumption the non-dimensional form of the Coulomb sliding law (2.15) becomes

$$T^{sxz} = -sgn(\overline{v^x})T^{szz}cot(\theta)\tan(\phi_{bed}) \quad at \quad z = b(x). \tag{2.22}$$

Assuming that the constitutive behavior of the material can be described by a simple Mohr-Coulomb yield criterion. By having postulated that the Coulomb constitutive relation for the material, is a nonlinear relation among the components of the solid tensor stress. Full reports expressing the Coulomb law are very complex to be used in Savage-Hutter derivation, because they yield the mass and momentum balance laws linearly ill-posed, then make the simplifications in the relations to be taken. However, it is based upon the results of shear cell and chute flow tests, and explanations of and justifications for this assumption are given in considerable detail in [67]. The Mohr-Coulomb yield criterion for a cohesionless material with an internal friction angle φ, expresses the alignment between the shear stress and the normal stress, by the following relation:

$$T^{sxz} = T^{szz}tan(\varphi), \tag{2.23}$$

This is shown schematically in terms of a standard Mohr-diagram (see figure 2.2) for the case of a constant internal friction angle and a constant bed friction angle ϕ_{bed}.

At the bed , the normal stress T^{szz} and the shear stress T^{sxz} must be such that they lie on the wall yield line as shown. Note that two possible Mohr circles can be drawn through the point corresponding to the (T^{szz}, T^{sxz}) stress state. That one corresponding to a larger value of the normal stress T^{sxx} (i.e. $T^{sxx} > T^{szz}$) we associate the passive state of stress (to use the common soil mechanics terminology) and the other we associate with the active state of stress. An earth pressure relation expresses the proportionality between the diagonal stress components, as follows:

$$T^{sxx} = K_{act/pas}T^{szz}, \tag{2.24}$$

where $K_{act/pas}$ is the earth pressure coefficient, determined by the equation:

$$K_{act/pas} = 2\frac{1 \mp [1 - \cos^2(\phi_{int})[1 + \tan^2(\phi_{bed})]]^{1/2}}{\cos^2(\phi_{int})} - 1, \tag{2.25}$$

with ϕ_{int} is the internal friction angle. The sign $\mp$ depends on whether an element of the material is being elongated ("active" coefficient $\partial v/\partial_x > 0$,

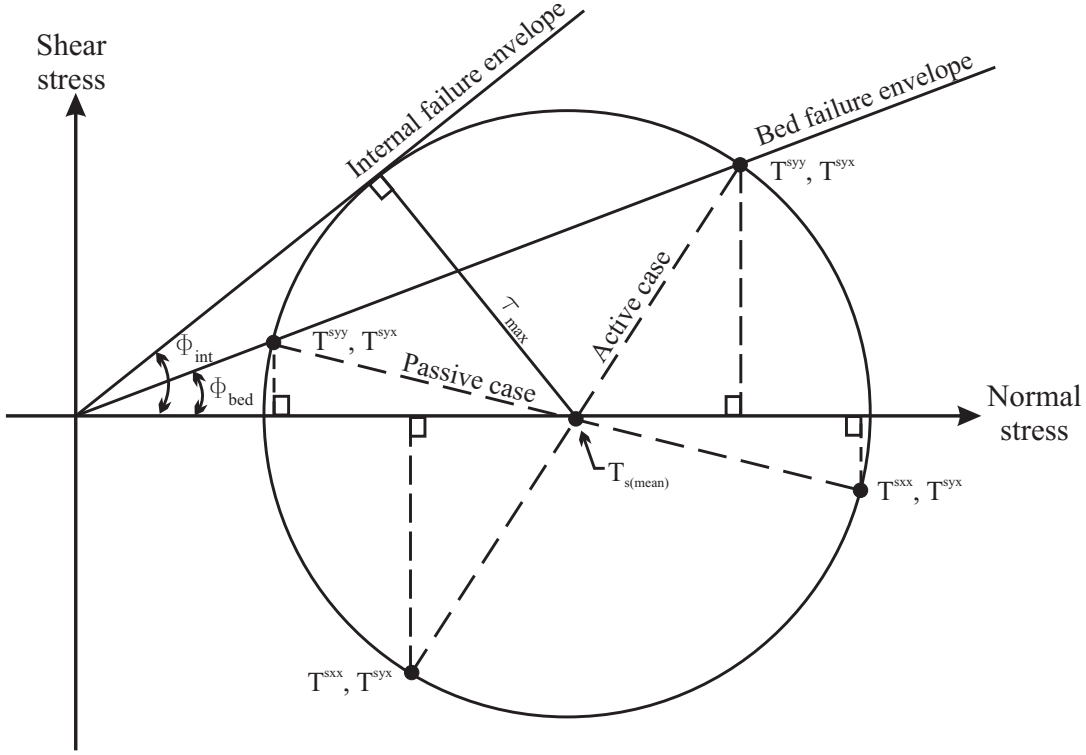

Fig. 2.2: Mohr stress circle and Coulomb failure envelopes for a granular material that is simultaneously slipping along a bed and failing internally. The radius of the stress circle defines the maximum internal shear stress.

with - sign) or compressed ("passive" coefficient $\partial v/\partial_x < 0$, with + sign) in the direction parallel to the bed.

The relation (2.17) with (2.18)-(2.24) becomes:

$$\begin{aligned}[(h-b)\overline{v^x}]_t + [\alpha(h-b)\overline{v^x}^2]_x = sin(\theta)(h-b) + \\ -\epsilon cos(\theta)K_{act/pas}\{[(h-b)T^{szz}]_x + T^{szz}b_x\} + \\ -cos(\theta)sgn(\overline{v^x})T^{szz}\tan(\phi_{bed}).\end{aligned} \tag{2.26}$$

From (2.13) after integration and taking account of the zero pressure condition at the free surface obtained the following overburden pressure:

$$T^{szz} = h(x,t) - b(x) = \widehat{h}(x,t) \tag{2.27}$$

and still has:

$$\widehat{h}T^{szz} = \frac{1}{2}[h(x,t) - b(x)] = \frac{1}{2}\widehat{h}(x,t) \tag{2.28}$$

So the relation (2.26) with (2.27) and (2.28) becomes:

$$[\widehat{h}\overline{v^x}]_t + [\alpha\widehat{h}\overline{v^x}^2]_x = sin(\theta)\widehat{h} - \epsilon cos(\theta)K_{act/pas}\{\widehat{h}_x^2 + \widehat{h}b_x\} + \\ -cos(\theta)sgn(\overline{v^x})\tan(\phi_{bed})\widehat{h}. \tag{2.29}$$

Finally, after integration of the first equation of the system (2.2) over the depth and use the kinematic boundary conditions at the free surface and at the base, the continuity equation becomes:

$$\widehat{h}_t + (\widehat{h}\overline{v^x})_x = 0. \tag{2.30}$$

The relation (2.31) using the (2.30) is simplified as:

$$\overline{v^x}_t + \overline{v^x v^x}_x = sin(\theta) - \epsilon cos(\theta)K_{act/pas}\{\widehat{h}_x + b_x\} + \\ -sgn(\overline{v^x})cos(\theta)\tan(\phi_{bed}), \tag{2.31}$$

taking a value of $\alpha = 1$.

Equations (2.30) and (2.31) comprise a system of two partial differential equations for the profile $\widehat{h}(x,t)$ and the transversely averaged velocity $\overline{v^x}$. Provided the internal angle of friction φ, the basal friction angle ϕ_{bed}, and the basal geometry (through the angle θ and the function $b(x)$ are known. The evolution in time of both $\widehat{h}(x,t)$ and $\overline{v^x}$ can be determined if an initial profile and a velocity distribution

$$\begin{cases} h(x,0) = h_0(x), \\ \\ \overline{v^x}(x,0) = \overline{v^x}_0(x), \end{cases} \tag{2.32}$$

are prescribed. In particular, for the motion of an avalanche along a planar bed the authors may set $b = 0$ and replace $\widehat{h}$ by h. So the considerations of the present model will be restricted to this case, and the system become:

$$\begin{cases} h_t + (hv^x)_x = 0, \\ \\ v_t^x + v^x v_x^x = sin(\theta) - sgn(v^x)cos(\theta)\tan(\phi_{bed}) - \beta h_x, \end{cases} \tag{2.33}$$

where we have omitted the over bars for simplicity and

$$\beta = \epsilon K_{act/pas}cos(\theta) \tag{2.34}$$

is a small constant. Boundary conditions which must imposed upon the system (5.8) are:

$$\begin{cases} h(x,t) = h_F(t) \quad at \quad x = x_F(t), \\ \\ h(x,t) = h_R(t) \quad at \quad x = x_R(t), \end{cases} \tag{2.35}$$

with $x = x_F(t)$ and $x = x_R(t)$ denoting the front and rear margins respectively, while $h_F(t)$ and $h_R(t)$ are prescribed functions of time. Note that $h_F(t) = h_R(t) = 0$ are obvious choices, but cliffs are also possible.

Finally, we mention that the margin velocities are given by:

$$\begin{cases} u_F = \frac{dx_F}{dt}, \\ \\ u_R = \frac{dx_R}{dt}. \end{cases} \tag{2.36}$$

Chapter 3

The Iverson model

In an extensive review of debris flows, Iverson [42] presented a thin layer model for a mixture of granular material and interstitial fluid in one spatial dimension.

Before dealing with the analysis of the model described by Iverson, we think it is useful to show a short review of the equations governing the theory of mixtures, which underlie this model.

The governing equations for a debris flow can be obtained from established theory of continuous mixtures [68]. Equations are formulated separately, even if strongly coupled, they describe the balance of conservation of mass and momentum, respectively for solid and liquid constituents of a debris flow. In addition, as it is usual for the classical theory of mixtures, these equations both for solid and liquid are assumed to be valued simultaneously be all positions.

It usually, these equations for the solid and the liquid are assumed to be applied simultaneously to all positions. One could also formulate an equation of balance of moment of momentum, but this is not necessary since it is assumed that the stress tensor is symmetric. Similarly, the thermodynamic energy balance is made redundant, because it is assumed that the mixture is isothermal. The mixture theory mass conservation equations for the solid and fluid constituents are, respectively:

$$\frac{\partial(\rho^s\varphi)}{\partial t} + \nabla\cdot(\rho^s\varphi\mathbf{v^s}) = m^s, \tag{3.1}$$

$$\frac{\partial[\rho^f(1-\varphi)]}{\partial t} + \nabla\cdot[\rho^f(1-\varphi)\mathbf{v^f}) = m^f, \tag{3.2}$$

where φ is the solid volume fraction, $\mathbf{v^s}$ and $\mathbf{v^f}$ are the solid and fluid velocities and and m^s and m^f are the respective rates of solid and fluid mass addition, per unit volume.

As the material of the debris flow is saturated, the volume fractions of solid and fluid must satisfy the condition of saturation. As a result, the equations (3.1) and (3.2) are coupled, and their sum gives an equivalent equation of conservation of the total mass of the mixture:

$$\frac{\partial \rho}{\partial t} + \nabla \cdot (\rho \mathbf{v}) = m^s + m^f, \tag{3.3}$$

where the total mass density of the mixture ρ and the barycentric velocity $\mathbf{v}$, are defined by:

$$\rho = \varphi + \rho^f (1 - \varphi) \tag{3.4}$$

$$\mathbf{v} = \frac{\rho^s \varphi \mathbf{v^s} + \rho^f (1 - \varphi) \mathbf{v^f}}{\rho} \tag{3.5}$$

Now, we consider the special case of conservation of mass, in which the variations of mass are zero ($m^s = m^f = 0$) and the solid and fluid constituents are individually incompressible.

By summing (3.1) and (3.2) we get the alternative forms of mass balance:

$$\nabla \cdot (1 - \varphi)(\mathbf{v^f} - \mathbf{v^s}) + \nabla \cdot \mathbf{v^s} = 0, \tag{3.6}$$

$$\nabla \cdot \mathbf{v} = 0, \tag{3.7}$$

After having substituted the fluid specific discharge,

$$\mathbf{q} = (1 - \varphi)(\mathbf{v^f} - \mathbf{v^s}),$$

in the equation (3.6) we get the standard form of the equation of continuity for deforming porous media subject to quasistatic [69] or inertial motion [70].

In this way it is exploited the analogy between the mixtures of debris flow and porous media. Finally, the (3.7) represents the standard continuity equation for an incompressible, single-phase continuum.

In general, from the theory of mixtures, the momentum balance equation of the solid and fluid phase are, respectively:

$$\rho^s\varphi[\partial\mathbf{v^s}/\partial t + \mathbf{v^s}\cdot\nabla\mathbf{v^s}] = \nabla\cdot\mathbf{T^s} + \rho^s\varphi\mathbf{g} + \mathbf{f} - m^s\mathbf{v^s}, \tag{3.8}$$

$$\rho^f(1-\varphi)[\partial\mathbf{v^f}/\partial t + \mathbf{v^f}\cdot\nabla\mathbf{v^f}] = \nabla\cdot\mathbf{T^f} + \rho^f(1-\varphi)\mathbf{g} - \mathbf{f} - m^f\mathbf{v^f}, \tag{3.9}$$

where $\mathbf{g}$ is gravitational acceleration, $\mathbf{T^s}$ and $\mathbf{T^f}$ are the solid phase and fluid phase stress tensors, respectively, and $\mathbf{f}$ is the interaction force per unit volume that results from momentum exchange between the solid and fluid constituents. Sign conventions define normal stresses as positive in tension and $\mathbf{f}$ as positive when it acts on the solid.

The last term of (3.8) and (3.9) arises from the nonzero terms on the right-hand sides of (3.1) and (3.2) and account for momentum change due to mass change. However, they do not account for forces that enable mass change, and they assume that mass enters or leaves with zero momentum.

By adding the (3.8) and (3.9), and considering the special case with ($m^s = m^f = 0$), the mixture is obtained, the equation of conservation of momentum:

$$\rho[\partial\mathbf{v}/\partial t + \mathbf{v}\cdot\nabla\mathbf{v}] = \nabla\cdot(\mathbf{T^s} + \mathbf{T^f} + \hat{\mathbf{T}}) + \rho\mathbf{g}, \tag{3.10}$$

in which

$$\hat{\mathbf{T}} = \rho^s\varphi(\mathbf{v^s} - \mathbf{v})(\mathbf{v^s} - \mathbf{v}) - \rho^f(1-\varphi)(\mathbf{v^f} - \mathbf{v})(\mathbf{v^f} - \mathbf{v}), \tag{3.11}$$

is a contribution to the stress of the mixture, resulting from the motion of fluid and solid constituents.

$\hat{\mathbf{T}}$ brings in (3.10), the convective acceleration terms of the mixture, given by $\mathbf{v}\cdot\nabla\mathbf{v}$.

It shows in a two-phase mixture (debris flow), represented as a single material, the stresses are more complex than those obtained by adding the stress of the solid and fluid $\mathbf{T^s} + \mathbf{T^f}$.

Finally we can observe that by excluding $\hat{\mathbf{T}}$, the equation (3.10) assuming the form of a single-phase continuum balance equation.

The basic equations of the mixture's theory (3.1-3.10) compared with those for single phase, show three significant advantages with respect to comparable single-phase equations:

1. they represent explicitly the volume fractions of solid, of fluid and changes in mass, allowing them to show the various compositions or evolution of a debris flow;

2. they include separately the stress tensor for the solid and fluid, which have a direct physical meaning.

   On the contrary, in the single-phase models of the stress tensor that amalgamates the effects of solids and fluids and their interactions. This formulation of stress, to describe the rheology of the mixture may need the use of many parameters poorly constrained.

3. the momentum mixture equations contain explicit solid-fluid interaction force. Such a force is missing in the single-phase models, that include they effect in the mixed stress tensor.

   Since the solid-fluid interactions vary from point to point within a debris flow, playing an important role physical, it is necessary to introduce an explicit representation of their effects.

3.1 A simple model for a Debris Flow Surges

There are two phenomena that characterize the unstable motion and non-uniform of a debris flow:

1. In a debris flow, the pressure of the fluid, which can not exists in a constant and uniform motion, is significantly greater than the hydrostatic pressure, thus increasing the efficiency of the flow. The significant influence of pore pressure on the mechanics of debris flow can be molded easily by introducing the actual pore pressure in a specially formulated hydraulic model (as we will see in Section 3.1).

2. The debris flow, move as a surge or series of surges, in which coarse-grained heads that lack high fluid pressure restrict the downslope motion of finer-grained debris that may be nearly liquefied by high fluid pressure.

The concentration of coarse material (clasts) at the surge heads, means that the hydraulic diffusivity is higher than in the main part of materials of debris flow. This is because the heads of the pulses appear unsaturated and exhibit small or no pore fluid pressure. The interaction of the surge heads with the almost liquid material, plays a key role in the determination of the unstable and non-uniform motion and limit the expansion of the debris flow. The remaining parts of the flow almost liquefied provide a small frictional resistance to motion, unlike the surge heads.

A rigorous evaluation of the interaction between the dry surge heads with the material liquefied almost requires the numerical analysis of the motion unstable and non-uniform flow.

However a simple analysis of steady-state, provides a framework for understanding the problem and interpretation of numerical results. Such analysis ([71]-[73]), assumes that the surge heads acts as a rigid body shifted, with resistance at the base of Coulomb and pushed back by a mass completely liquefied.

This analysis ignores other forms of resistance, considering only those associated with internal deformation, ignore all the inertial effects and time-dependent, whereas the evolution of the shape of the flow and finally, ignore the multi-dimensional effects that can not be represented with a balance one-dimensional forces.

We consider here, the simple model of the pulse of a debris flow, shown in Figure 3.1.

The surge moves steadily on a uniform slope inclined at the angle θ.

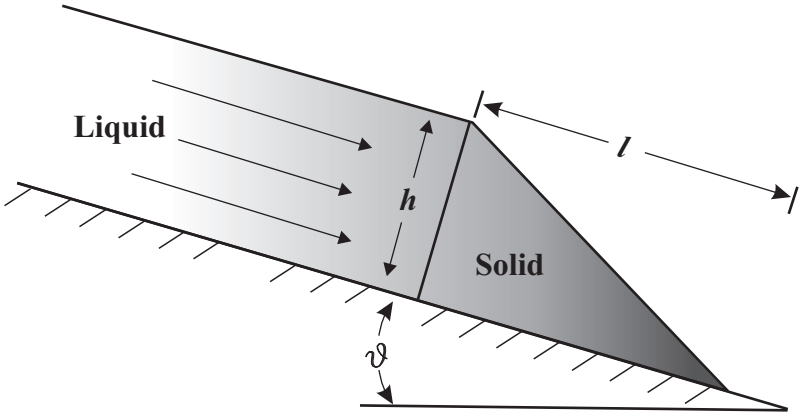

Fig. 3.1: Schematic vertical cross section of the rigid body model of a debris-flow surge, with geometric parameters defined ([71], [72]).

The surge head has a triangular cross-sectional shape with height h equal to the debris flow thickness measured normal to the slope. The length l of the surge head is measured parallel to the slope.

The mass of the surge head is then $\frac{1}{2}\rho_h lw$, where ρ_h is the bulk density of the head and w is its breadth normal to the plane of the page.

The basal shear force τ and normal force σ due to the action of gravity on the head are simply:

$$\tau = \frac{1}{2}\rho_h ghlw \sin\theta, \tag{3.12}$$

and

$$\sigma = \frac{1}{2}\rho_h ghlw \cos\theta, \tag{3.13}$$

The slope basal parallel Coulomb resistance, sliding of the head, is described by $-\sigma \tan\phi$, and the slope parallel force of the liquefied debris flow body pushing against the upslope face of the head is described by $\frac{1}{2}\rho_b gh^2 lw \cos\theta$, where ρ_b is the density of the liquefied body. This expression assumes that the streamlines of flow parallel the slope.

Steady motion of the head then requires to be zero the sum of the slope parallel forces acting on the head:

$$\frac{1}{2}\rho_h ghlw\sin\theta - \frac{1}{2}\rho_h ghlw\cos\theta + \frac{1}{2}\rho_b gh^2 lw\cos\theta = 0, \tag{3.14}$$

Combining the terms of (3.14) [72]we get:

$$\frac{h}{l} = \frac{\rho_h}{\rho_b}(\tan\phi - \tan\theta). \tag{3.15}$$

Moreover, if we assume $\rho_h \approx \rho_b$, for reasonable approximation debris flow, the (3.15) can be expressed as:

$$\frac{h}{l} = (\tan\phi - \tan\theta). \tag{3.16}$$

The quantitative predictions of (3.15) and (3.16) must be interpreted with great caution because of several factors neglected in the analysis. However, they provide some insight for the interpretation of the behavior of debris flow and to predict more elaborate models.

(3.16) shows that on steep slopes, when $\theta \to \phi$, we obtain $\frac{h}{l} \to 0$.

This implies that the momentum tends to accelerate on the steep slope, unless the length of the head is much larger than its height.

Furthermore, in addition, pulses with identical values of l, rise height h larger and with greater acceleration, overtaking the smaller pulses.
Instead, for small angles of slope, when $\theta \to 0$, (3.16) becomes $\frac{h}{l} = \tan\phi$, this implies that the pulse will slow down and stop, unless, which requires that the heads of the pulses are short and steep.

Typically an angle of friction $\phi \to 30^o$ is sufficient to stop the movement, in fact, the length exceeds the value so that the frictional resistance of the head of the pulse is capable of stopping the movement of the flow.

A more realistic assessment of the role of the head of the pulse requires a model such as that described in the following section.

3.2 Hydraulic modeling and prediction of debris flow motion

This model formulated by Iverson [42], known as "hydraulic model", uses the simplifications of the hydraulics theory and is one of the most refined for the prediction of unstable and non-uniform motion of a debris flow, and its limits of expansion and flooding.

In this model are still used of depth-averaged equations of motion. However, are neglect some key physical phenomena, such as the rigorous treatment of the evolution of the granule temperature and non-hydrostatic pore pressure.

To account for debris flows variable composition, the possibility of boundary slip, and the mechanics of initiation and deposition as well as flow, the hydraulic model described here uses internal and basal friction angles and pore fluid viscosity to characterize flow resistance. This simplifies the rigorous testing of the model because the values of the angles of friction and viscosity of the fluid can be measured independently rather than being calibrated.

In fact, the calibration is a problem of debris flows because the transport mechanisms of the time and energy dissipation differ significantly depending on the type of event.

The mathematical formulation is based on the change of hydraulic theory for dry granular flows developed by Savage and Hutter [29].

To clarify the assumptions of hydraulic formulation we refer to the relationships described in the theory of mixture.

A simpler form of the equations of momentum of the mixture (3.8) and (3.9), can be obtained by focusing attention on the motion of solids, and analyzing the motion of fluid in relation to that of solids. So, it is defined that

$$\frac{\mathbf{q}}{(1-\varphi)} = \mathbf{v^f} - \mathbf{v^s}.$$

where $\mathbf{q}$ is the specific discharge and $(1-\varphi)$ is the volume fraction of the fluid

Substituting this relation into the equation of momentum of the fluid, we get:

$$\rho^f(1-\varphi)[\frac{\partial}{\partial t}\left(\frac{\mathbf{q}}{1-\varphi}+\mathbf{v^s}\right)+\frac{\mathbf{q}}{1-\varphi}\cdot\nabla\left(\frac{\mathbf{q}}{1-\varphi}+\mathbf{v^s}\right)+\mathbf{v^s}\cdot\nabla\left(\frac{\mathbf{q}}{1-\varphi}+\mathbf{v^s}\right)=$$

$$=\nabla\cdot\mathbf{T^f}+\rho^f(1-\varphi)\mathbf{g}-\mathbf{f}, \tag{3.17}$$

Darcy's law provides an estimate of the largest plausible $\mathbf{q}$ in (3.19) because data show that hydraulic head gradients in debris flows commonly approach but seldom exceed liquefaction-inducing gradients, which roughly is equal 1. Thus the hydraulic conductivity, for example, provides a good estimate of the maximum magnitude of $\mathbf{q}$, and the conductivity rarely exceeds 0.01 m/s for debris flow materials. In contrast, $\mathbf{v^s}$ typically exceeds 1 m/s.

By this rationale, $\mathbf{v^s}$ generally exceeds $\dfrac{\mathbf{q}}{1-\varphi}$ by more than an order of magnitude, then assuming

$$\left|\frac{\mathbf{q}}{1-\varphi}\right| << |\mathbf{v^s}| \tag{3.18}$$

the (3.19) becomes:

$$\rho^f(1-\varphi)\left[\frac{\partial \mathbf{v^s}}{\partial t} + \mathbf{v^s}\cdot\nabla\mathbf{v^s}\right] = \nabla\cdot\mathbf{T^f} + \rho^f(1-\varphi)\mathbf{g} - \mathbf{f}, \tag{3.19}$$

This equation implies that inertial forces affecting fluid motion are practically indistinguishable from those affecting solid motion, except insofar as the fluid and solid masses per unit volume of mixture differ.

By adding (3.19) with (3.8), we obtain a simplified equation of momentum of the solid-fluid mixture:

$$\rho\left[\frac{\partial \mathbf{v^s}}{\partial t} + \mathbf{v^s}\cdot\nabla\mathbf{v^s}\right] = \nabla\cdot(\mathbf{T^s} + \mathbf{T^f}) + \rho\mathbf{g}, \tag{3.20}$$

where ρ is the density of the mixture defined by (3.4), we also note that the solid-fluid interaction force f does not appear explicitly, but implicitly lies in the combination of solid-fluid stress tensor $\mathbf{T^s} + \mathbf{T^f}$.

The assumption (3.18), produces a further simplification of the mass balance equation (3.6), which reduces to the following form:

$$\nabla\cdot\mathbf{v^s} = 0. \tag{3.21}$$

The equations (3.20) and (3.21) are the equations governing the debris flow. They differ from the equations governing the motion of granular solids to a single-phase, because they involve the total mass density ρ of the mixture and the influence of the fluid stress $\mathbf{T^f}$ (implicitly considered in the equation of momentum of the mixture).

We consider a two-dimensional flow through an infinitely wide planar surface, inclined at an angle θ to the horizontal, as shown in Figure 3.2.

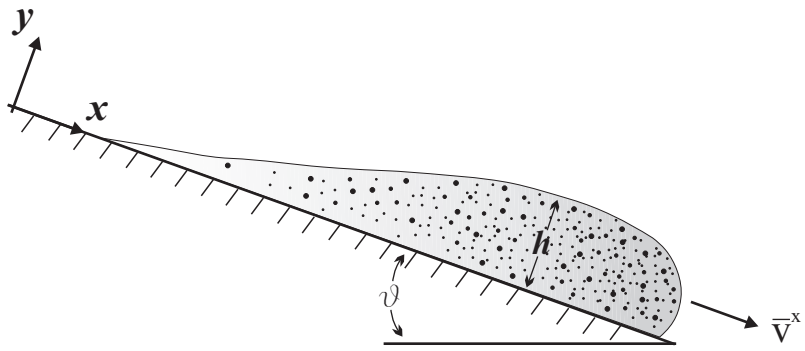

Fig. 3.2: Schematic vertical cross section of an unsteady, deforming debris flow surge moving down an inclined plane. The flow depth h and depth-averaged velocity $\overline{v}^x$ vary as functions of x and t.

The equations (3.20) and (3.21) generalized to two spatial coordinates x and y become:

$$\frac{\partial v_x}{\partial x} + \frac{\partial v_y}{\partial y} = 0, \tag{3.22}$$

$$\rho\left[\frac{\partial v_x}{\partial t} + v_x\frac{\partial v_x}{\partial x} + v_y\frac{\partial v_y}{\partial y}\right] = -\frac{\partial T^s_{xx}}{\partial x} - \frac{\partial T^s_{yz}}{\partial y} - \frac{\partial T^f_{xx}}{\partial x} + \\ -\frac{\partial T^f_{yz}}{\partial y} + \rho g \sin\theta, \tag{3.23}$$

$$\rho\left[\frac{\partial v_y}{\partial t} + v_y\frac{\partial v_y}{\partial y} + v_x\frac{\partial v_y}{\partial x}\right] = -\frac{\partial T^s_{yy}}{\partial y} - \frac{\partial T^s_{xy}}{\partial x} - \frac{\partial T^f_{yy}}{\partial y} + \\ -\frac{\partial T^f_{xy}}{\partial x} + \rho g \cos\theta, \tag{3.24}$$

Since all velocities refer to the solid phase, we omitted the subscript s, also the speed of the x and y subscripts denote the Cartesian components parallel and normal to the inclined plane.

Sign conventions for stress components have been reversed so that compression and left-lateral shear are positive [29].

The subscripts denote the Cartesian components of the stress of the solid and fluid, the first subscript indicates the direction normal to the plane of action of components of stress, and the second subscript indicates the direction of action.

Finally, the subscripts (x, y) and (y, x) are interchangeable because it is assumed that the stress tensor is symmetric.

To normalize the equations (3.22-3.24), we introduce two scale lengths: L the characteristic length of flow in x direction, and H the characteristic height of flow in y direction.

Therefore, the parameter $\epsilon = \dfrac{H}{L}$ describes the ratio of these lengths of scale and is considered generally much smaller than 1.

Instead, the characteristic time scale is given by the free fall in the x direction $(L/g)^{\frac{1}{2}}$, as the potential free fall is leading the movement of debris flow.

These time and length scales in turn lead to different scales of speed, in x direction $(Lg)^{\frac{1}{2}}$ and y direction $\epsilon(Lg)^{\frac{1}{2}}$, and also imply that $v_x >> v_y$. Finally, the scale of stress are the stress that existed on the basis of a constant flow and uniform height H, $\rho g H \sin\theta$ for shear stress and $\rho g H \cos\theta$ for normal stress and pore pressure.

In summary, using the following scaling transformation:

$$\begin{cases} (x, y, t) = L(\tilde{x}, \frac{H}{L}\tilde{z}, (\frac{L}{g})^{\frac{1}{2}}\tilde{t}), \\ (v^x, \mathbf{v^y}) = (gL)^{\frac{1}{2}}(\tilde{v}^x, \frac{H}{L}\tilde{v}^y), \\ (T_{xx}, T_{yy}) = \rho^s g H \sin\theta(\tilde{T}_{xx}, \tilde{T}_{yy}) \\ (T_{xy}, T_{yx}) = \rho^s g H \cos\theta(\tilde{T}_{xy}, \tilde{T}_{yx}) \end{cases} \tag{3.25}$$

The system of equations (3.22-3.24) with scaling transformation (3.25), by dropping tilde, multiplying each term of (3.22) by $(L/g)^{\frac{1}{2}}$, dividing each term of (3.23) and (3.24) by ρg and taking the limit as $\epsilon \to 0$, we get the following

three scalar equations written in component form:

$$\frac{\partial v_x}{\partial x} + \frac{\partial v_y}{\partial y} = 0, \tag{3.26}$$

$$\frac{\partial v_x}{\partial t} + v_x \frac{\partial v_x}{\partial x} + v_y \frac{\partial v_y}{\partial y} = \sin\theta \left[1 - \frac{\partial T^s_{yz}}{\partial y} - \frac{\partial T^f_{yz}}{\partial y} \right] + \\ + \epsilon \cos\theta \left[- \frac{\partial T^s_{xx}}{\partial x} - \frac{\partial T^f_{xx}}{\partial x} \right], \tag{3.27}$$

$$0 = \cos\theta \left[-1 - \frac{\partial T^s_{yy}}{\partial y} - \frac{\partial T^f_{yy}}{\partial y} \right]. \tag{3.28}$$

These equations differ from governing equation of Savage and Hutter [29] only by including fluid stresses.
Equations (3.26-3.28) have two key properties:

1. The y direction momentum balance (3.28) has a simple form identical to that for steady, uniform flow; its integration shows that the total normal stress at any depth is simply the static stress $\rho g(h - y)\cos\theta$.

2. The x direction momentum balance (3.27) includes longitudinal normal stress gradient terms preceded by the small parameter ϵ, which apparently indicates that such terms can be neglected.

However, as was explained by Savage and Hutter, neglect of longitudinal normal stress gradients is untenable because it produces a stress field identical to that for steady, uniform flow, which negates any hope of modeling surge-like motion.

The physical rationale for retaining this term becomes more apparent when the equations are integrated over the flow depth.

The final step in the simplification of the equations of government is to introduce the depth integration, which incorporates the assumptions with respect to stress and produces constitutive equations without explicit dependence on y.

The process is linear, but rather prolonged, then try to summarize the results easily. It includes repeated application of Leibniz's rule for integrating derivatives and incorporates kinematic boundary conditions, which state that

the mass does not enter and exit the free surface (where $y = h$) and the bed (where $y = 0$),

$$\frac{\partial h}{\partial t} + v_x \frac{\partial h}{\partial x} - v_y = 0 \qquad at \qquad y = (x, t) \tag{3.29}$$

$$v_y = 0 \qquad at \qquad y = 0 \tag{3.30}$$

It also involves the assumption that the debris flow surface is free of all stresses,

$$T^s_{xx} = T^s_{yy} = T^s_{xy} = T^f_{xx} = T^f_{yy} = T^f_{xy} = 0 \qquad at \qquad y = (x, t) \tag{3.31}$$

and it employs depth-averaged velocities and normal stresses defined by

$$\overline{v_x} = \frac{1}{h} \int_0^h v_x dy, \tag{3.32}$$

$$\overline{T^s_{xx}} = \frac{1}{h} \int_0^h T^s_{xx} dy, \tag{3.33}$$

$$\overline{T^s_{yy}} = \frac{1}{h} \int_0^h T^s_{yy} dy, \tag{3.34}$$

$$\overline{T^f_{xx}} = \frac{1}{h} \int_0^h T^f_{xx} dy, \tag{3.35}$$

$$\overline{T^f_{yy}} = \frac{1}{h} \int_0^h T^f_{yy} dy, \tag{3.36}$$

$$\overline{v^2_x} = \frac{1}{h} \int_0^h v^2_x dy = \alpha \overline{v^2_x}, \tag{3.37}$$

The value of α in (3.37) [29], provides information on the deviation of the vertical velocity profile uniformity. If a debris flow moves only for basal slip, is applied 1.

For a description of the constitutive stress in (3.27), we use the simple relationship of Coulomb granular solids, in dimensionless form:

$$T^s_{xy} = -sgn(v_x) T^s_{yy} \cot\theta \tan\phi_{bed/int}, \tag{3.38}$$

where $\phi_{bed/int}$ indicates the appropriate friction angle for bed slip or internal deformation, $sgn(v_x)$ denotes the sign (+ or -) of (v_x) and $\cot\theta$ is introduced because of the different scalings for shear and normal stress components.

Finally, in (3.38) does not appear explicitly the effects of pore pressure, but implicitly, because the T^s_{yy} and T^f_{yy} refer to (3.28). Thus as fluid pressures T^f_{yy} grow in magnitude, the magnitudes of T^s_{yy} and T^s_{yx} diminish.

Moreover, the Coulomb rule leads directly to the following expression of T^s_{xx} and T^s_{yy} obtained from classical Rankine [79] earth pressure theory:

$$T^s_{xx} = K_{act/pas} T^s_{yy}, \tag{3.39}$$

where $K_{act/pas}$ is an earth pressure coefficient that has different values depending on whether the flow is actively extending $\left(\dfrac{\partial \overline{v}_x}{\partial x} > 0\right)$ or passively compressing $\left(\dfrac{\partial \overline{v}_x}{\partial x} < 0\right)$, and its expression presented without derivation by Savage and Hutter:

$$K_{act/pas} = 2\frac{1 \mp [1 - \cos^2(\phi_{int})[1 + \tan^2(\phi_{bed})]]^{1/2}}{\cos^2(\phi_{int})} - 1, \tag{3.40}$$

where the sign "-" applies to the active coefficient, and the sign "+" applies to the passive.

Equations (3.26-3.40) provide all information necessary to complete the formulation of hydraulic equations.

Integration of equation (3.26) from $y = 0$ to $y = h$, with application of the kinematic boundary conditions (3.29-3.30) produces a depth-averaged mass conservation equation:

$$\frac{\partial h}{\partial t} + \frac{\partial h \overline{v}_x}{\partial x} = 0. \tag{3.41}$$

Integration of (3.28) from $y = 0$ to $y = h$ yields a steady momentum balance in the y direction, which states that the sum of the nondimensional

solid and fluid stress balances the y component of the nondimensional total mixture weight

$$T^s_{yy} + T^f_{yy} = h(x,t) - y. \tag{3.42}$$

This in turn leads to nondimensional expressions for the total (solid plus fluid) normal stress at the bed and for the y direction depth-averaged total normal stress,

$$T^s_{yy} + T^f_{yy} = h, \qquad at \qquad y = 0 \tag{3.43}$$

$$\overline{T}^s_{yy} + \overline{T}^f_{yy} = \frac{1}{h}\int_0^h (h-y)dy = \frac{1}{2}h. \tag{3.44}$$

Integration of the normalized x direction momentum equation (3.27) from $y = 0$ to $y = h$, gives the following expression:

$$\begin{aligned} \frac{\partial}{\partial t}(h\overline{v}_x) + \frac{\partial}{\partial x}(\alpha h\overline{v}_x^2) &= h\sin\theta + \\ +(T^s_{yx|y=0})\sin\theta + (T^f_{yx_|y=0})\sin\theta &+ \\ -\epsilon\cos\theta\frac{\partial}{\partial x}(h\overline{T}^s_{xx}) - \epsilon\cos\theta\frac{\partial}{\partial x}(h\overline{T}^f_{xx}). & \end{aligned} \tag{3.45}$$

Terms on the right-hand side of (3.45) can be interpreted as follows. The first term represents the gravitational driving stress. The second term represents frictional resistance to slip at the base of the flow and can be evaluated by applying the Coulomb equation (3.38) and the normal stress equation (3.43) at the flow base

$$(T^s_{yx|y=0})\sin\theta = -sgn(\overline{v}_x)(h - p_{bed})\cos\theta\tan\phi_{bed} \tag{3.46}$$

where $h - p_{bed}$ is the nondimensional basal effective stress and $\phi_{bed} = T^f_{yx|y=0}$ is the nondimensional basal pore pressure.

The third term on the right-hand side of (3.45) represents flow resistance due to shear of the fluid at the flow base. It can be evaluated using Newton's

law of viscosity [42], which yields

$$(T^f_{yx|y=0}) \sin\theta = -(1-\varphi)\overline{\mu}\left(\frac{\partial v_x}{\partial y}\right)_{|y=0} \tag{3.47}$$

where $\overline{\mu}$ is the appropriate, nondimensional depth-averaged viscosity, given by

$$\overline{\mu} = \frac{\mu}{\left[\rho g \overline{h}^2 / g\overline{l}^{1/2}\right]}. \tag{3.48}$$

Application of (3.48) requires knowledge of the fluid velocity gradient at the bed, $\left(\frac{\partial v_x}{\partial y}\right)_{|y=0}$, which is generally unknown but can be obtained from estimates of the vertical velocity profile. The estimates are constrained by assuming no slip of fluid at the bed and a mean fluid velocity of $\overline{v}_x$. For example, if the velocity profile is linear, then $\left(\frac{\partial v_x}{\partial y}\right)_{|y=0} = \frac{\overline{v}_x}{h}$. If the velocity profile is parabolic, then a simple analysis of laminar flow down an incline shows that $\left(\frac{\partial v_x}{\partial y}\right)_{|y=0} = \frac{3\overline{v}_x}{h}$. If the velocity profile is blunt, with shear strongly concentrated near the bed, a good descriptor is $\left(\frac{\partial v_x}{\partial y}\right)_{|y=0} = (n+2)\frac{\overline{v}_x}{h}$, where $n = 1$ indicates a parabolic profile and $n > 1$ indicates blunter profiles; this form is used below.

The fourth term on the right-hand side of (3.45) represents the longitudinal stress gradient due to interaction of solid grains. It can be evaluated using (3.39) and (3.44), yielding

$$-\epsilon\cos\theta\frac{\partial}{\partial x}(h\overline{T}^s_{xx}) = -\epsilon K_{act/pas}\cos\theta\frac{\partial}{\partial x}\left(\frac{h^2}{2} - h\overline{T}^f_{yy}\right). \tag{3.49}$$

As is indicated by the presence of $\overline{T}^f_{yy}$ in (3.49), the longitudinal solid stress gradient is mediated by fluid pressure.

The final term in (3.45) represents the longitudinal stress gradient due to the fluid pressure alone. Because fluid pressure is isotropic, it can be rewritten with $\overline{T}^f_{yy}$ in place of $\overline{T}^f_{xx}$,

$$-\epsilon\cos\theta\frac{\partial}{\partial x}(h\overline{T}^f_{xx}) = -\epsilon K_{act/pas}\cos\theta\frac{\partial}{\partial x}\left(\frac{h^2}{2} - h\overline{T}^f_{yy}\right). \tag{3.50}$$

The utility of (3.49) and (3.50) is enhanced by evaluating the integral (3.36) to calculate $\overline{T}^f_{yy}$ for a condition in which the fluid pressure increases linearly from zero at the debris flow surface to a maximum of p_{bed} at the bed (a condition consistent with the hydraulic theory assumptions). Integration shows that we can write

$$\frac{\partial h\overline{T}^f_{yy}}{\partial x} = h\frac{p_{bed}}{\partial x}.$$

The final form of the x direction momentum equation results from incorporating (3.41) and (3.46-3.50) in (3.45), assuming $\alpha = 1$, collecting and canceling like terms, and dividing by h, which yields

$$\frac{\partial \overline{v}_x}{\partial x} + \overline{v}_x\frac{\partial \overline{v}_x}{\partial t} = \sin\theta - sgn(\overline{v}_x)\left(1 - \frac{p_{bed}}{h}\right)\cos\theta\tan\phi_{bed} + \\ -(1-\varphi)\overline{\mu}(n+2)\left(\frac{\overline{v}_x}{h^2}\right) + \\ -\epsilon\cos\theta\frac{\partial}{\partial x}[K_{act/pas}(h - p_{bed}) + p_{bed}]. \qquad (3.51)$$

Together, (3.51) and (3.41) form a set of two equations in two unknowns, $\overline{v}_x(x,t)$ and $h(x,t)$, which can be solved provided that the basal pore fluid pressure $p_{bed}(x,t)$ and the necessary initial and boundary conditions are specified.

The need to specify rather than predict basal pore pressures is inherent to the hydraulic model; fluid pressure deviations from hydrostatic values result from velocity components normal to the bed, and neglect of such velocities in (3.28) precludes the possibility of predicting non hydrostatic pressures.

Thus inclusion of non hydrostatic pressures $p_{bed}(x,t)$ may seem to contradict the hydraulic model assumptions. The inclusion is justified, however, on the grounds that the consolidation process responsible for generating non hydrostatic fluid pressures typically operates on timescales substantially longer than the debris flow duration.

Thus as a first approximation, high pore pressures, once established, may be assumed to persist in debris flows, and pore pressures may be treated as parameters in hydraulic model calculations.

Inspection of the individual terms in (3.51) reveals how the hydraulic model encapsulates debris flow physics.

The inertial terms on the left-hand side of (3.51) show that both rigid body accelerations and convective accelerations may be important.

On the right-hand side of (3.51), if the first two terms are viewed in isolation, they depict a static balance of forces identical to that used in infinite slope stability analyses for cases in which there is zero cohesion and an arbitrary distribution of pore pressure [74]-[75].

If the last term on the right-hand side is included, this static force balance assumes a form comparable to that of two-dimensional slope stability analyses that use methods of slices, and in this case the interslice forces are represented by depth-averaged Rankine stresses.

Thus the model subsumes classical models of the statics of landslides with spatially varied pore pressures as a limiting case, which applies to incipient debris flow motion.

The third term on the right-hand side of (3.51) represents the effects of shear resistance due to fluid viscosity.

The motion of a frictionless but viscous mass is represented by the special case where $\phi_{bed/int} = 0$ or, alternatively, $pbed = h$ (in which case the mass is completely liquefied by pore pressure).

The final term is perhaps the most interesting and important term in (3.2), for it describes the longitudinal stress variation that accompanies variations in flow depth and surge-like motion.

The term shows that a great change in debris flow behavior occurs as p_{bed} ranges from 0 to h. If $p_{bed} = h$ and the sediment mass behaves like a liquid, normal stresses are isotropic, equal to the static pressure, and independent of the local style of deformation. If $p_{bed} = 0$ and the debris behaves like a Coulomb solid, normal stresses are anisotropic, and the longitudinal normal stress depends strongly on whether the sediment mass is locally extending $\left(\frac{\partial \overline{v}_x}{\partial x} > 0\right)$ or compressing $\left(\frac{\partial \overline{v}_x}{\partial x} < 0\right)$ as it deforms and moves downslope.

Consequently, the model predicts that strong local gradients in the longitudinal normal stress can occur for two reasons: either the style of deformation changes locally from extending to compressing, or the pore pressure varies locally from high to low.

Thus, depending on the deformation style and pore pressure distribution, the model expressed by (3.41) and (3.51) can represent unsteady flow behavior that ranges from that of a granular avalanche, as modeled by Savage and Hutter [29]-[67], to that of a liquid surge, as modeled by Hunt [76].

Furthermore, the front of a fully developed debris flow may act like a compressing granular solid and support high lateral stresses, while the trailing flow acts more like a fluid.

This phenomenon explains how debris flow surges with steep snouts and gradually tapered tails can move downstream with only modest attenuation.

The initial and boundary conditions used in conjunction with (3.41) and

(3.51) are identical to those described by Savage and Hutter [29].

The initial conditions specify the zero velocity and static geometry of the mass that mobilizes into a debris flow,

$$\overline{v}_x(x,0) = 0 \tag{3.52}$$

$$h(x,0) = h_0(x) \tag{3.53}$$

Boundary conditions stipulate that the height of the deforming mass is zero at the front margin ($x = x_F$) and rear margin ($x = x_R$),

$$h(x_F,t) = 0 \tag{3.54}$$

$$h(x_R,t) = 0 \tag{3.55}$$

These zero-depth boundary conditions are connected to the velocities at the front and rear flow margins by the relations

$$\overline{v}_x^F(x,0) = \frac{dx_F}{dt} \tag{3.56}$$

$$\overline{v}_x^R(x,0) = \frac{dx_R}{dt} \tag{3.57}$$

Finally, the pore pressure distribution $p_{bed}(x,t)$ must be specified.

Chapter 4

The Iverson and Denlinger model

This model is a generalization of the depthaveraged, two-dimensional grain-fluid mixture model of Iverson [42], who in turn generalized the one-phase grain flow model of Savage and Hutter [29].

The new generalization yields depth-averaged mass and momentum balance equations that describe finite masses of variably fluidized grain-fluid mixtures that move unsteadily across a threedimensional terrain, from initiation to deposition.

In generalizing to three spatial dimensions we address key physical issues concerning with preservation of frame invariance, symmetry of conjugate shear stresses, magnitudes of lateral forces, and distributions of pore fluid pressure.

Here, along the guidelines of the paper of Iverson and Denlinger [35] we consider the relevant equations for debris flow resulting from the theory of mixtures (see Section 3): :

$$\nabla \cdot \mathbf{v^s} = 0. \tag{4.1}$$

$$\rho \left[\frac{\partial \mathbf{v^s}}{\partial t} + \mathbf{v^s} \cdot \nabla \mathbf{v^s} \right] = \nabla \cdot (\mathbf{T^s} + \mathbf{T^f}) + \rho \mathbf{g}, \tag{4.2}$$

A key step in further simplifying the equations of motion involves depth averaging to eliminate explicit dependence on z which is the coordinate normal to the bed.

Depth averaging requires decomposing the vector equations (4.1) and (4.2) into component equations in locally defined x, y, z orthogonal direc-

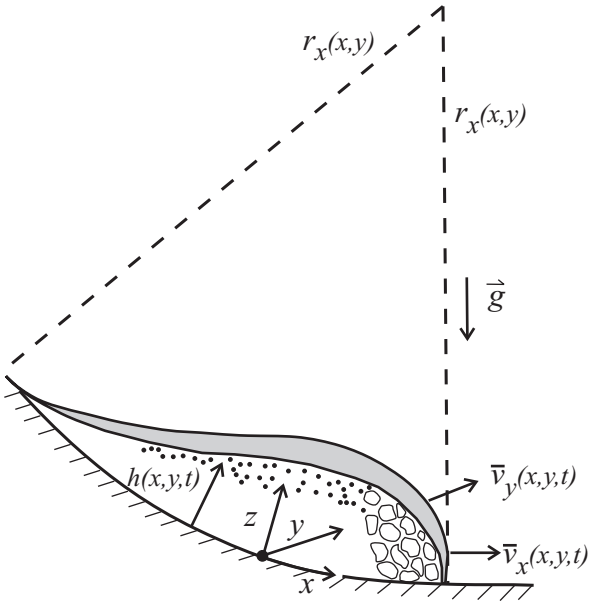

Fig. 4.1: Schematic cut-away view of an unsteady flow down a curvilinear slope, illustrating the local coordinate system and dependent variables $h(x, y, t)$, $v_x(x, y, t)$, $v_y(x, y, t)$ that describe depth-averaged flow. The x component of bed curvature is specified by the local radius of curvature r_x.

tions, then integrating each component equation from the base of the flow at $z = 0$ to the surface of the flow at $z = h$ (see Figure 4.1).

The pertinent mathematical manipulations are rather lengthy, and we omit some details here. However, the details are similar to those in [78] derivation of the standard shallow water equations and in [34] derivation of dry granular avalanche equations.

The derivation makes frequent use of Leibniz' theorem for interchanging the order of integrations and differentiations [77] and of kinematic boundary conditions that specify that mass neither enters nor leaves at the free surface or base of the flow:

$$\frac{\partial h}{\partial t} + v_x \frac{\partial h}{\partial x} + v_y \frac{\partial h}{\partial y} - v_z = 0 \qquad at \qquad z = (x, y, t) \tag{4.3}$$

$$v_z = 0 \qquad at \qquad z = 0 \tag{4.4}$$

In these equations and in hereinafter, all v denote the solid-phase velocity,

and subscripts x, y, and z denote Cartesian components of vector and tensor quantities.

Depth averaging also implies that the total normal stress (the sum of solid and fluid normal stresses) in the z direction balances the z component of the mixture weight:

$$T^s_{zz} + T^f_{zz} = (h - z)\rho g_z. \tag{4.5}$$

Equation (4.5), in turn, leads to expressions for the total normal stress at the bed and for the depth-averaged total normal stress in the z direction,

$$T^s_{zz|z=0} + T^f_{zz|z=0} = \rho g_z h. \tag{4.6}$$

$$\overline{T}^s_{zz} + \overline{T}^f_{zz} = \frac{1}{h}\int_0^h \rho g_z (h - z) dz = \frac{1}{2}\rho g_z h. \tag{4.7}$$

In (4.6), (4.7), and equations hereinafter, overbars denote depth-averaged quantities defined by integrals similar to that in (4.7).

Thus depth-averaged velocities are defined by

$$\overline{v}_x = \frac{1}{h}\int_0^h v_x dz \tag{4.8}$$

$$\overline{v}_y = \frac{1}{h}\int_0^h v_y dz \tag{4.9}$$

and depth-averaged stress components (denoted generically by subscript ij) are defined by

$$\overline{T}_{ij} = \frac{1}{h}\int_0^h T_{ij} dz. \tag{4.10}$$

Using these definitions together with (4.1) and (4.2), we obtain depth-averaged mass and momentum conservation equations for motion in the x and y directions:

$$\frac{\partial h}{\partial t} + \frac{\partial (h\overline{v}_x)}{\partial x} + \frac{\partial (h\overline{v}_y)}{\partial y} = 0, \tag{4.11}$$

$$\rho\left[\frac{\partial (h\overline{v}_x)}{\partial t} + \frac{\partial (h\overline{v}_x^2)}{\partial x} + \frac{\partial (h\overline{v}_x\overline{v}_y)}{\partial y}\right] =$$

$$= -\int_0^h \left[\frac{\partial T^s_{xx}}{\partial x} + \frac{\partial T^f_{xx}}{\partial x} + \frac{\partial T^s_{yx}}{\partial y} + \frac{\partial T^f_{yx}}{\partial y} + \frac{\partial T^s_{zx}}{\partial z} + \frac{\partial T^s_{zx}}{\partial z} - \rho g_x \right] dz, \quad (4.12)$$

$$\rho \left[\frac{\partial (h\overline{v}_y)}{\partial t} + \frac{\partial (h\overline{v}_y^2)}{\partial y} + \frac{\partial (h\overline{v}_y \overline{v}_x)}{\partial x} \right] =$$

$$= -\int_0^h \left[\frac{\partial T^s_{yy}}{\partial y} + \frac{\partial T^f_{yy}}{\partial y} + \frac{\partial T^s_{xy}}{\partial x} + \frac{\partial T^f_{xy}}{\partial x} + \frac{\partial T^s_{zy}}{\partial z} + \frac{\partial T^s_{zy}}{\partial z} - \rho g_y \right] dz. \quad (4.13)$$

The factor h that appears explicitly or implicitly in each term of these equations can be eliminated from the left-hand side of (4.12) and (4.13) by combining these equations with (4.11) [42]. However, here we retain the factor h so that individual terms have "conservative"' forms that represent fluxes of mass or momentum insofar as possible [78].

We use an "uniform slab" approximation, which assumes that stresses at any location and time (x, y, z, t) depend only on the local thickness, $h(x, y, t)$ and not on thickness gradients $\partial h/\partial x$ and $\partial h/\partial y$. Despite this approximation, thickness gradients influence the overall momentum balance, because all stress components are differentiated in space and multiplied by h as a result of the mathematical operations in (4.12) and (4.13).

Before evaluating Coulomb stress components, we replace the local solid stresses in (4.12) and (4.13) with depth-averaged stresses and basal shear stresses obtained by evaluating the integrals on the right-hand sides of (4.12) and (4.13) and using Leibniz' theorem to simplify the resulting expression. For (4.12) we find:

$$-\int_0^h \left[\frac{\partial T^s_{xx}}{\partial x} + \frac{\partial T^s_{yx}}{\partial y} + \frac{\partial T^s_{zx}}{\partial z} \right] dz = -\frac{\partial (h\overline{T}^s_{xx})}{\partial x} - \frac{\partial (h\overline{T}^s_{yx})}{\partial y} + T^s_{zx|z=0}, \quad (4.14)$$

and we find an analogous expression (with x and y interchanged) for (4.13).

Evaluation of individual Coulomb stress components follows a rationale like that in [42] two-dimensional analysis, with one important complication: whereas a depthaveraged two-dimensional stress field involves no transverse shear stresses $(\overline{T}^s_{yx}, \overline{T}^s_{xy})$, such shear stresses appear in both the x and y direction momentum equations used here.

Moreover, these conjugate shear stresses must satisfy $\overline{T}^s_{yx} = \overline{T}^s_{xy}$ to maintain the stress symmetry that preserves mechanical equilibrium in the $x -$

y plane. This shear stress symmetry also requires equality of the depth-averaged intergranular normal stresses $\overline{T}^s_{xx}$ and $\overline{T}^s_{yy}$ because shear stresses are proportional to normal stresses in deforming Coulomb materials.

Following Savage and Hutter [29], Gray et al.[34], and Iverson [42], we relate the depth-averaged normal stresses $\overline{T}^s_{xx}$ and $\overline{T}^s_{yy}$ to the depth-averaged z direction normal stress $\overline{T}^s_{zz}$ by using a lateral stress coefficient, $k_{act/pass}$, derived from Coulomb theory

$$\overline{T}^s_{xx} = \overline{T}^s_{yy} = K_{act/pas}\overline{T}^s_{zz}. \tag{4.15}$$

Unlike Gray et al. [34], however, we use a scalar lateral stress coefficient, which applies in the x and y directions simultaneously. Use of a scalar coefficient ensures frame invariance in the $x - y$ plane and preserves the stress symmetry $\overline{T}^s_{yx} = \overline{T}^s_{xy}$ described above, whereas use of multiple coefficients may violate invariance and symmetry.

At each point in a flow, our model stipulates that one of three deterministic values of the lateral stress coefficient applies. The coefficient values are given by

$$K_{act/pas} = 2\frac{1 \mp [1 - \cos^2(\phi_{int})[1 + \tan^2(\phi_{bed})]]^{1/2}}{\cos^2(\phi_{int})} - 1, \tag{4.16}$$

where "$-$" in "$\mp$" applies to the "*active*" coefficient for diverging flow, K_{act}, and "$+$" applies to the "*passive*" coefficient for converging flow, K_{pas}. These coefficient definitions are more general than those of classical Rankine earth pressure coefficients commonly used in soil mechanics [79] because (6.13) is derived by assuming that Coulomb failure occurs simultaneously along the bed (where $\phi = \phi_{bed}$) and within the overlying sediment mixture (where $\phi = \phi_{int}$) [42]. For the special case in which $\phi_{bed} = 0$, the coefficient definitions in (6.13) reduce to the classical Rankine definitions [80]. For most values of ϕ_{bed}, corresponding values of $K_{act/pas}$ indicate that lateral stresses in regions of converging flow exceed bed-normal stresses, whereas lateral stresses in regions of diverging flow are less than bed-normal stresses. Lateral normal stresses where flow converges typically exceed those where flow diverges by a factor of 2 to 10. An exception to this behavior occurs if the bed has maximum roughness, in which case, $\phi_{bed} = \phi_{int}$ and (6.13) reduces to a single-valued expression:

$$K_{act/pas} = \frac{1 + \sin^2\phi_{int}}{1 - \sin^2\phi_{int}}, \tag{4.17}$$

The uniqueness of this value indicates that a slab of Coulomb material can move downslope with zero velocity divergence (implying no thinning or thickening) only if the bed friction angle equals the internal friction angle.

We express the depth-averaged lateral stresses in the granular solids by combining (4.15) and (4.7) to obtain

$$\overline{T}^s_{xx} = \overline{T}^s_{yy} = K_{act/pas}\left(\frac{1}{2}\rho g_z h - \overline{T}^f_{zz}\right), \tag{4.18}$$

and we evaluate the depth-averaged fluid normal stress $\overline{T}^s_{zz}$ in (4.18) by identifying this stress as the pore fluid pressure. We assume that the pore fluid pressure varies linearly from a maximum of p_{bed} at the base of the flow to zero (i.e., atmospheric reference pressure) at the flow surface, yielding

$$\overline{T}^f_{zz} = \frac{1}{h}\int_0^h T^f_{zz} dz = \frac{1}{2}T^f_{zz|z=0} = \frac{1}{2}p_{bed}, \tag{4.19}$$

The assumption of linear variation of fluid pressure is appropriate because nonlinear variation would imply locally unbalanced forces in the z direction, violating the static force balance in (4.5). Linear variation of fluid pressure also allows us to express the fluid pressure as a fraction λ of the total basal normal stress given by (4.6), yielding

$$p_{bed} = \lambda \rho g_z h, \tag{4.20}$$

This definition, similar to that of Hubbert and Rubey [81], aids brevity and indicates that $\lambda = 1$ represents a case of zero basal effective stress or complete liquefaction. Combining (4.18), (4.19), and (5.5) yields the expression we use for the solid lateral normal stresses:

$$\overline{T}^s_{xx} = \overline{T}^s_{yy} = K_{act/pas}\left[\frac{1}{2}\rho g_z h(1-\lambda)\right]. \tag{4.21}$$

Next, we derive an expression for the transverse solid shear stresses $\overline{T}^s_{yx}$, $\overline{T}^s_{xy}$ by first noting that equality of $\overline{T}^s_{xx}$ and $\overline{T}^s_{yy}$ implies that these depth-averaged normal stresses equal the mean normal stress in the $x-y$ plane. Combine the (4.21) with the form of the Coulomb rule applicable on these planes ([82], [83]) to obtain the shear stress equation:

$$\overline{T}^s_{yx} = \overline{T}^s_{xy} = -sgn\left(\frac{\partial \overline{v}_x}{\partial y}\right)\{K_{act/pas}[1/2\rho g_z h(1-\lambda)]\}\sin\phi_{int}. \tag{4.22}$$

Here we introduce the factor $-sgn(\partial\overline{v}_x/\partial y)$ to designate the sign (+ or -) opposite that of the argument $(\partial\overline{v}_x/\partial y)$, which ensures that shear stresses oppose shear straining in the $x-y$ plane (see Figures 2 and 3).

Basal sliding necessarily accompanies bulk mixture motion unless $\phi_{bed} \geq \phi_{int}$ and frictional locking occurs at the bed. We evaluate solid shear stresses at the bed by combining (5.5) with the Coulomb equation for basal sliding ([82], [83]) and the equation for the z direction normal stress at the bed (4.6), which yields

$$T^s_{zx|z=0} = -sgn(\overline{v}_x)[\rho g_z h(1-\lambda)] \tan\phi_{bed}. \tag{4.23}$$

and an analogous equation $T^s_{zy|z=0}$. In these equations, factors of the form $-sgn(\overline{v}_x)$ stipulate that basal Coulomb stresses oppose basal sliding. These sign factors are exactly analogous to that in (4.21) but involve only the pertinent velocity component (rather than its gradient) because velocity gradients in the z direction do not appear in the depth-averaged model.

Resistance due to basal sliding friction is modified by changes in bed slope that affect the apparent weight of the moving mass. For example, where the bed slope decreases in the downstream direction, part of the depth-averaged momentum flux per unit area $\rho\overline{v}_x^2$ is directed into the bed and resisted by the reaction force provided by the underlying Earth (assumed to be infinitely massive and immobile). This external reaction force redirects the flow's depth-averaged momentum flux to keep it parallel to the bed. However, the action-reaction at the bed also locally increases the normal stress at the bed by an amount $(\rho h\overline{v}_x^2)/r_x$, where r_x is the radius of local bed curvature in the x direction and $\overline{v}_x^2/r_x$ is the associated centripetal acceleration (Figure 3). Thus, for curving beds, (4.23) generalizes to

$$T^s_{zx|z=0} = -sgn(\overline{v}_x)\left[\rho g_z h(1-\lambda)\left(1+\frac{\overline{v}_x^2}{r_x g_z}\right)\right]\tan\phi_{bed}. \tag{4.24}$$

Equation (4.24) reduces to (4.23) in the limit $r_x \to \infty$ applicable to planar beds, and it applies to both bed concavities with positive curvature ($r_x > 0$) and bed convexities with negative curvature ($r_x < 0$). (For combinations of velocity and convex curvature that satisfy $\overline{v}_x^2 = -r_x g_z$, (4.24) implies that bed friction vanishes because the mass becomes effectively weightless as it descends in free fall.) Savage and Hutter [29] and Gray et al. [34] obtained results like (4.24) through formal transformations from linear to curvilinear coordinates. Their scaling analyses demonstrated that other terms generated by such coordinate transformations are generally negligible. Consequently,

(4.24) contains the only term we use for adapting (4.11), (4.12), and (4.13) to curving terrain.

We assume that fluid-phase stresses in (4.12) and (4.13) obey the conventional linear law that governs the behavior of Newtonian fluids (e.g., water). Fluid stresses include both an isotropic pressure component that not does not depend on viscous deformation (as used in (4.19) and a deviatoric, viscous component [e.g., [84], [85]]. More complicated, non-Newtonian fluid stresses could be included instead, but no compelling data indicate that this complication is warranted.

To streamline our presentation, we take advantage of results well-known from derivations of the standard Navier-Stokes equations for flow of incompressible Newtonian fluids [e.g., [84], [85]]. Adapting the Navier-Stokes equations, we find that the fluid stress terms in (4.12) can be expressed by

$$-\int_0^h \left[\frac{\partial T_{xx}^f}{\partial x}+\frac{\partial T_{yx}^f}{\partial y}+\frac{\partial T_{zx}^f}{\partial z}\right]dz = \\ =-\int_0^h \left[\frac{\partial p}{\partial x}-(1-\varphi)\mu\left(\frac{\partial^2 v_x)}{\partial x^2}+\frac{\partial^2 v_x)}{\partial y^2}+\frac{\partial^2 v_x)}{\partial z^2}\right)\right]dz, \tag{4.25}$$

and we find an analogous expression (with x and y interchanged) for (4.13). As discussed during evaluation of solid stresses, we multiply the pore fluid viscosity μ by the fluid volume fraction $(1-\varphi)$ because only this fraction of the mixture produces viscous stresses.

Consistent with (4.19) and (5.5), we assume that the fluid pressure in (4.25) varies linearly from a maximum of pbed at the bed to zero at the free surface. Using this assumption and Leibniz' theorem, we integrate the pressure term in (4.25) directly, yielding

$$-\int_0^h \frac{\partial p}{\partial x}dz=-\frac{\partial}{\partial x}\int_0^h \lambda\rho g_z(h-z)dz=-\lambda\rho g_z h\frac{\partial h}{\partial x}=-h\frac{\partial p_{bed}}{\partial x} \tag{4.26}$$

Equation (4.26) establishes the relationship between longitudinal fluid pressure gradients and their representation in the depth-averaged model.

Similarly, term-by-term integration of the velocity derivatives on the right-hand side of (4.25) establishes the relationship between viscous stress gradients and their depth averages. For example, using Leibniz' theorem and some algebraic manipulation, we find that the term involving $\dfrac{\partial^2 v_x}{\partial x^2}$ in (4.25)

can be written as

$$\int_0^h (1-\varphi)\mu\frac{\partial^2 v_x}{\partial x^2}dz = (1-\varphi)\mu\Bigg[h\frac{\partial^2 \overline{v}_x}{\partial x^2} + 2\frac{\partial}{\partial x}(\overline{v}_x) - v_x(h))\frac{\partial h}{\partial x} + \\ +(\overline{v}_x) - v_x(h))\frac{\partial^2 h}{\partial x^2}\Bigg], \tag{4.27}$$

where $v_x(h)$ specifies the value of v_x at the flow surface. An equation analogous to (4.27) results from integration of the viscous term involving $\dfrac{\partial^2 v_x h}{\partial y^2}$ in (4.25). Employing the same uniform-slab approximation ($\partial h/\partial x = 0$) used to derive the Coulomb stress equations, the right-hand side of (4.27) simplifies and reduces the equation to

$$\int_0^h (1-\varphi)\mu\frac{\partial^2 v_x}{\partial x^2}dz = (1-\varphi)\mu h\frac{\partial^2 \overline{v}_x}{\partial x^2}. \tag{4.28}$$

The same simplification reduces the analogous equation for $\dfrac{\partial^2 v_x}{\partial y^2}$ to The final viscous stress term in (4.25) can be integrated directly, yielding

$$\int_0^h (1-\varphi)\mu\frac{\partial^2 v_x}{\partial x^2}dz = (1-\varphi)\mu\left[\frac{\partial v_x}{\partial z}_{|z=h} - \frac{\partial v_x}{\partial z}_{|z=0}\right] = -3(1-\varphi)\mu\frac{\overline{v}_x}{h}. \tag{4.29}$$

The last form of this equation results from assuming a no-slip basal boundary condition for fluid flow and a parabolic velocity profile in the z direction [84].

Combination of the results from (4.25) through (4.29) indicates that the depth-averaged fluid stress terms in (4.12) can be represented by

$$-\int_0^h \left[\frac{\partial T^f_{xx}}{\partial x} + \frac{\partial T^f_{yx}}{\partial y} + \frac{\partial T^f_{zx}}{\partial z}\right]dz = -h\frac{\partial p_{bed}}{\partial x} + \\ +(1-\varphi)\mu h\frac{\partial^2 \overline{v}_x}{\partial x^2} + (1-\varphi)\mu h\frac{\partial^2 \overline{v}_x}{\partial y^2} - 3(1-\varphi)\mu\frac{\overline{v}_x}{h}, \tag{4.30}$$

An analogous expression (with x and y interchanged) represents the fluid stress terms in (4.13).

The final form of the depth-averaged x direction momentum equation results from combining (4.10) and (4.12) with (4.18), (4.19), (5.5), (4.21), (4.22), (4.24), and (4.30) and using the substitution

$$\frac{\partial(h^2/2)}{\partial x} = h\left(\frac{\partial h}{\partial x}\right)$$

to eliminate explicit dependence on h^2. After this elimination, (5.5) may be used to eliminate λ in favor of p_{bed}, which improves physical clarity. The final result is the x momentum equation

$$\begin{aligned}
\rho\left[\frac{\partial(h\overline{v}_x)}{\partial t} + \frac{\partial(h\overline{v}_x^2)}{\partial x} + \frac{\partial(h\overline{v}_x\overline{v}_y)}{\partial y}\right] = \\
= -sgn(\overline{v}_x)(\rho g_z h - p_{bed})\left(1 + \frac{\partial(\overline{v}_x^2)}{r_x g_z}\right)\tan\phi_{bed} - 3(1-\varphi)\mu\frac{\overline{v}_x}{h} + \\
-hK_{act/pas}\frac{\partial}{\partial x}(\rho g_z h - p_{bed}) - h\frac{\partial p_{bed}}{\partial x} + (1-\varphi)\mu h\frac{\partial^2\overline{v}_x}{\partial x^2} + \\
-sgn\frac{\partial(\overline{v}_x)}{\partial y}hK_{act/pas}\frac{\partial}{\partial y}(\rho g_z h - p_{bed})\sin\phi_{int} + \\
+(1-\varphi)\mu h\frac{\partial^2\overline{v}_x}{\partial y^2} + \rho g_x h. \qquad (4.31)
\end{aligned}$$

The y direction momentum equation is obtained by interchanging x and y in (4).

Terms on the right-hand side of (4.31) are grouped by line according to type of stress: the first line represents basal shear stresses, the second line represents longitudinal normal stresses, the third and fourth lines represent transverse shear stresses, and the fifth line represents the driving stress due to the gravitational body force. Combined with the mass balance equation (4.11), equation (4.31) and its y direction analog provided a set of three governing equations in three unknowns, $\overline{v}_x(x,y,t)$, $\overline{v}_y(x,y,t)$ and $h(x,y,t)$, which we use to compute flows of dense solid-fluid mixtures.

Importantly, (4.31) and its y direction analog are invariant with respect to rotation of the x and y coordinates about the z axis. This frame invariance is crucial if the equations are used to solve problems involving motion over irregular topography, for which flow paths are unknown a priori.

Examination of limiting cases reveals another key feature of our governing equations. For cases in which no pore fluid pressure or viscosity are present, the equations reduce to a set applicable to granular avalanches with purely frictional energy dissipation. At the other extreme, for cases in which the mass is fully liquefied by persistent high pore fluid pressure ($p_{bed} = \rho g_z h$), the equations reduce to a set applicable to Newtonian fluid flow with purely viscous dissipation. For intermediate cases the equations indicate a combination of frictional and viscous energy dissipation that changes in response to spatial and temporal changes in pore pressure. Before we consider pore pressure evolution, however, we describe initial and boundary conditions for the governing mass and momentum conservation equations.

To solve the governing equations, we use initial conditions that specify zero flow velocity and an initial thickness distribution, $h_0(x, y)$,

$$\overline{v}_x(x, y, 0) = \overline{v}_y(x, y, 0) = 0, \qquad and \qquad h(x, y, 0) = h_0(x, y). \tag{4.32}$$

These conditions represent a static mass of specified volume and geometry that is poised to descend a slope. In principle, we could use the static limits of our model equations to identify sectors of a landscape where a sloping mass has reached Coulomb equilibrium and imminent failure, but we have not yet implemented a search algorithm to perform this task.

We use boundary conditions that specify the flow thickness is zero at coordinates that denote the margins (x_M, y_M) of the flowing mass,

$$h(x_M, y_M) = 0. \tag{4.33}$$

These conditions are connected to the velocities at the flow margins by

$$\overline{v}_x(x_M, y, t) = \frac{dx_M}{dt}, \qquad and \qquad \overline{v}_y(x, y_M, t) = \frac{dy_M}{dt}. \tag{4.34}$$

Chapter 5

A model for two flows classes

We consider, here, the motion of a geophysical mass flow along a rough inclines, modeled in order to use the models described in the previous chapters. In particular, we take into account the one-phase model of Savage and Hutter [29] described in chapter 2 and the two-phase model of Iverson [42] described in chapter 3 by recalling on its generalization developed by Iverson and Denlinger [35] described in chapter 4.

These systems will be considered in one space dimension, that is in the x-direction.

In the following, after neglecting for simplicity the subscripts in the x components and the overbars, we put

$$\frac{\partial}{\partial t} = (\ )_t \qquad \frac{\partial}{\partial x} = (\ )_x$$

The Savage and Hutter model system reads

$$\begin{cases} h_t + (hv)_x = 0, \\ \\ v_t + vv_x = sin(\theta) - sgn(v)cos(\theta)\tan(\phi_{bed}) - \beta h_x, \end{cases} \tag{5.1}$$

where v is the velocity component, h is the depth flow, ϕ_{bed} is the angle of friction for bed slip, θ is the angle that the base of the mass flow makes with the horizontal, consequently $sin(\theta)$ and $cos(\theta)$ are the local components of gravity. Moreover we have put

$$\beta = \epsilon K_{act/pas} cos(\theta) \tag{5.2}$$

being $K_{act/pas}$ the earth pressure coefficient, introduced in chapter 2 and determined by the equation:

$$K_{act/pas} = 2\frac{1 \mp [1 - \cos^2(\phi_{int})[1 + \tan^2(\phi_{bed})]]^{1/2}}{\cos^2(\phi_{int})} - 1, \tag{5.3}$$

with ϕ_{int} is the internal friction angle.

Finally, as known ϵ is the small constant given from the ratio $\frac{H}{L}$, where H is the characteristic thickness and L is the characteristic flow length.

Instead, Iverson model system reads

$$\begin{cases} h_t + (hv)_x = 0, \\ \\ v_t + vv_x = \sin(\theta) - sgn(v)\left(1 - \dfrac{p_{bed}}{h}\right)\cos(\theta)\tan(\phi_{bed}) + \\ -(1-\varphi)\mu(n+2)\left(\dfrac{v_x}{h^2}\right) + \\ \\ -\epsilon\cos(\theta)[K_{act/pas}(h - p_{bed}) + p_{bed}]_x. \end{cases} \tag{5.4}$$

where v, h, ϕ_{bed}, ϕ_{int}, θ, ϵ and $K_{act/pas}$ have the same meaning as the (5.1). μ is a nondimensional depth-averaged viscosity, which is generally unknown but can be obtained from estimates of the vertical velocity profile, as explained in Section 3, through the term n. In the following the viscous shear term involving is omitted for three reasons.

1. Scaling analyses [42] indicate that this term is commonly orders of magnitude smaller than other terms in (5.4).

2. Lack of knowledge of the appropriate n value makes evaluation of the viscous shear term uncertain, and it is undesirable to introduce a poorly constrained "fitting" parameter in the model.

3. Omission of the viscous shear term reduces the model to a straightforward force balance in which Coulomb friction provides all resistance to motion, and fluid stresses merely mediate the Coulomb friction. This facilitates comparison of model results with those for the dry Coulomb flows of Savage and Hutter [29].

Finally, we recall the term $p_{bed}(x,t)$ in (5.4) is the basal pore pressure, determines the degree of mixture fluidization and must itself be determined to complete the solutions for v and h. Assumes a linear variation of fluid pressure that also allows us to express the fluid pressure as a fraction λ of the total basal normal stress given by

$$p_{bed} = \lambda \rho g_z h, \tag{5.5}$$

This definition [35], similar to that of Hubbert and Rubey [81], aids brevity and indicates that $\lambda = 1$ represents a case of zero basal effective stress or complete liquefaction. So, Iverson and Denlinger [35] describe a model in which pore pressure simultaneously advects downstream with the flowing debris and diffuses normal to the bed. Only the computed basal pore pressure (indicated by λ) enters depth-averaged calculations of flow dynamics. In their numerical simulations of watersaturated debris flows they employ the advective diffusion model and assume that pore pressures are hydrostatic until the debris begins to move. When movement commences, we specify that pore pressures rise linearly over the course of 1 sec. to a value $\lambda = 0.9$ and then begin to decay diffusively as they advect downstream. This behavior mimics behavior measured in debris flow initiation experiments ([86]-[87]).

Similarly Iverson [42] says the last term of the second equation of system (5.4) shows a great change in debris flow behavior occurs as p_{bed} ranges from 0 to h. If $p_{bed} = h$ and the sediment mass behaves like a liquid, while if $p_{bed} = 0$ the debris behaves like a Coulomb solid.

So, in the system (5.4), in very simplified way, we have put

$$p_{bed} = \alpha h, \tag{5.6}$$

where $0 \leq \alpha \leq 1$ is a constant. So, if α=1 the mass flows behaves like a liquid, instead if α=0 the mass flows behaves like a solid.

For the function $sign(v)$, common to both systems (5.1) and (5.4), Savage and Hutter [29] in order to find some similarity solution assumed that the bed slope and the bed friction angle are such that is always $sign(v) = 1$. In the following, in order to regularize the function $sign(v)$, we have substituted it with the function

$$f(v) = arctan\frac{v}{\epsilon}, \tag{5.7}$$

that for $\epsilon << 1$ is a good approximation of $sign(v)$.

We can say, that the systems (5.1-5.4), with (5.6) and (5.7) belong to the following class

$$\begin{cases} h_t + (hv)_x = 0, \\ \\ v_t + \epsilon C h_x + v v_x = A - f(v) B D, \end{cases} \tag{5.8}$$

where we denote

$$A = \sin\theta, \qquad B = \cos\theta \tan\phi_{bed},$$

$$C = \begin{cases} K_{act/pas} cos(\theta) & \text{in order to get (5.1)} \\ \\ cos(\theta)[K_{act/pas}(1-\alpha)+\alpha] & \text{in order to get (5.4)} \end{cases}$$

and

$$D = \begin{cases} 1 & \text{in order to get (5.1)} \\ \\ (1-\alpha) & \text{in order to get (5.4)} \end{cases}$$

The system (5.8) in matrix form reads:

$$\mathbf{U}_t + \mathbf{A}\mathbf{U}_x = \mathbf{F} \tag{5.9}$$

where

$$\mathbf{U} = \begin{bmatrix} h \\ v \end{bmatrix}$$

$$\mathbf{A} = \begin{bmatrix} v & h \\ \epsilon C & v \end{bmatrix}$$

$$\mathbf{F} = \begin{bmatrix} 0 \\ A - f(v) B D \end{bmatrix}.$$

It is easy to verify that the characteristic equation of the system (5.8) is

$$P(\lambda) := det(\mathbf{A} - \lambda \mathbf{I}) =$$

$$= \lambda^2 - 2\lambda v + (v^2 - \epsilon C h) = 0, \tag{5.10}$$

and admits the real roots

$$\lambda_{1,2} = v \mp \sqrt{\epsilon C h}, \tag{5.11}$$

then, by recalling that $h > 0$, the system is always hyperbolic.

The corresponding right and left eigenvectors are respectively:

$$\mathbf{r}_{1,2}^T = \left[\mp \sqrt{\frac{h}{\epsilon C}}, 1 \right], \tag{5.12}$$

and

$$\mathbf{l}_{1,2} = \left[\mp \sqrt{\frac{\epsilon C}{h}}, 1 \right]. \tag{5.13}$$

5.1 Weak discontinuity propagation in a constant state

Let Σ denotes the weak discontinuity surface of equation

$$\psi(x,t) = 0 \tag{5.14}$$

across which the field

$$\mathbf{U} = \begin{bmatrix} h \\ v \end{bmatrix}$$

is continuous but discontinuities in its first derivatives are permitted. By denoting the jump of the first derivatives across Σ with

$$\delta := \left[\frac{\partial}{\partial\psi}\right] = \left(\frac{\partial}{\partial\psi}\right)_{\psi=0^+} - \left(\frac{\partial}{\partial\psi}\right)_{\psi=0^-} \tag{5.15}$$

At any point of surface ψ is defined the normal speed of the wave propagation $\lambda\mathbf{n}$, where:

$$\begin{cases} \lambda = \dfrac{\psi_t}{|\nabla\psi|} \\ \mathbf{n} = \dfrac{\nabla\psi}{|\nabla\psi|} \end{cases} \tag{5.16}$$

Following Hadamard [88], we write:

$$[\mathbf{U}] = 0, \tag{5.17}$$

that indicates $\mathbf{U}$ is continuous across the surface ψ, while, according with a well established procedure [89], [45] we have

$$[\mathbf{U}_x] = \psi_x\mathbf{\Pi}, \qquad [\mathbf{U}_t] = \psi_t\mathbf{\Pi} \tag{5.18}$$

where the vector $\mathbf{\Pi}$ denotes the amplitude of discontinuities in the first derivatives, which satisfies the characteristic condition

$$(A_0 - \lambda_0\mathbf{I})\mathbf{\Pi} = 0. \tag{5.19}$$

Here the subscript "0" means that a function of the field $\mathbf{U}$ is evaluated at the unperturbed state $\mathbf{U}_0$.

We assume that the *unperturbed state*:

$$\mathbf{U}_0 = \mathbf{U}_* := \begin{bmatrix} h_* \\ v_* \end{bmatrix}$$

where the constant value of h_* and v_* are solutions of the system (5.8), h_* is an arbitrary value of h, while v_* is obtained by solving the following equation:

$$A - arctan\frac{v}{\epsilon}BD = 0. \tag{5.20}$$

Then

$$v_* = \epsilon \tan\left(\frac{A}{BD}\right). \tag{5.21}$$

In the constant state the characteristic equation becomes:

$$P_*(\lambda) = \lambda^2 - 2\lambda v_* + (v_*^2 - \epsilon C h_*) = 0, \tag{5.22}$$

and the solutions are:

$$\lambda_*^{(1,2)} = v_* \mp \sqrt{\epsilon C h_*}.$$

We consider the discontinuity wave propagating with speed $\lambda = \lambda_*^{(2)}$, through a constant state $\mathbf{U}_*$. The corresponding right eigenvectors $\mathbf{r}^{(2)}$ and left eigenvectors $\mathbf{l}^{(2)}$ valued in the unperturbed state $\mathbf{U} = \mathbf{U}_*$ are respectively:

$$\mathbf{r}_*^{(2)^T} = [r_1^{(2)}, r_2^{(2)}]^T_{\mathbf{U}=\mathbf{U}_*}$$

$$\begin{aligned} r_{1_*}^{(2)} &= \sqrt{\frac{h_*}{\epsilon C}}, \\ r_{2_*}^{(2)} &= 1, \end{aligned}$$

and

$$\mathbf{l}_*^{(4)} = [l_1^{(2)}, l_2^{(2)}]_{\mathbf{U}=\mathbf{U}_*},$$

$$\begin{aligned} l_{1_*}^{(2)} &= \sqrt{\frac{\epsilon C}{h_*}}, \\ l_{2_*}^{(2)} &= 1. \end{aligned}$$

By following [89], [45],the equation of evolution of weak discontinuities, in the constant state $\mathbf{U}_*$, is written as:

$$\frac{d\Pi}{d\sigma} + (\nabla\lambda^{(2)} \cdot \mathbf{r}^{(2)})_* \Pi^2 = \nu_* \Pi \tag{5.23}$$

where $d/d\sigma = \partial_t + \lambda^{(2)}\partial_x$ is the time derivative along the characteristic,

$$\nu_* = \left(\frac{\boldsymbol{\nabla}(\mathbf{F} \cdot \mathbf{l}^{(2)}) \cdot \mathbf{r}^{(2)}}{\mathbf{l}^{(2)} \cdot \mathbf{r}^{(2)}} \right)_{\mathbf{U}=\mathbf{U}_*} = -\frac{\epsilon B D}{2(\epsilon^2 + v_*^2)}, \tag{5.24}$$

moreover, of course,

$$(\boldsymbol{\nabla}\lambda^{(2)} \cdot \mathbf{r}^{(2)})_* = \frac{3}{2} \tag{5.25}$$

By integrating, from (5.23), following [45] we get:

$$\boldsymbol{\Pi} = \boldsymbol{\eta}/\phi \tag{5.26}$$

with

$$\phi = 1 + \int_0^\sigma (\nabla\lambda^{(2)} \cdot r^{(2)})_* \eta d\tau, \tag{5.27}$$

and

$$\boldsymbol{\eta} = \eta \mathbf{r}_*^{(2)} \tag{5.28}$$

being η the solution of the Cauchy problem:

$$\begin{cases} d\eta/d\sigma = \nu_* \eta, \\ \eta_0 = \Pi(0), \end{cases} \tag{5.29}$$

that is

$$\eta = \Pi(0) \exp \nu_* \sigma. \tag{5.30}$$

Taking into account (5.30) it follows

$$\phi = 1 + \frac{(\nabla \lambda^{(2)} \cdot r^{(2)})_*}{\nu_*} \Pi(0)(\exp \nu_* \sigma - 1). \tag{5.31}$$

If the wave satisfies the *genuine non linearity condition* $\nabla \lambda^{(2)} \cdot \mathbf{r^{(2)}} \neq 0$ it is possible that exists for suitable amplitudes $\Pi(0)$, a *critical time* σ_{cr} which makes zero the denominator ϕ. So at this instant the discontinuity becomes unbounded. Usually the critical time corresponds to the formation of a strong discontinuity (shock), that is, corresponds to that instant when the field $\mathbf{U}$ becomes discontinuous across the wave front ψ. From (5.31) it is a simple matter to get

$$\sigma_{cr} = \frac{1}{\nu_*} ln \left(1 - \frac{\nu_*}{\Pi(0)(\nabla \lambda^{(2)} \cdot r^{(2)})_*} \right) =$$

$$= -\frac{2(\epsilon^2 + v_*^2)}{\epsilon B D} ln \left(1 + \frac{\epsilon B D}{3\Pi(0)(\epsilon^2 + v_*^2)} \right) \tag{5.32}$$

It is worthwhile stressing that for $\nu_* < 0$ exists a *threshold* value of initial discontinuity:

$$\Pi(0)_{thres} = \frac{\nu_*}{(\nabla \lambda^{(2)} \cdot r^{(2)})_*} \tag{5.33}$$

that separates the values of $\Pi(0)$ that brings to zero the discontinuity and the values of $\Pi(0)$ that brings to infinite the discontinuity in a finite time σ_{cr}.

In details the possibility to get $\sigma_{cr} > 0$, being $\nu_* < 0$ is fulfilled if:

$$0 < 1 - \frac{\nu_*}{\Pi(0)(\nabla \lambda^{(2)} \cdot r^{(2)})_*} < 1 \tag{5.34}$$

this implies the following subcase:

$$\Pi(0) < 0, \quad (\nabla \lambda^{(2)} \cdot r^{(2)})_* > 0 \quad \Pi(0) < \Pi(0)_{thres}. \tag{5.35}$$

5.1.1 Some geophysical mass flows

Here we analyze the discontinuity propagation in a constant state, starting from the experimental data of geophysical mass flows [43] as Debris Flow (Yake Dake), Pyroclastic Flow (Mount St.Helens) and Avalanche (Elm Rock).

These flows are characterized by a common value of the angles of internal friction and bed friction ($\phi_{int} = 50^o$ and $\phi_{bed} = 25^o$), with which the value of the earth pressure coefficient, obtained from equation (6.13), is $K_{pas} = 7.25$. In the following, we show the numerical data and numerical results of these flows for both systems (5.1) and (5.4) (see Table 6.1, 6.2 and 6.3).

Debris Flow	**System (5.1)**	**System (5.4)**
K_{pas}	7.25	7.25
θ	11^o	11^o
α	0.4	0.4
ϵ	0.002	0.002
A	0.19	0.19
B	0.46	0.46
C	7.12	4.66
D	1.0	0.6
h	2	2
$\lambda^{(2)}$	0.17	0.14
$(\nabla\lambda^{(2)} \cdot r^{(2)})_*$	1.5	1.5
ν_*	-114.43	-68.65
η	$e^{(-114.43\sigma)}$	$e^{(-68.65\sigma)}$
ϕ	$-0.00018 + e^{(-114.43\sigma)}$	$-0.0058 + e^{(-68.65\sigma)}$
$\Pi(0)_{thres}$	-76.2	-45
$\Pi(0)$	-76.3	-76.3
σ_{cr}	0.075	0.013

Table 5.1: Numerical data and numerical results of the systems (5.1) and (5.4) for Debris Flows (Yake Dake).

Pyroclastic Flow	**System (5.1)**	**System (5.4)**
K_{pas}	7.25	7.25
θ	2^o	2^o
α	0.6	0.6
ϵ	0.0005	0.0005
A	0.03	0.03
B	0.47	0.47
C	7.24	3.50
D	1.0	0.4
h	1	1
$\lambda^{(2)}$	0.06	0.04
$(\nabla\lambda^{(2)} \cdot r^{(2)})_*$	1.5	1.5
ν_*	-466.02	-186.41
η	$e^{(-466.02\sigma)}$	$e^{(-186.41\sigma)}$
ϕ	$-0.001 + e^{(-466.02\sigma)}$	$-0.005 + e^{(-186.41\sigma)}$
$\Pi(0)_{thres}$	-310	-124
$\Pi(0)$	-311	-311
σ_{cr}	0.014	0.0027

Table 5.2: Numerical data and numerical results of the systems (5.1) and (5.4) for Pyroclastic Flows (Mount St.Helens).

Avalanche	**System (5.1)**	**System (5.4)**
K_{pas}	7.25	7.25
θ	28^o	28^o
α	0.5	0.5
ϵ	0.005	0.005
A	0.47	0.47
B	0.41	0.41
C	6.40	3.64
D	1.0	0.5
h	10	10
$\lambda^{(2)}$	0.57	0.43
$(\nabla\lambda^{(2)} \cdot r^{(2)})_*$	1.5	1.5
ν_*	-41.16	-20.55
η	$e^{(-41.16\sigma)}$	$e^{(-20.55\sigma)}$
ϕ	$-0.020 + e^{(-41.16\sigma)}$	$-0.021 + e^{(-20.55\sigma)}$
$\Pi(0)_{thres}$	-27	-13
$\Pi(0)$	-28	-28
σ_{cr}	0.095	0.19

Table 5.3: Numerical data and numerical results of the systems (5.1) and (5.4) for Avalanches (Elm Rock).

We can observe that for the same experimental data of geophysical mass flows previous considered, in particular for the same value of the initial discontinuity $\Pi(0)$, satisfying (5.35), the system (5.4) provides a critical time σ_{cr} less than the (5.1). This is clearly due to the existence of a second phase in the system (5.4) that brings the discontinuity amplitude to become infinite faster than the system (5.1).

In figures (5.1-5.6) we have shown the evolution of weak discontinuities with respect to σ, concerned with the previous geophysical mass flows. In these figures it is easy to ascertain that the value of the discontinuity amplitude becomes unbounded in a finite critical time σ_{cr}.

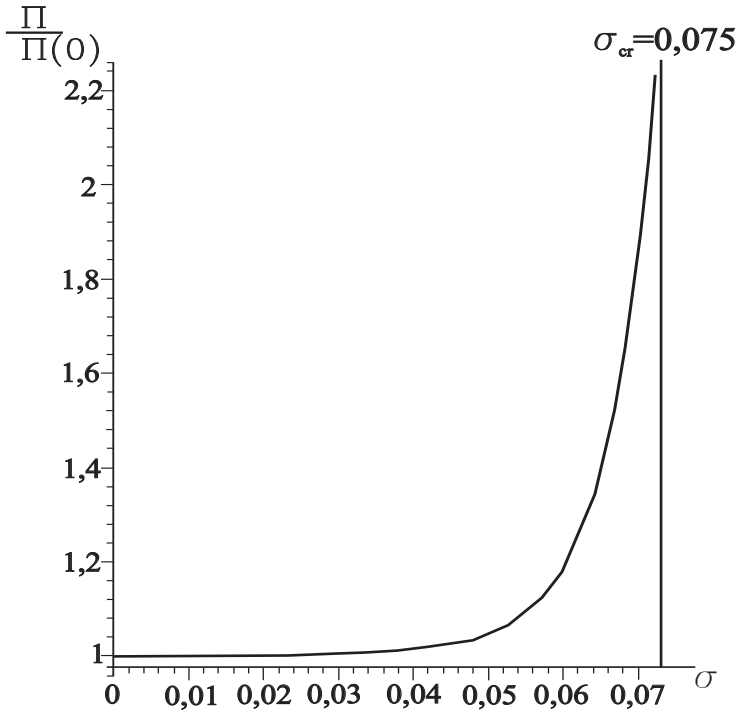

Fig. 5.1: The evolution of discontinuity amplitude of the systems (5.1) in a Debris Flows (Yake Dake).

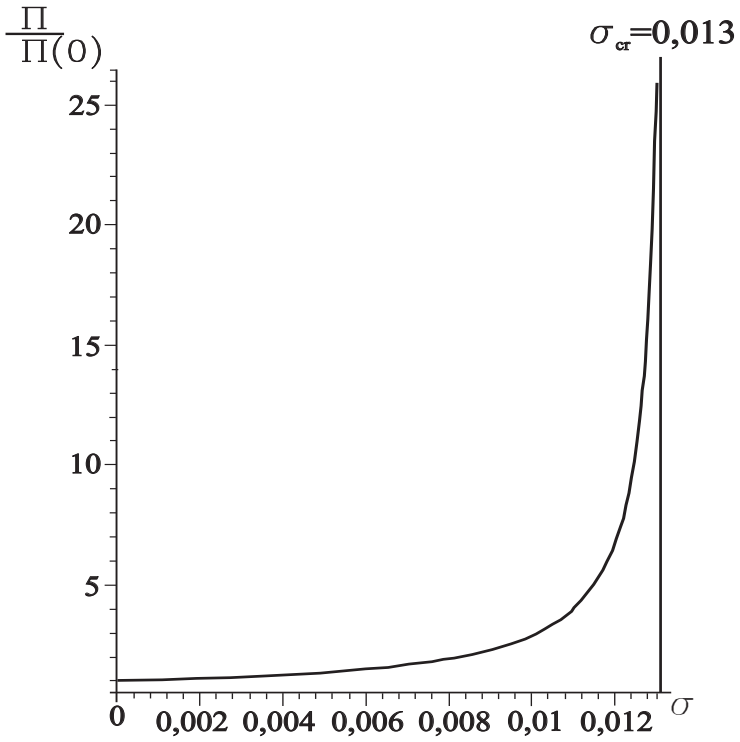

Fig. 5.2: The evolution of discontinuity amplitude of the systems (5.4) in a Debris Flows (Yake Dake).

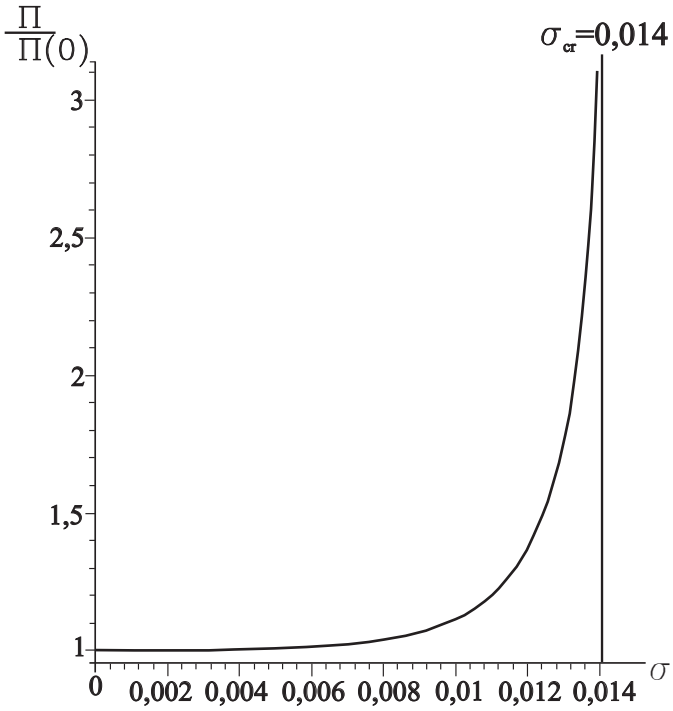

Fig. 5.3: The evolution of discontinuity amplitude of the systems (5.1) in a Pyroclastic Flow (Mount St.Helens).

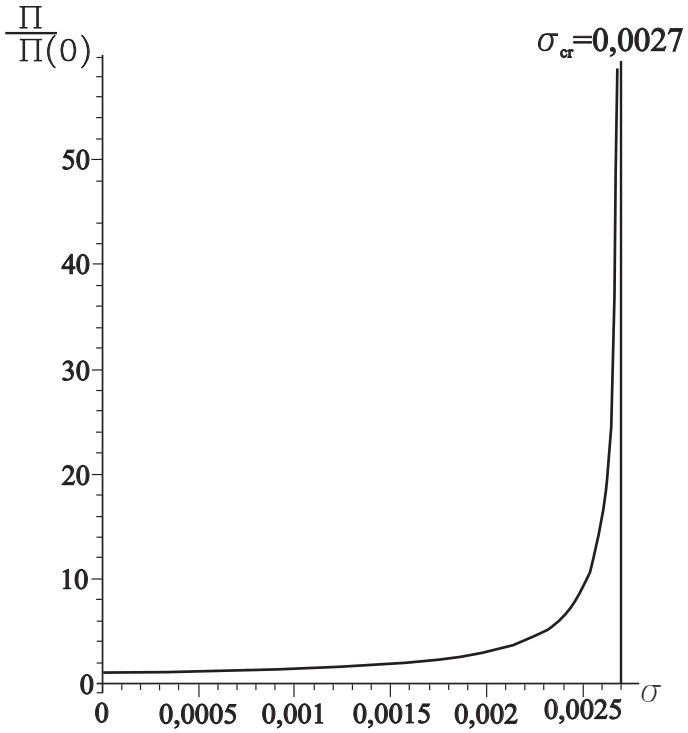

Fig. 5.4: The evolution of discontinuity amplitude of the systems (5.4) in a Pyroclastic Flow (Mount St.Helens).

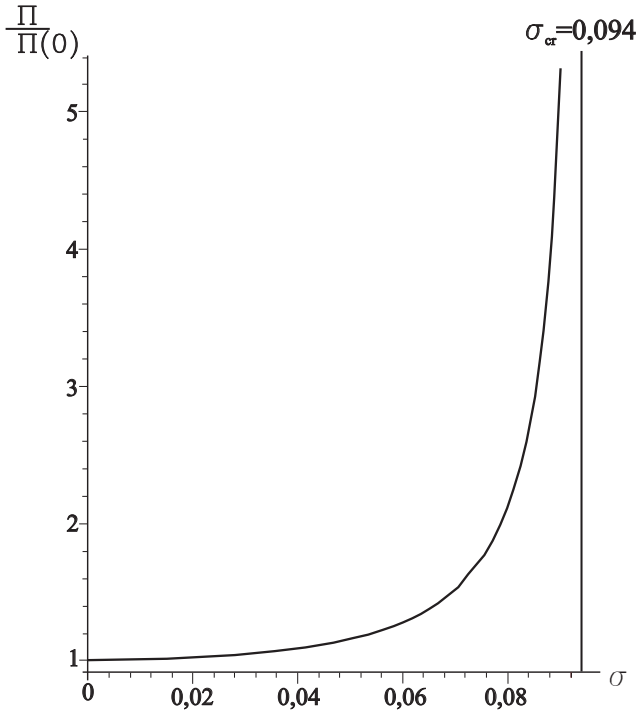

Fig. 5.5: The evolution of discontinuity amplitude of the systems (5.1) in Avalanche (Elm Rock).

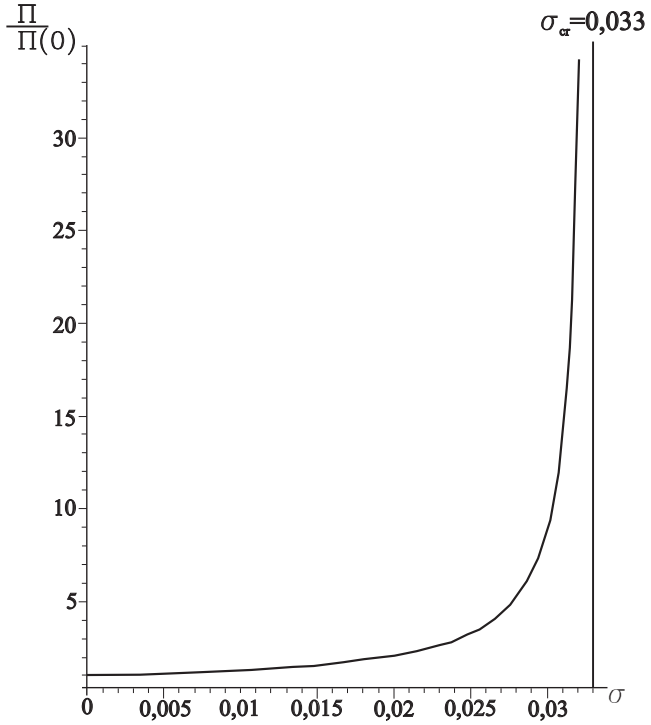

Fig. 5.6: The evolution of discontinuity amplitude of the systems (5.4) in Avalanche (Elm Rock).

In figures 5.7, 5.8 and 5.9 we have shown the evolution of weak discontinuities with respect to σ, concerned with the previous geophysical mass flows. In these figures it is easy to ascertain that the value of the discontinuity amplitude becomes unbounded in a finite critical time σ_{cr}.

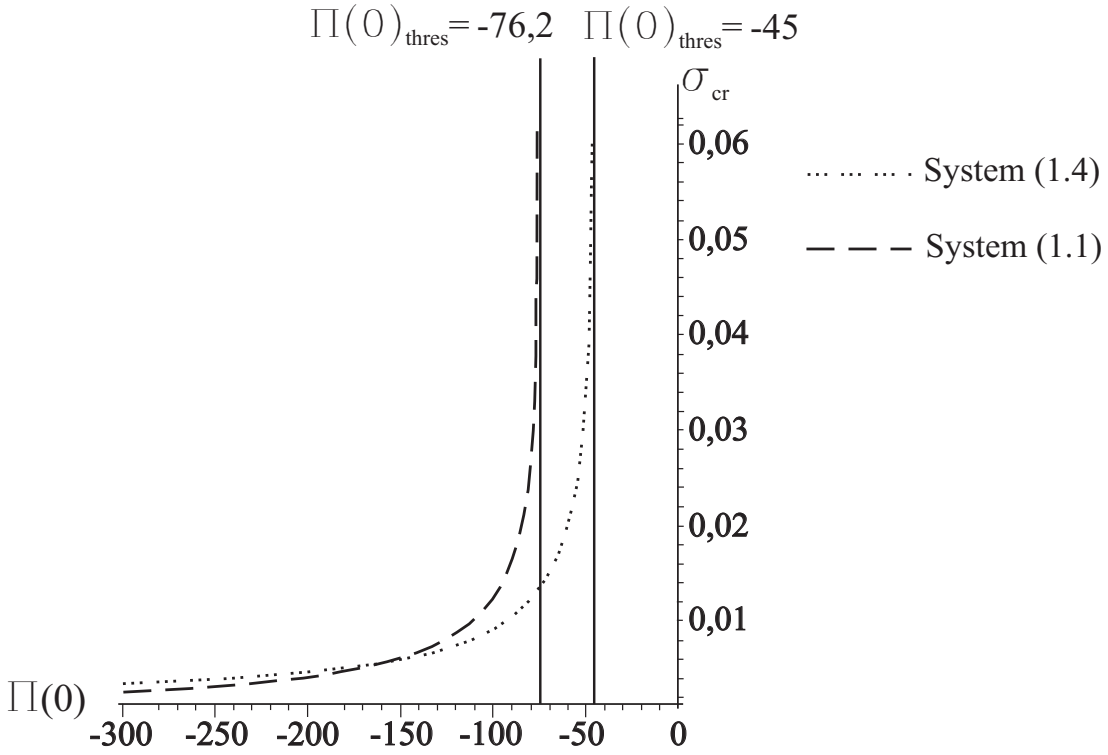

Fig. 5.7: The evolution of discontinuity amplitude of the systems (5.1) and (5.4) in a Debris Flows (Yake Dake).

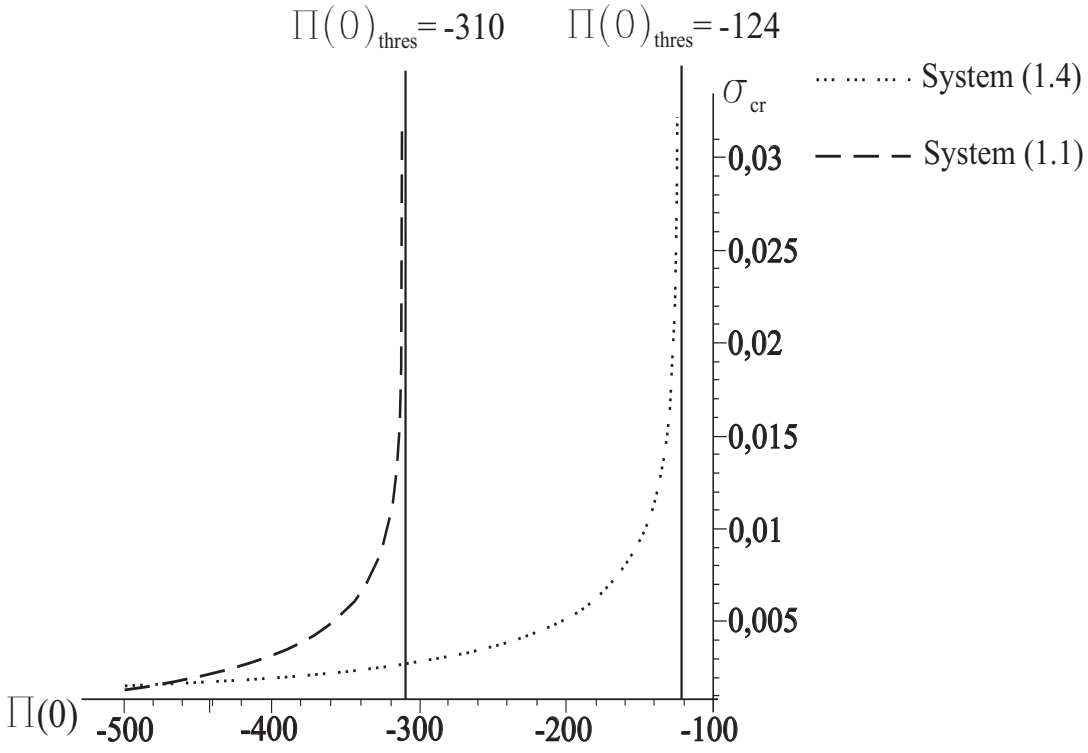

Fig. 5.8: The evolution of discontinuity amplitude of the systems (5.1) and (5.4) in a Pyroclastic Flow (Mount St.Helens).

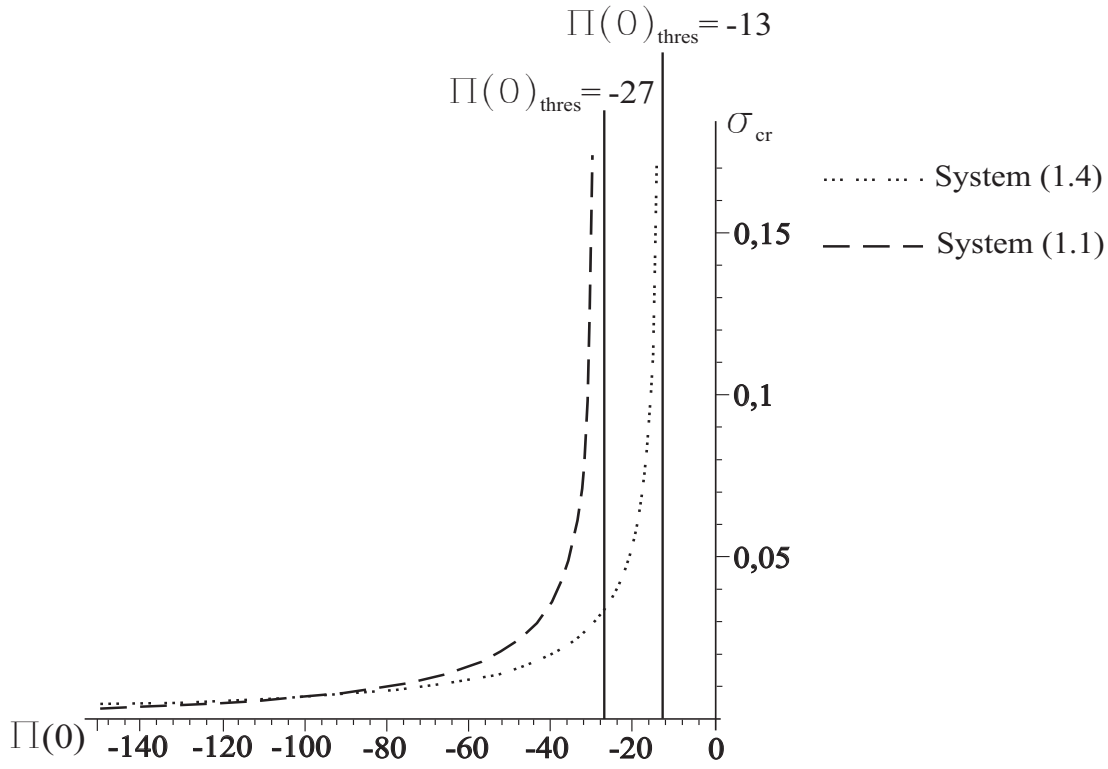

Fig. 5.9: The evolution of discontinuity amplitude of the systems (5.1) and (5.4) in Avalanche (Elm Rock).

Chapter 6

The two-fluid model

Along the guidelines of the paper of Pitman and Le [90], we consider, here, the (1+3)-dimensional model equations, describing a thin layer of a mixture of incompressible solid frictional granular material and interstitial incompressible fluid, each one of constant specific density ρ^s and ρ^f, respectively. In the following, we neglect any erosion of the base and assume that the components of the mixture are moving over a variable terrain. At any point of the terrain, we consider a Cartesian coordinate system xyz, defined so that the plane xy is tangent to the basal surface and z axis is the normal direction. Moreover, it is assumed that the mixture is moving without a preferred direction in the xy-plane.

Mass and momentum balance equations [91] for the two constituent phases are written as

$$\partial_t(\rho^s\varphi) + \nabla\cdot(\rho^s\varphi\mathbf{v}) = 0, \tag{6.1}$$

$$\partial_t(\rho^f(1-\varphi)) + \nabla\cdot(\rho^f(1-\varphi)\mathbf{u}) = 0, \tag{6.2}$$

$$\rho^s\varphi(\partial_t\mathbf{v} + (\mathbf{v}\cdot\nabla)\mathbf{v}) = -\nabla\cdot\mathbf{T}^s - \varphi\nabla\cdot\mathbf{T}^f + \mathbf{f} + \rho^s\varphi\mathbf{g}, \tag{6.3}$$

and

$$\rho^f(1-\varphi)(\partial_t\mathbf{u} + (\mathbf{u}\cdot\nabla)\mathbf{u}) = -(1-\varphi)\nabla\cdot\mathbf{T}^f - \mathbf{f} + \rho^f(1-\varphi)\mathbf{g}, \tag{6.4}$$

where φ is the solid volume fraction, $\mathbf{v}$ and $\mathbf{u}$ are the solid and fluid velocities, $\mathbf{T}^s$ and $\mathbf{T}^f$ the solid and fluid stress tensors, and $\mathbf{g}$ the gravity acceleration vector. $\mathbf{f}$ represents all non-buoyant interaction forces of the fluid on the particle. These forces are characterized using a simple drag interaction:

$$\mathbf{f} = (1-\varphi)\beta(\mathbf{u}-\mathbf{v}), \tag{6.5}$$

β being a phenomenological function [92] given by

$$\beta = \frac{(\rho^s - \rho^f)\varphi g}{v_T(1-\varphi)^m}, \tag{6.6}$$

where v_T is a characteristic velocity, g is the magnitude of the gravitational force and m is related to the Reynold number of the flow.

In agreement with Savage and Hutter [29] developments, the system of equations (1-4) is put in a non dimensional form by using the following scaling transformation:

$$\begin{cases} (x,y,z,t) = L(\tilde{x},\tilde{y},\frac{H}{L}\tilde{z},\frac{1}{(gL)^{\frac{1}{2}}}\tilde{t}), \\ (\mathbf{v},\mathbf{u}) = (gL)^{\frac{1}{2}}(\tilde{\mathbf{v}},\tilde{\mathbf{u}}), \\ \mathbf{T}^s = \rho^s g H \tilde{\mathbf{T}}^s, \\ \mathbf{T}^f = \rho^f g H \tilde{\mathbf{T}}^f, \end{cases} \tag{6.7}$$

where H is the characteristic thickness in the z-direction and L is the characteristic flow length in the x and y direction.

In the following we consider the component of the scaled solid and fluid momentum balances along x, y and z axes. From eqn. (6.3) with scaling transformation (6.7), by dropping tilde and dividing each term by $\rho^s g$, after putting $\epsilon = \dfrac{H}{L} << 1$, we get the following three scalar equations:

$$\begin{cases} \varphi(v_{x,t} + (\mathbf{v}\cdot\nabla)v_x) = -(\epsilon T^s_{xx,x} + \epsilon T^s_{xy,y} + T^s_{xz,z}) + \\ \qquad\qquad -\frac{\rho^f}{\rho^s}(\nabla\cdot\mathbf{T}^f)_x + \frac{f_x}{\rho^s g} + \varphi g_x, \\ \varphi(v_{y,t} + (\mathbf{v}\cdot\nabla)v_y) = -(\epsilon T^s_{xy,x} + \epsilon T^s_{yy,y} + T^s_{yz,z}) + \\ \qquad\qquad -\frac{\rho^f}{\rho^s}(\nabla\cdot\mathbf{T}^f)_y + \frac{f_y}{\rho^s g} + \varphi g_y, \\ \epsilon\varphi(v_{z,t} + (\mathbf{v}\cdot\nabla)v_z) = -(\epsilon T^s_{xz,x} + \epsilon T^s_{yz,y} + T^s_{zz,z}) \\ \qquad\qquad -\frac{\rho^f}{\rho^s}(\nabla\cdot\mathbf{T}^f)_z + \epsilon\frac{f_z}{\rho^s g} + \varphi g_z, \end{cases} \tag{6.8}$$

In a similar way from eqn. (6.4) dividing each term by $\rho^f(1-\varphi)g$, we obtain:

$$\begin{cases} \varphi(u_{x,t} + (\mathbf{u}\cdot\nabla)u_x) = -(\epsilon T^f_{xx,x} + \epsilon T^f_{xy,y} + T^f_{xz,z}) - \frac{f_x}{\rho^f(1-\varphi)g} + g_x, \\ \varphi(u_{y,t} + (\mathbf{u}\cdot\nabla)u_y) = -(\epsilon T^f_{xy,x} + \epsilon T^f_{yy,y} + T^f_{yz,z}) - \frac{f_y}{\rho^f(1-\varphi)g} + g_y, \\ \epsilon\varphi(u_{z,t} + (\mathbf{u}\cdot\nabla)u_z) = -(\epsilon T^f_{xz,x} + \epsilon T^f_{yz,y} + T^f_{zz,z}) - \epsilon\frac{f_z}{\rho^f(1-\varphi)g} + g_z. \end{cases} \tag{6.9}$$

For a more direct comparison of theory with the experiments, we exclude the viscosity, so the only fluid stress considered is a pressure. Moreover, a Coulomb friction law, expressing collinearity between shear stresses and normal stresses is assumed:

$$T^s_{*z} = -sgn(v_*)\nu^b T^s_{zz}, \tag{6.10}$$

where $\nu^b = \tan\phi_{bed}$ is the friction coefficient and ϕ_{bed} is the angle of friction for bed slip, while $*$ can be either x and y and $sgn(v^*)$ determine the force opposing to the motion in $*$-direction. It is worth stressing that in recent works, it has been shown that the Coulomb friction coefficient of the particle phase at the bed can be considered, at least for particular values of the concentration of particles, to depend on a certain inertial parameter, see e.g ([93]-[95]) and references therein.

In order to determine the xy shear stress [35] we use the following Coulomb relation

$$T^s_{xy} = -sgn(v_{x,y})\sin(\phi_{int})K_{act/pas}T^s_{zz} \equiv \alpha_{xy}T^s_{zz}, \tag{6.11}$$

where $\phi = \phi_{int}$ denotes the internal friction angle.

Finally, an earth pressure relation is employed for the solid phase [29, 35, 43, 34, 82]; this assumes that the basal shear stress is proportional to the normal stress,

$$T^s_{**} = K_{act/pas}T^s_{zz} \equiv \alpha_{**}T^s_{zz}, \tag{6.12}$$

where $K_{act/pas}$ is the earth pressure coefficient, determined by the equation:

$$K_{act/pas} = 2\frac{1 \mp [1 - \cos^2(\phi_{int})[1 + \tan^2(\phi_{bed})]]^{1/2}}{\cos^2(\phi_{int})} - 1, \tag{6.13}$$

the sign $\mp$ depends on whether the sediment mass is locally extending ("active" coefficient $\partial v/\partial_x > 0$, with - sign) or compressing ("passive" coefficient $\partial v/\partial_x < 0$, with + sign) as it deforms and moves downslope.

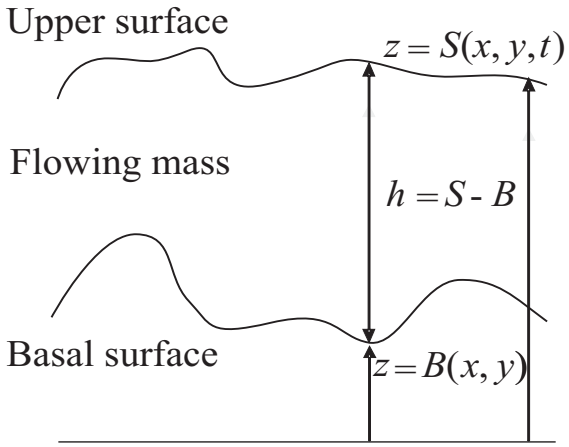

Fig. 6.1: Model Topography

In agreement with Savage and Hutter [29], the earth pressure coefficient can be obtained with reference to the Mohr stress circle and Coulomb failure (for its derivation see also Appendix C in [42]). In the special case where $\phi_{bed} = 0$, equation (6.13) reduces to the classical Rankine [79, 80] definitions commonly used in soil mechanics. After some algebraic manipulations, it is possible, from the mass balance equations, to write:

$$\nabla \cdot (\varphi \mathbf{v} + (1 - \varphi)\mathbf{u}) = 0)$$

that implies that the mixture is isochoric. This allows to depth average for the mixture between the basal surface $z = B(x, y)$ and the upper free surface $z = S(x, y, t)$ (figure 1) and write the mass balance equations and the momentum balance equations in a depth averaged form. An averaged quantity $\bar{A}$ is defined as:

$$\bar{A} = \frac{1}{S - B} \int_B^h A dz,$$

where $h = S - B$.

So the mass balance equations is written:

$$\int_B^h \nabla \cdot (\varphi \mathbf{v} + (1 - \varphi)\mathbf{u}) dz = 0,$$

that at the upper free surface $z = S(x, y)$, becomes:

$$\begin{aligned} \varphi h + (1 - \varphi)h]_{,t} + [\varphi v_x + (1 - \varphi)u_x]h_{,x} + [\varphi v_y + (1 - \varphi)u_y]h_{,y} + \\ -[\varphi v_z + (1 - \varphi)u_z] = 0, \end{aligned} \tag{6.14}$$

and likewise at the basal surface $z = B(x, y, t)$ is:

$$[\varphi v_x + (1-\varphi)u_x]B_{,x} + [\varphi v_y + (1-\varphi)u_y]B_{,y} + \\ +[\varphi v_z + (1-\varphi)u_z] = 0. \tag{6.15}$$

In this way it is possible to derive from mass balance equations the follow equation for the total mass of the solid and fluid

$$\hat{h}_{,t} + \left[\hat{h}(\bar{\varphi}\bar{v_x} + (1-\bar{\varphi})\bar{u_x})\right]_{,x} + \left[\hat{h}(\bar{\varphi}\bar{v_y} + (1-\bar{\varphi})\bar{u_y})\right]_{,y} = 0 \tag{6.16}$$

As it is necessary to follow the evolution of the depth-averaged volume fraction, but there is no obvious candidate equation to which we could appeal, we turn to the mass balance law for the solid phase and depth average, beginning with the follow integration:

$$\int_B^h \varphi_{,t} + \nabla \cdot (\varphi \mathbf{v}) dz = 0,$$

which becomes

$$\left[\int_B^h \varphi dz\right]_{,t} + \left[\int_B^h \varphi v_x dz\right]_{,x} + \left[\int_B^h \varphi v_y dz\right]_{,y} + \varphi v_{z|h} - \varphi v_{x|h} h_{,x} +$$

$$-\varphi v_{y|h} h_{,y} - \varphi_{|h} h_{,t} - \varphi v_{z|B} + \varphi v_{x|B} B_{,x} + \varphi v_{y|B} B_{,y} = 0,$$

In order for the boundary terms to vanish here, the solid and fluid phases must separately satisfy material-free surface and basal surface conditions, just as the mixture does ((6.15) and (6.16)). If no erosion or infiltration occurs, it is reasonable to assume the motion of each species is tangent to the basal surface.

Imposing the material surface condition on the upper free surface is less justified. If the fluid and solid velocities do not differ by much, consideration of flows for which the x or y velocity is zero suggest special conditions under which each phase does in fact satisfy a material-free surface condition. We make the assumption, recognizing it is subject to error: at $z = h$,

$$\varphi h, t + (\varphi v_x) h, x + (\varphi v_y) h, y - \varphi v_z 0,$$

and

$$[(1-\varphi)h, t + [(1-\varphi)u_x]h_{,x} + [(1-\varphi)u_y]h_{,y} - [(1-\varphi)u_z] = 0.$$

With this assumption the equation for solid mass balance equation is:

$$(\hat{h}\bar{\varphi})_{,t} + (\hat{h}\bar{\varphi}\bar{v_x})_{,x} + (\hat{h}\bar{\varphi}\bar{v_y})_{,y} = 0 \tag{6.17}$$

where $\bar{u_x}$, $\bar{u_y}$, $\bar{v_x}$, $\bar{v_y}$, $\bar{\varphi}$, are the depth averaged velocities and the depth averaged volume fraction respectively , while $\hat{h} = h - z$.

To be sure, the imposition of individual phase mass balance requires experimental validation. The justification offered here breaks down when the difference $\mathbf{v} - \mathbf{u}$ is not small, such as at the time of final deposition, where interesting phase separation occurs.

Now going to consider the momentum balance equations, in order to write them in a depth averaged form, we observe that by putting $\epsilon = 0$ in the fluid z-momentum equation, in the spirit of the shallow water approximation, we get that the fluid is hydrostatic, and :

$$T^f_{zz,z} = g_z, \tag{6.18}$$

while from the solid z-momentum equation, by putting $\epsilon = 0$, it follows:

$$T^s_{zz,z} + \frac{\rho^f}{\rho^s}\varphi T^f_{zz,z} = \varphi g_z. \tag{6.19}$$

so, by using (6.18), it is possible to write the following relation:

$$T^s_{zz,z} = \left(1 - \frac{\rho^f}{\rho^s}\right)\varphi g_z = \left(1 - \frac{\rho^f}{\rho^s}\right)\varphi T^f_{zz,z}. \tag{6.20}$$

which affirm that the normal solid stress in the z-direction at any height is equal to the reduced weight of the solid material overburden.

Then by integrating(6.18) and imposing the boundary conditions we find:

$$T^f_{zz} = -g_z(h - z). \tag{6.21}$$

that after depth averaging reads:

$$\bar{T}^f_{zz} = -\frac{1}{2}g_z\hat{h}. \tag{6.22}$$

In a similar way from:

$$T^s_{zz,z} = \left(1 - \frac{\rho^f}{\rho^s}\right)\varphi T^f_{zz,z}, \tag{6.23}$$

we get

$$\bar{T}^s_{zz} = \left(1 - \frac{\rho^f}{\rho^s}\right)\varphi(-g_z)\frac{\hat{h}}{2}. \tag{6.24}$$

Now remains to describe the process which bring the x and y-components of momentum balance equation in depth averaged form. In several steps of the derivation that follows, we will use the approximation $\bar{\varphi f} \approx \bar{\varphi}\bar{f}$, and we do not indicate every place at which this is performed. For more details the interested reader can see to appendix B of [90].

Consider the x momentum equation for the motion of the solid phase. The left-hand side of this can be written:

$$LHS = (\varphi v_x)_{,t} + (\varphi v_x v_x)_{,x} + (\varphi v_x v_y)_{,y} + (\varphi v_x v_z)_{,z}$$

Depth averaging and using boundary conditions yields

$$\int_B^h LHS dz = \left(\int_B^h \varphi v_x dz \right)_{,t} + \left(\int_B^h \varphi v_x^2 dz \right)_{,x} + \left(\int_B^h \varphi v_x v_y dz \right)_{,y}.$$

Instead, the right-hand side of x momentum equation can be written:

$$RHS = -(\epsilon T^s_{xx,x} + \epsilon T^s_{xy,y} + T^s_{xz,z}) - \frac{\rho^f}{\rho^s}(\nabla \cdot \mathbf{T}^f)_x +$$

$$+ \left(1 - \frac{\rho^f}{\rho^s}\right) \frac{\varphi(1-\varphi)}{v_T(1-\varphi)^m}(u_x - v_x) + \varphi g_x$$

and depth averaging yields:

$$\int_B^h RHS dz = \underbrace{-\int_B^h (\epsilon T^s_{xx,x} + \epsilon T^s_{xy,y} + T^s_{xz,z}) dz}_{A} + \tag{6.25}$$

$$\underbrace{-\int_B^h \frac{\rho^f}{\rho^s}(\nabla \cdot \mathbf{T}^f)_x dz}_{B} + \int_B^h \left(1 - \frac{\rho^f}{\rho^s}\right) \frac{\varphi(1-\varphi)}{v_T(1-\varphi)^m}(u_x - v_x) dz$$

$$+ \int_B^h \varphi g_x dz$$

Observe that:

$$\int_B^h T^f_{xx,x} dz = \left[\int_B^h T^f_{xx} dz \right]_x - T^f_{xx|z=h} h_{,x} + T^f_{xx|z=B} B_{,x}.$$

From the assumptions (6.10-6.12), the term B of the (6.26) becomes:

$$B = -\epsilon\frac{\rho^f}{\rho^s}\int_B^h \varphi T^f_{xx,x}dz = -\epsilon\frac{\rho^f}{\rho^s}\left(\int_B^h \varphi dz \int_B^h T^f_{xx,x}dz\right) =$$
$$= -\epsilon\frac{\rho^f}{\rho^s}\left[\frac{g^z\widehat{h}^2}{2} + g_z\widehat{h}B_{,x}\right].$$

Finally, using the following fluid and solid stress relation:

$$\bar{T}^s_{zz} = \left(1 - \frac{\rho^f}{\rho^s}\right)\bar{\varphi}\bar{T}^f_{zz}, \tag{6.26}$$

term A is approximated as:

$$A = -\epsilon\int_B^h \alpha_{xx}T^s_{zz,x}dz - \epsilon\int_B^h \alpha_{xy}T^s_{zz,y}dz - \epsilon\int_B^h \alpha_{xz}T^s_{zz,z}dz =$$
$$= -\epsilon\left[\int_B^h \alpha_{xx}T^s_{zz}dz - \alpha_{xx}T^s_{zz|z=h}h_x + \alpha_{xx}T^s_{zz|z=B}B_x\right]_x =$$
$$= -\epsilon\left[\int_B^h \alpha_{xy}T^s_{zz}dz - \alpha_{xy}T^s_{zz|z=h}h_y + \alpha_{xy}T^s_{zz|z=B}B_x\right]_y =$$
$$= -\alpha_{xz}T^s_{zz|z=h} - T^s_{zz|z=B}.$$

Because the upper free surface is stress free, all terms $T^s_{zz|z=h}$ vanish, so the previous expression A becomes:

$$A = -\epsilon\left(1 - \frac{\rho^f}{\rho^s}\right)\left[\widehat{h}\alpha_{xx}\bar{\varphi}\bar{T}^f_{zz}\right]_{,x} - \epsilon\left(1 - \frac{\rho^f}{\rho^s}\right)\left[\widehat{h}\alpha_{xy}\bar{\varphi}\bar{T}^f_{zz}\right]_{,y} +$$
$$+\left(1 - \frac{\rho^f}{\rho^s}\right)(-\epsilon\alpha_{xx}B_{,x} - \epsilon\alpha_{xy}B_{,y} + \alpha_{xz})g_z\widehat{h}\bar{\varphi}.$$

Combining all terms yields the following solids x-momentum equation:

$$
\begin{aligned}
&(\widehat{h}\bar{\varphi}\overline{v_x})_{,t} + (\widehat{h}\bar{\varphi}\overline{v_x v_x})_{,x} + (\widehat{h}\bar{\varphi}\overline{v_x v_y})_{,y} = \\
&\quad = -\frac{\epsilon}{2}\left(1-\frac{\rho^f}{\rho^s}\right)\left(\alpha_{xx}\widehat{h}^2\bar{\varphi}g_z\right)_{,x} - \frac{\epsilon}{2}\left(1-\frac{\rho^f}{\rho^s}\right)\left(\alpha_{xy}\widehat{h}^2\bar{\varphi}g_z\right)_{,y} + \\
&+\left(1-\frac{\rho^f}{\rho^s}\right)(-\epsilon\alpha_{xx}B_{,x} - \epsilon\alpha_{xy}B_{,y} + \alpha_{xz})\widehat{h}\bar{\varphi}g_z - \frac{\epsilon}{2}\frac{\rho^f}{\rho^s}\bar{\varphi}(\widehat{h}^2 g_z)_{,x} + \\
&\quad -\epsilon\frac{\rho^f}{\rho^s}\widehat{h}\bar{\varphi}g_z B_{,x} + \left(1-\frac{\rho^f}{\rho^s}\right)\frac{\widehat{h}\bar{\varphi}(1-\bar{\varphi})^{1-m}}{v_T}(\overline{u_x}-\overline{v_x}) + \widehat{h}\bar{\varphi}g_x.
\end{aligned}
$$

The y-solid momentum equation can be derived in a similar fashion and yields:

$$
\begin{aligned}
&(\widehat{h}\bar{\varphi}\overline{v_y})_{,t} + (\widehat{h}\bar{\varphi}\overline{v_x v_y})_{,x} + (\widehat{h}\bar{\varphi}\overline{v_y v_y})_{,y} = \\
&\quad = -\frac{\epsilon}{2}\left(1-\frac{\rho^f}{\rho^s}\right)\left(\alpha_{xy}\widehat{h}^2\bar{\varphi}g_z\right)_{,x} - \frac{\epsilon}{2}\left(1-\frac{\rho^f}{\rho^s}\right)\left(\alpha_{yy}\widehat{h}^2\bar{\varphi}g_z\right)_{,y} + \\
&+\left(1-\frac{\rho^f}{\rho^s}\right)(-\epsilon\alpha_{xy}B_{,x} - \epsilon\alpha_{yy}B_{,y} + \alpha_{yz})\widehat{h}\bar{\varphi}g_z - \frac{\epsilon}{2}\frac{\rho^f}{\rho^s}\bar{\varphi}(\widehat{h}^2 g_z)_{,y} + \\
&\quad -\epsilon\frac{\rho^f}{\rho^s}\widehat{h}\bar{\varphi}g_z B_{,y} + \left(1-\frac{\rho^f}{\rho^s}\right)\frac{\widehat{h}\bar{\varphi}(1-\bar{\varphi})^{1-m}}{v_T}(\overline{u_y}-\overline{v_y}) + \widehat{h}\bar{\varphi}g_y.
\end{aligned}
$$

We now proceed to derive an equation for the fluid motion. Depth averaging for the fluid presents fewer difficulties than in the solid equations. The x-momentum equation takes the form:

$$
\begin{aligned}
&(\widehat{h}\overline{u_x})_{,t} + (\widehat{h}\overline{u_x u_x})_{,x} + (\widehat{h}\overline{u_x u_y})_{,y} = \\
&= -\frac{\epsilon g_z}{2}\widehat{h}_{,x}^2 - \left(\frac{1-\frac{\rho^f}{\rho^s}}{\rho^f/\rho^s}\right)\frac{\widehat{h}\bar{\varphi}}{v_T(1-\bar{\varphi})^m}(\overline{u_x}-\overline{v_x}) + \widehat{h}g_x.
\end{aligned}
$$

The fluid y-momentum equation is similar:

$$
\begin{aligned}
&(\widehat{h}\overline{u_y})_{,t} + (\widehat{h}\overline{u_x u_y})_{,x} + (\widehat{h}\overline{u_y u_y})_{,y} = \\
&= -\frac{\epsilon g_z}{2}\widehat{h}_{,y}^2 - \left(\frac{1-\frac{\rho^f}{\rho^s}}{\rho^f/\rho^s}\right)\frac{\widehat{h}\bar{\varphi}}{v_T(1-\bar{\varphi})^m}(\overline{u_y}-\overline{v_y}) + \widehat{h}g_y.
\end{aligned}
$$

Finally after having depth averaged the momentum equations of the thin layer in the shallow flows approximation it is possible to write by dropping hat for sake of simplicity, the full system of equations of the two fluid model as follows

$$
\begin{cases}
h_{,t} + [h(\varphi v_x + (1-\varphi)u_x)]_{,x} + [h(\varphi v_y + (1-\varphi)u_y)]_{,y} = 0, \\
(h\varphi)_{,t} + (h\varphi v_x)_{,x} + (h\varphi v_y)_{,y} = 0, \\
(h\varphi v_x)_{,t} + (h\varphi v_x^2)_{,x} + (h\varphi v_x v_y)_{,y} = -\frac{1}{2}a(h^2\varphi)_{,x} - \frac{1}{2}a_1(h^2\varphi)_{,y} + \\
-b\varphi h h_{,x} - h\varphi[(a+b)B_{,x} + a_1 B_{,y} - sgn(v)\nu^b(1-\gamma)g] + \\
+(1-\gamma)\frac{h\varphi(1-\varphi)^{1-m}}{v_T}(u_x - v_x) + h\varphi g_x, \\
(h\varphi v_y)_{,t} + (h\varphi v_x v_y)_{,x} + (h\varphi v_y^2)_{,y} = -\frac{1}{2}a_1(h^2\varphi)_{,x} - \frac{1}{2}a_2(h^2\varphi)_{,y} + \\
-b\varphi h h_{,y} - h\varphi[a_1 B_{,x} + (a_2+b)B_{,y} + sgn(v)\nu^b(1-\gamma)g] + \\
+(1-\gamma)\frac{h\varphi(1-\varphi)^{1-m}}{v_T}(u_y - v_y) + h\varphi g_y, \\
[h(1-\varphi)u_x]_{,t} + [h(1-\varphi)u_x u_x]_{,x} + [h(1-\varphi)u_x u_y]_{,y} = \\
-\frac{1}{2}c[h^2(1-\varphi)]_{,x} - \left(\frac{1-\gamma}{\gamma}\right)\frac{h\varphi(1-\varphi)^{1-m}}{v_T}(u_x - v_x) + hg_x, \\
[h(1-\varphi)u_y]_{,t} + [h(1-\varphi)u_x u_y]_{,x} + [h(1-\varphi)u_y u_y]_{,y} = \\
-\frac{1}{2}c[h^2(1-\varphi)]_{,y} - \left(\frac{1-\gamma}{\gamma}\right)\frac{h\varphi(1-\varphi)^{1-m}}{v_T}(u_y - v_y) + hg_y,
\end{cases}
\tag{6.27}
$$

where

$$
\begin{cases}
\gamma = \frac{\rho^f}{\rho^s} < 1, \quad a = \epsilon(1-\gamma)\alpha_{xx}g, \quad a_1 = \epsilon(1-\gamma)\alpha_{xy}g, \\
a_2 = \epsilon(1-\gamma)\alpha_{yy}g, \quad b = \epsilon\gamma\, g, \quad c = \epsilon\, g.
\end{cases}
\tag{6.28}
$$

6.1 The one dimensional case

For our purposes here, we consider the special case of a flow in one space dimension. That is, consider the model equation (3.29) confined so that all motion is in the x-direction only, and set all y-derivatives, y-stress terms and y-velocities to zero. Finally, we assume the bottom surface $B = B(x, y)$, which describes the bottom topography, to be flat, that is, $B = B_0 \equiv 0$. Then, in the one dimensional case (x-direction e.g.), after neglecting the subscripts in the x components of $\mathbf{u}$ and $\mathbf{v}$, by putting

$$(\,)_{,t} = (\,)_t \quad (\,)_{,x} = (\,)_x$$

and removing the limiting cases $h = 0,\ \varphi = 0,\ \varphi = 1$, we write:

$$\begin{cases} h_t + [\varphi\, v + (1-\varphi)\, u]h_x + h(v-u)\varphi_x + h\varphi\, v_x + h(1-\varphi)u_x = 0, \\ \varphi_t + \frac{1}{h}[\varphi\,(v-u)(1-\varphi)]h_x + [v - \varphi\,(v-u)]\varphi_x + \varphi(1-\varphi)v_x + \\ \quad -\varphi(1-\varphi)u_x = 0, \\ v_t + (a+b)h_x + \frac{ah}{2\varphi}\varphi_x + vv_x = (1-\gamma)\frac{(1-\varphi)^{1-m}}{v_T}(u-v) + \\ \quad -sgn(v)\nu^b(1-\gamma)g, \\ u_t + ch_x - \frac{ch}{2(1-\varphi)}\varphi_x + uu_x = -\left(\frac{1-\gamma}{\gamma}\right)\frac{\varphi(1-\varphi)^{-m}}{v_T}(u-v). \end{cases} \tag{6.29}$$

The system (6.29) in matrix form reads:

$$\mathbf{U}_t + \mathbf{A}\mathbf{U}_x = \mathbf{F} \tag{6.30}$$

where

$$\mathbf{U} = \begin{bmatrix} h \\ \varphi \\ v \\ u \end{bmatrix}$$

$$\mathbf{A} = \begin{bmatrix} \varphi\, v + (1-\varphi)\, u & h\,(v-u) & h\varphi & h\,(1-\varphi) \\ \frac{\varphi\,(1-\varphi)(v-u)}{h} & v - \varphi\ (v-u) & \varphi\,(1-\varphi) & -\varphi\ (1-\varphi) \\ a+b & \frac{ah}{2\varphi} & v & 0 \\ c & -\frac{ch}{2-2\,\varphi} & 0 & u \end{bmatrix}$$

$$\mathbf{F} \;=\; \begin{bmatrix} 0 \\ 0 \\ (1-\gamma)\frac{(1-\varphi)^{1-m}}{v_T}(u-v) - sgn(v)\nu^b(1-\gamma)g \\ -(\frac{1-\gamma}{\gamma})\frac{\varphi(1-\varphi)^{-m}}{v_T}(u-v) \end{bmatrix}.$$

The characteristic equation of the system (6.29) is

$$P(\lambda) \;:=\; det(\mathbf{A} - \lambda\mathbf{I}) =$$

$$= (\lambda - v)^2(\lambda - u)^2 - \tfrac{h}{2}[a(1+\varphi) + 2\varphi\, b](\lambda - u)^2 +$$

$$-\tfrac{ch}{2}(2-\varphi)(\lambda - v)^2 + \tfrac{ch^2}{2}(a + b\varphi) = 0 \tag{6.31}$$

6.1.1 Eigenvalues

The problem of hyperbolicity of the system is related to the reality of the roots of equation (6.31).

In [90], the case of the parameter $\epsilon = 0$, has been considered and it has been observed that in this case, taking (6.28) into account, equation (6.31) reduces to:

$$(\lambda - v)^2(\lambda - u)^2 = 0 \tag{6.32}$$

That is, there are two double real roots. It is easy to verify that for $\epsilon = 0$ the system (6.29) is hyperbolic. Of course for ϵ small the system is still hyperbolic.

In view of further applications we observe that the constant vector

$$\mathbf{U}_* := \begin{bmatrix} h_* \\ \varphi_* \\ 0 \\ 0 \end{bmatrix}, \tag{6.33}$$

with $h_* > 0$ and $0 < \varphi_* < 1$, gives a two parameters family of solutions for the system (6.29). Here, according to [46] we show as the system can be hyperbolic around a constant solution $\mathbf{U}_*$.

After having put $\mathbf{U} = \mathbf{U}_*$, the characteristic equation becomes a quartic equation in λ:

$$P_*(\lambda) := \lambda^4 - \frac{h_*}{2}\left[a(1+\varphi_*) + 2\varphi_* b - c(2-\varphi_*)\right]\lambda^2 + \frac{ch_*^2}{2}(a + b\varphi_*) = 0, \tag{6.34}$$

whose roots are written as

$$\lambda_*^i = \pm\frac{1}{2}\sqrt{\mathcal{A} \pm h_*\sqrt{\Delta_*}} \qquad i = 1, 2, 3, 4 \tag{6.35}$$

where

$$\mathcal{A} = h_*\left[(a - 2c) + \varphi_*(a + 2b + c)\right], \tag{6.36}$$

and

$$\Delta_* = (a-2c)^2 + \varphi_*^2(a+2b+c)^2 + 2\varphi_*(a-2c)(a+2b+c) - 8c(a+b\varphi_*). \tag{6.37}$$

The eigenvalues $\lambda_*^i \;\; i = 1, 2, 3, 4$ will be real if and only if both $\mathcal{A}$ and Δ_* are non negative. In fact, due to Descartes rule, it follows that the values of

$$\lambda^2 = \frac{1}{4}\left(\mathcal{A} \pm h_*\sqrt{\Delta_*}\right) \tag{6.38}$$

are not only real but also non-negative. Then all the eigenvalues λ_*^i are real $(i = 1, 2, 3, 4)$.

From (6.36) and (6.37), taking (6.28) into account, it is a simple matter to ascertain that in order that $\mathcal{A}$ and Δ_* are both non-negative it is necessary and sufficient that both:

$$[\alpha_{xx}(1-\gamma) + 2\gamma + 1]\varphi_* + [\alpha_{xx}(1-\gamma) - 2] \geq 0. \tag{6.39}$$

and

$$[\alpha_{xx}(1-\gamma) + 2\gamma + 1]^2\varphi_*^2 + 2[\alpha_{xx}^2(1-\gamma)^2 - \alpha_{xx}(2\gamma-1)(\gamma-1) + \\ -(8\gamma+2)]\varphi_* + \alpha_{xx}^2(1-\gamma)^2 - 12\alpha_{xx}(1-\gamma) + 4 \geq 0. \tag{6.40}$$

So, for values of α_{xx}, γ and φ_* of relevant physical interest, satisfying the previous conditions, we can say that the system (6.29) is hyperbolic around a solution $\mathbf{U}_*$.

6.1.2 Some geophysical mass flows

Here we discuss some real cases due the observation of geophysical mass flows [43] as Debris Flow (Yake Dake), Pyroclastic Flow (Mount St.Helens) and Avalanche (Elm Rock). In this case we have considered typical values of the physical parameters, appearing in (6.39) and (6.40).

These flows are characterized by a common value of the angles of internal friction and bed friction ($\phi_{int} = 50^o$ and $\phi_{bed} = 25^o$), with which the value of the earth pressure coefficient, obtained from equation (6.13), is $\alpha_{xx} = K_{pas} = 7.25$. Now in the following we show the specializations of the constraints (6.39) and (6.40) for the values of α_{xx} and γ, concerned with the aforesaid flows. And find the range of the values of φ_* which allows real eigenvalues.

1. For Debris Flow (Yake Dake), $\gamma = 0.4$ ($\rho^s = 2600Kg/m^3$, $\rho^f = 1200Kg/m^3$), $\alpha_{xx} = 7.25$, the (6.39) and (6.40) become:

$$6.15\varphi_* + 2.35 \geq 0; \tag{6.41}$$

and the (6.40):

$$37.82\varphi_*^2 + 25.7\varphi_* - 29.2 \geq 0; \tag{6.42}$$

the range of the values of φ_* is:

$$\varphi_* \in [0.61, 1[.$$

2. For Pyroclastic Flow (Mount St.Helens), the parameters are $\gamma = 0,0007$ ($\rho^s = 2600Kg/m^3$ and $\rho^f = 2Kg/m^3$), $\alpha_{xx} = 7.25$ and the (6.39) becomes:

$$8.24\varphi_* + 5.24 \geq 0; \tag{6.43}$$

and the (6.40):

$$68\varphi_*^2 + 86.49\varphi_* - 30.45 \geq 0; \tag{6.44}$$

the range of the values of φ_* is:

$$\varphi_* \in [0.29, 1[.$$

3. For Avalanche (Elm Rock), the parameters are $\gamma = 0,0008$ ($\rho^s = 2400Kg/m^3$ and $\rho^f = 2Kg/m^3$), $\alpha_{xx} = 7.25$ and the (6.39) becomes:

$$8.24\varphi_* + 5.24 \geq 0; \tag{6.45}$$

and the (6.40):

$$67.99\varphi_*^2 + 86.47\varphi_* - 30.45 \geq 0; \tag{6.46}$$

the range of the values of φ_* is:

$$\varphi_* \in [0.29, 1[.$$

In figure 6.2, 6.3 and 6.4 we show the feature of the eigenvalues corresponding to some values of φ_*, referring to previous cases.

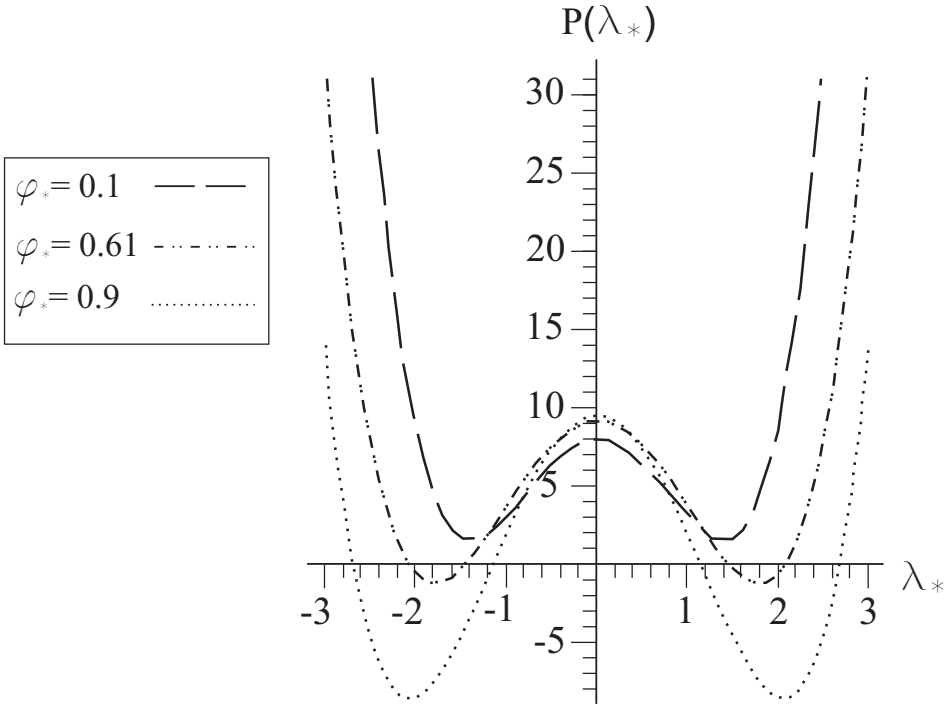

Fig. 6.2: Debris Flows (Yake Dake). Feature for some values of φ_*.

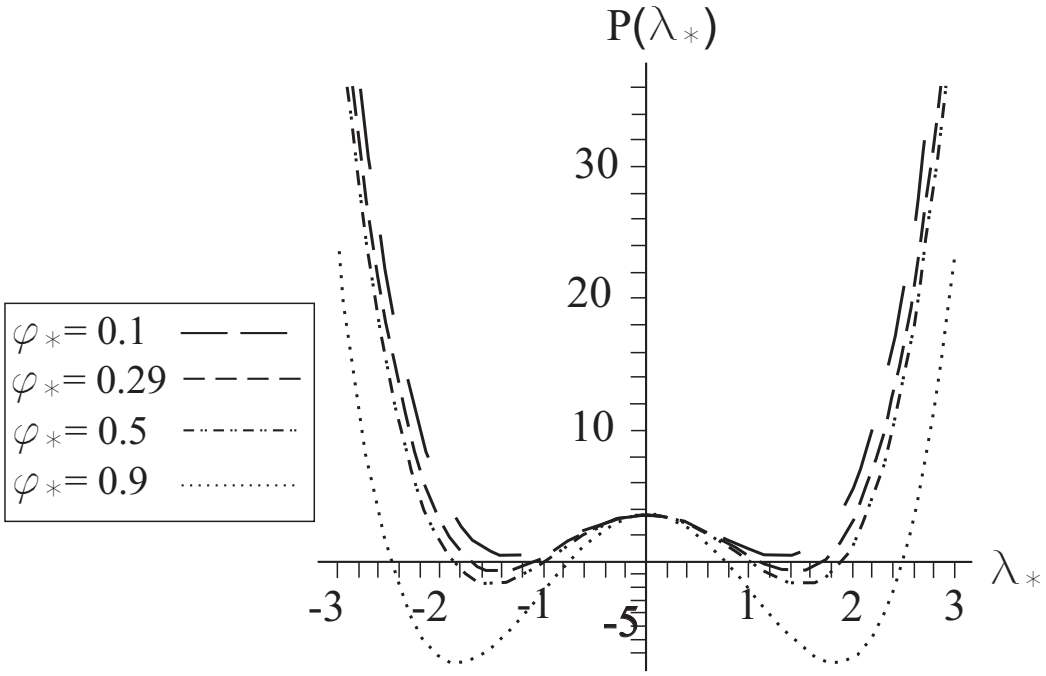

Fig. 6.3: Pyroclastic Flows (Mount St.Helens). Feature of characteristic polynomial $P(\lambda_*)$ for some values of φ_*.

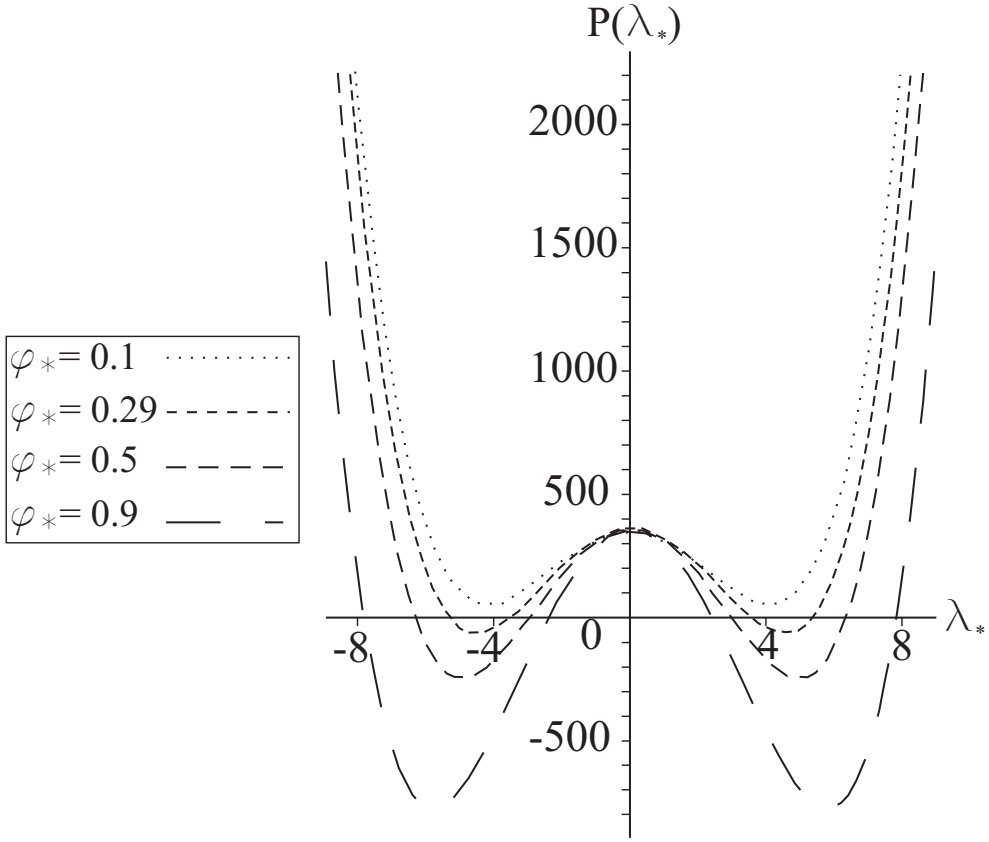

Fig. 6.4: Avalanches (Elm Rock). Feature of characteristic polynomial $P(\lambda_*)$ for some values of φ_*.

So we can conclude that for values of φ_* satisfying (6.39) and (6.40) the system is hyperbolic not only in $\mathbf{U}_*$ but also for continuity reasons in a suitable neighborhood of $\mathbf{U}_*$.

6.1.3 Approximate computations of λ^i

After these results, more generally, we can compute the values of λ_i by using a perturbation expansion with respect to small parameter $\eta = \sqrt{\epsilon}$ starting from the constant state $\mathbf{U}_*$.

So by assuming that $\lambda, h, \varphi, u, v$ are analytic function of small parameter η we are able expanding them in power series as follows:

$$\begin{cases} \lambda^i = \lambda^i_* + \eta\lambda^i_1 + \eta^2\lambda^i_2 ....., \\ h = h_* + \eta h_1 + \eta^2 h_2 ....., \\ \varphi = \varphi_* + \eta\varphi_1 + \eta^2\varphi_2 ....., \\ u = \eta u_1 + \eta^2 u_2 ....., \\ v = \eta v_1 + \eta^2 v_2 ..... \end{cases} \tag{6.47}$$

After having truncated (6.47) at the first power of η we substituted them in the $P(\lambda)$ and obtain, by neglecting all powers of η greater than one, an approximate characteristic polynomial:

$$\begin{gathered} P_1(\lambda^i) := P_0(\lambda^i_*) + \\ +\eta\Big\{2[2\lambda^i_1 - (u_1 + v_1)]{\lambda^i_*}^3 + \tfrac{1}{2}[(\varphi_* h_1 + \varphi_1 h_0)(c - a - 2b) + \\ -h_1(a + 2c)]{\lambda^i_*}^2 + h_*\{(u_1 - \lambda^i_1)[a(1 + \varphi_*) + 2b\varphi_*] + \\ +(v_1 - \lambda^i_1)c(2 - \varphi_*)\}\lambda^i_* + ch_*\Big[\tfrac{b}{2}(h_*\varphi_1 + 2h_1\varphi_*) + ah_1\Big]\Big\} = 0. \end{gathered} \tag{6.48}$$

When

$$P_0(\lambda^i_*) = P(\lambda^i_*) \tag{6.49}$$

Then by requiring:

$$\begin{cases} P_0(\lambda^i_*) = 0 \\ 2[2\lambda^i_1 - (u_1 + v_1)]{\lambda^i_*}^3 + \tfrac{1}{2}[(\varphi_* h_1 + \varphi_1 h_*)(c - a - 2b) + \\ -h_1(a + 2c)]{\lambda^i_*}^2 + h_*\{(u_1 - \lambda^i_1)[a(1 + \varphi_*) + 2b\varphi_*] + \\ +(v_1 - \lambda^i_1)c(2 - \varphi_*)\}\lambda^i_* + ch_*\Big[\tfrac{b}{2}(h_*\varphi_1 + 2h_1\varphi_*) + ah_1\Big] = 0, \end{cases} \tag{6.50}$$

it follows

$$\lambda_*^i = \pm\frac{1}{2}\sqrt{\mathcal{A} \pm h_*\sqrt{\Delta_*}}, \qquad i = 1,2,3,4 \tag{6.51}$$

and

$$\lambda_1^i = \frac{-2(v_1+u_1){\lambda_*^i}^3 + \frac{1}{2}[(\varphi_* h_1 + \varphi_1 h_*)(c-a-2b) - h_1(a+2c)]{\lambda_*^i}^2}{\lambda_*^i[4{\lambda_*^i}^2 - ah_*(1+\varphi_*) - ch_*(2-\varphi_*) - 2h_* b\varphi_*]} +$$
$$+\frac{\{cv_1h_*(2-\varphi_*) + u_1h_*[a(1+\varphi_*)+2b\varphi_*]\}\lambda_0^i}{\lambda_*^i[4{\lambda_*^i}^2 - ah_*(1+\varphi_*) - ch_*(2-\varphi_*) - 2h_*b\varphi_*]} +$$
$$+\frac{ch_*[\frac{b}{2}(h_*\varphi_1 + 2h_1\varphi_*) + ah_1]}{\lambda_*^i[4{\lambda_0^i}^2 - ah_*(1+\varphi_*) - ch_*(2-\varphi_*) - 2h_*b\varphi_*]}. \qquad i = 1,2,3,4.$$

So,

$$\lambda^i \approx \pm\frac{1}{2}\sqrt{\mathcal{A} \pm h_*\sqrt{\Delta_*}} +$$
$$+\eta\left\{\frac{-2(v_1+u_1){\lambda_*^i}^3 + \frac{1}{2}[(\varphi_* h_1 + \varphi_1 h_*)(c-a-2b) - h_1(a+2c)]{\lambda_*^i}^2}{\lambda_*^i[4\lambda_*^2 - ah_*(1+\varphi_*) - ch_*(2-\varphi_*) - 2h_* b\varphi_*]} +\right.$$
$$+\frac{\{cv_1h_*(2-\varphi_*) + u_1h_*[a(1+\varphi_*)+2b\varphi_*]\}\lambda_*^i}{\lambda_*^i[4\lambda_*^2 - ah_*(1+\varphi_*) - ch_*(2-\varphi_*) - 2h_*b\varphi_*]} +$$
$$\left.+\frac{ch_*[\frac{b}{2}(h_*\varphi_1 + 2h_1\varphi_*) + ah_1]}{\lambda_*^i[4\lambda_*^2 - ah_*(1+\varphi_*) - ch_*(2-\varphi_*) - 2h_*b\varphi_*]}\right\}, \qquad i = 1,2,3,4.$$

6.1.4 Eigenvectors

The components of the right eigenvectors $\mathbf{r}^i = [r_1^i, r_2^i, r_3^i, r_4^i]^T$ are:

$$r_1^i = -\frac{(\lambda^i - u)[ah(\varphi - 1) + 2(\lambda^i - v)^2] + (\lambda^i - v)[2\varphi(\lambda^i - u)(v - u) - ch\varphi]}{c[\varphi(u - v)(\lambda^i - v) - 2(\lambda^i - v)^2 + h(a + \varphi b)]},$$

$$r_2^i = \frac{2\varphi(\varphi - 1)\{(\lambda^i - u)[h(a + b) - v^2] + \lambda^{i^2}(v - u) + (\lambda^i - v)(u^2 - ch)\}}{ch[\varphi(u - v)(\lambda^i - v) - 2(\lambda^i - v)^2 + h(a + \varphi b)]},$$

$$r_3^i = \frac{(\lambda^i - u)\{av(1 - \varphi) + 2b[\varphi u + v(1 - \varphi)]\} - 2\lambda^{i^2}(a + b)}{c[\varphi(u - v)(\lambda^i - v) - 2(\lambda^i - v)^2 + h(a + \varphi b)]} +$$

$$-\frac{au^2(1 + \varphi) - ch(a + b\varphi)}{c[\varphi(u - v)(\lambda^i - v) - 2(\lambda^i - v)^2 + h(a + \varphi b)]}$$

$$r_4^i = 1,$$

and the components of the left eigenvectors $\mathbf{l^i} = [l_1^i, l_2^i, l_3^i, l_4^i]$ reads:

$$l_1^i = \frac{c[\varphi(u - v)(\lambda^i - v) - 2(\lambda^i - v)^2 + h(a + \varphi b)]}{(u - \lambda^i)\{2(\lambda^i - v)^2 - h[\varphi(a + 2b) + a]\}},$$

$$l_2^i = \frac{ch\{(\lambda^i - v)[u(\varphi - 1) + v(2 - \varphi) - \lambda^i] + h(a + \varphi b)\}}{(\varphi - 1)(u - \lambda^i)\{2(\lambda^i - v)^2 - h[\varphi(a + 2b) + a]\}},$$

$$l_3^i = \frac{ch\varphi}{2(\lambda^i - v)^2 - h[\varphi(a + 2b) + a]},$$

$$l_4^i = 1.$$

6.2 Weak discontinuity propagation in a constant state

Let Σ denotes the weak discontinuity surface of equation

$$\psi(x,t) = 0 \tag{6.52}$$

across which the field

$$\mathbf{U} = \begin{bmatrix} h \\ \varphi \\ v \\ u \end{bmatrix}$$

is continuous but discontinuities in its first derivatives are permitted. By denoting the jump of the first derivatives across Σ with

$$\delta := \left[\frac{\partial}{\partial\psi}\right] = \left(\frac{\partial}{\partial\psi}\right)_{\psi=0^+} - \left(\frac{\partial}{\partial\psi}\right)_{\psi=0^-} \tag{6.53}$$

we obtain from the system (6.29) the compatibility conditions for weak discontinuities [89] and [45], which allows us to write (see Section 5.1 of this thesis):

$$\delta\mathbf{U}^{(i)} := \mathbf{\Pi} = \Pi\mathbf{r}_0^{(i)} \tag{6.54}$$

where $\mathbf{r}_0^{(i)}$ is the right eigenvector, corresponding to $\lambda^{(i)}$, evaluated for the *unperturbed state* $\mathbf{U}_o$. We consider the discontinuity wave propagating with speed $\lambda = \lambda_*^{(4)}$, through a constant state $\mathbf{U}_*$, characterized by:

$$\mathbf{U}_* := \begin{bmatrix} h_* \\ \varphi_* \\ 0 \\ 0 \end{bmatrix}$$

The characteristic equation, in the unperturbed state $\mathbf{U} = \mathbf{U}_o = \mathbf{U}_*$,

$$det(\mathbf{A} - \lambda \mathbf{I})|_{\mathbf{U}_*=0},$$

becomes

$$P_*(\lambda) = \lambda^4 - \frac{h_*}{2}[a(1+\varphi_*) + 2\varphi_* b)\lambda^2 - \frac{ch_*}{2}(2-\varphi_*)\lambda^2 + \\ + \frac{ch_*^2}{2}(a + b\varphi_*) = 0. \tag{6.55}$$

Assuming that the constitutive parameters and the components of $\mathbf{U}_*$ satisfies (6.39) and (6.40), we can affirm that solutions of (6.2) are real so we write them as

$$\lambda_*^{(1,2)} = -\frac{1}{2}\sqrt{\mathcal{A} \pm h_*\sqrt{\Delta_*}},$$

$$\lambda_*^{(3,4)} = \frac{1}{2}\sqrt{\mathcal{A} \pm h_*\sqrt{\Delta_*}},$$

The corresponding right eigenvectors $\mathbf{r}^{(4)}$ and left eigenvectors $\mathbf{l}^{(4)}$ valued in the unperturbed state $\mathbf{U} = \mathbf{U}_*$ defined by are respectively:

$$\mathbf{r}_*^{(4)^T} = [r_1^{(4)}, r_2^{(4)}, r_3^{(4)}, r_4^{(4)}]^T_{\mathbf{U}=\mathbf{U}_*}$$

$$r_{1_*}^{(4)} = -\frac{\lambda_*^{(4)}[ah_*(\varphi_* - 1) + 2\lambda_*^{(4)^2} - ch_*\varphi_*]}{c[h_*(a + \varphi_* b) - 2\lambda_*^{(4)^2}]},$$

$$r_{2_*}^{(4)} = \frac{2\lambda_*^{(4)}\varphi_*(\varphi_* - 1)(a + b - c)}{c[h_*(a + \varphi_* b) - 2\lambda_*^{(4)^2}]},$$

$$r_{3_*}^{(4)} = \frac{ch_*(a + b\varphi_*) - 2\lambda_*^{(4)^2}(a + b)}{c[h_*(a + \varphi_* b) - 2\lambda_*^{(4)^2}]},$$

$$r_{4_*}^{(4)} = 1,$$

and

$$\mathbf{l}_*^{(4)} = [l_1^{(4)}, l_2^{(4)}, l_3^{(4)}, l_4^{(4)}]_{\mathbf{U}=\mathbf{U}_*},$$

$$l_{1_*}^{(4)} = -\frac{c[h_*(a+\varphi_* b) - 2\lambda_*^{(4)^2}]}{\lambda_*^{(4)}\{2\lambda_*^{(4)^2} - h_*[\varphi_*(a+2b)+a]\}},$$

$$l_{2_*}^{(4)} = \frac{ch_*[\lambda_*^{(4)^2} + h_*(a+b\varphi_*)]}{\lambda_*^{(4)}(\varphi_*-1)\{2\lambda_*^{(4)^2} - h_*[\varphi_*(a+2b)+a]\}},$$

$$l_{3_*}^{(4)} = \frac{ch_*\varphi_*}{2\lambda_*^{(4)^2} - h_*[\varphi_*(a+2b)+a]},$$

$$l_{4_*}^{(4)} = 1.$$

In order to write of weak discontinuity evolution equation [45], we observe that from (6.31) it is possible to derive the following relation:

$$\frac{\partial P}{\partial h} + P'(\lambda)\lambda_h = 0, \tag{6.56}$$

where

$$P'(\lambda) = (\lambda - v)[ch(\varphi - 2) + 2(\lambda - u)(2\lambda - v - u)] + \\ -h(\lambda - u)[a(1+\varphi) + 2\varphi\, b],$$

denote the derivative of $P(\lambda)$ with respect to λ.

From (6.56) which we get

$$\lambda_h = -\frac{1}{P'(\lambda)}\frac{\partial P}{\partial h}. \tag{6.57}$$

After having obtained in similar way $\lambda_\varphi, \lambda_v, \lambda_u$ we are able to write:

$$\nabla\lambda = \begin{bmatrix} \lambda_h \\ \lambda_\varphi \\ \lambda_v \\ \lambda_u \end{bmatrix} =$$

$$= \begin{bmatrix} \frac{\frac{1}{2}\{[a(1+\varphi)+2\varphi\, b](\lambda-u)^2 + c(2-\varphi)(\lambda-v)^2 - 2ch(a+\varphi\, b)\}}{P'(\lambda)} \\ \frac{\frac{h}{2}[(a+2b)(\lambda-u)^2 - c(\lambda-v)^2 - chb]}{P'(\lambda)} \\ \frac{(\lambda-v)[2(\lambda-u)^2 - ch(2-\varphi))]}{P'(\lambda)} \\ \frac{(\lambda-u)\{2(\lambda-v)^2 - h[a(1+\varphi)+2\varphi\, b]\}}{P'(\lambda)} \end{bmatrix}$$

The equation of evolution of weak discontinuities in the constant state $\mathbf{U}_*$, neglecting friction and the function sgn(v), following Boillat [45] (see also recently e.g. [96], [97]), is written as:

$$\frac{d\Pi}{d\sigma} + (\nabla\lambda^{(4)} \cdot \mathbf{r^{(4)}})_* \Pi^2 = \nu_* \Pi \tag{6.58}$$

where $d/d\sigma = \partial_t + \lambda^{(4)}\partial_x$ is the time derivative along the characteristic,

$$\nu_* = \left(\frac{\boldsymbol{\nabla}(\mathbf{F}\cdot\mathbf{l}^{(4)})\cdot\mathbf{r}^{(4)}}{\mathbf{l}^{(4)}\cdot\mathbf{r}^{(4)}} \right)_{\mathbf{U}=\mathbf{U}_*} = \frac{-a\gamma\, \lambda_{4_*}[2\lambda_*^{(4)2} + ah_*(\varphi_*-1) - ch_*\varphi_*]}{\mathcal{C}} +$$

$$+ \frac{\mathcal{B}[2\lambda_*^{(4)2} - ah_*(1+\varphi_*) - h_*\varphi_*(2b+\gamma\, c)]}{\mathcal{C}}, \tag{6.59}$$

with

$$\mathcal{B} = 2\lambda_*^{(4)2}(c-1)(1-\gamma)(1-\varphi_*)^{(1-m)}[2\lambda_*^{(4)2} - ah_*(1+\varphi_*) - 2h_*\varphi_* b]$$

and

$$\mathcal{C} = c\gamma\, v_T[2\lambda_*^{(4)2} - 2h_*\varphi_* b]\{[2\lambda_*^{(4)2} - ah_*(1-\varphi_*) - ch_*\varphi_*][h_*(a+\varphi_* b) - \lambda_*^{(4)2}] +$$
$$-c\gamma\, v_T[ah_*(1+\varphi_*)]\{[2\lambda_*^{(4)2} - ah_*(1-\varphi_*) - ch_*\varphi_*][h_*(a+\varphi_* b) - \lambda_*^{(4)2}] +$$
$$-2\varphi_* h_*(a+b-c)[h_*(a+\varphi_* b) - \lambda_*^{(4)2}] + h_*\varphi_*[ch_*(a+\varphi_* b) - 2\lambda_*^{(4)2}(a+b)] +$$
$$+[h_*(a+\varphi_* b) - 2\lambda_*^{(4)2}][2\lambda_*^{(4)2} - h_* a(1+\varphi_* - 2h_*\varphi_* b)]\}.$$

moreover, of course,

$$(\boldsymbol{\nabla}\lambda^{(4)} \cdot \mathbf{r}^{(4)})_* = \frac{\lambda_*^{(4)^2}\{2\lambda_*^{(4)^2}[a(\varphi_*+5) + 2b(\varphi_*+2) - c(\varphi_*-6)]}{\mathcal{D}} +$$
$$+\frac{2ah_*\varphi_* c(\varphi_*-2) - a^2h_*(\varphi_*+1)^2 - 2abh_*\varphi_*[2(a+b)(\varphi_*-1)}{\mathcal{D}} +$$
$$-\frac{c(2\varphi_*+9)] + ch_*[4(a+\varphi_* b) + 22a + c\varphi_*^2 - 8b]\}}{\mathcal{D}} + \tag{6.60}$$
$$+\frac{2ch_*^2\{a[2-a(\varphi_*-1)] - \varphi_* b[b - b^2 - c(3-\varphi_*)]}{\mathcal{D}} +$$
$$+\frac{(a+\varphi_* b)[a(1+\varphi_*) + 2\varphi_* b]\}}{\mathcal{D}},$$

with

$$\mathcal{D} = 2c[2\lambda_*^{(4)^2} - h_*(a+\varphi_* b)]\{4\lambda_*^{(4)^2} - ch_*(2-\varphi_*) - h[a(1+\varphi_*) + 2\varphi_* b]\}$$

From (6.58) by integrating, following [45] we get:

$$\boldsymbol{\Pi} = \boldsymbol{\eta}/\phi \tag{6.61}$$

where

$$\boldsymbol{\eta} = \eta\mathbf{r}_*^{(4)} \tag{6.62}$$

being η the solution of the Cauchy problem:

$$\begin{cases} d\eta/d\sigma = \nu_*\eta, \\ \\ \eta_0 = \Pi(0), \end{cases} \tag{6.63}$$

that is

$$\eta = \Pi(0) \exp \nu_* \sigma. \tag{6.64}$$

Being

$$\phi = 1 + \int_0^\sigma (\nabla \lambda^{(4)} \cdot r^{(4)})_* \eta d\tau, \tag{6.65}$$

from (6.64) it follow

$$\phi = 1 + \frac{(\nabla \lambda^{(4)} \cdot r^{(4)})_*}{\nu_*} \Pi(0)(\exp \nu_* \sigma - 1) \tag{6.66}$$

If the wave satisfies the *genuine non linearity condition* $\nabla \lambda^{(4)} \cdot \mathbf{r^{(4)}} \neq 0$ it is possible that exists for suitable amplitudes $\Pi(0)$, a *critical time* σ_{cr} which makes zero the denominator ϕ. So at this instant the discontinuity becomes unbounded. Usually the critical time corresponds to the formation of a strong discontinuity (shock), that is, corresponds to that instant when the field $\mathbf{U}$ becomes discontinuous across the wave front ψ. From (6.66) it is a simple matter to get

$$\sigma_{cr} = \frac{1}{\nu_*} ln \left(1 - \frac{\nu_*}{\Pi(0)(\nabla \lambda^{(4)} \cdot r^{(4)})_*} \right) \tag{6.67}$$

It is worthwhile stressing that for $\nu_* > 0$ the possibility of critical time is depending only of the sign of $\Pi(0)$. Instead for $\nu_* < 0$ exists a *threshold* value of initial discontinuity:

$$\Pi(0)_{thres} = \frac{\nu_*}{(\nabla \lambda^{(4)} \cdot r^{(4)})_*} \tag{6.68}$$

that separates the values of $\Pi(0)$ that brings to zero the discontinuity and the values of $\Pi(0)$ that brings to infinite the discontinuity in a finite time σ_{cr}.

In details the possibility to get $\sigma_{cr} > 0$ is fulfilled in the following cases:

1. $\nu_* > 0 \quad$ implies $\quad \dfrac{\nu_*}{\Pi(0)(\nabla\lambda^{(4)} \cdot r^{(4)})_*} < 0$

   so that two subcases arise

   (a) $\Pi(0) > 0, \quad (\nabla\lambda^{(4)} \cdot r^{(4)})_* < 0$

   (b) $\Pi(0) < 0, \quad (\nabla\lambda^{(4)} \cdot r^{(4)})_* > 0$

2. $\nu_* < 0 \quad$ implies $\quad 0 < 1 - \dfrac{\nu_*}{\Pi(0)(\nabla\lambda^{(4)} \cdot r^{(4)})_*} < 1$

   also in this subcases arise

   (a) $\Pi(0) > 0, \quad (\nabla\lambda^{(4)} \cdot r^{(4)})_* < 0 \quad \Pi(0) > \Pi(0)_{thres}$

   (b) $\Pi(0) < 0, \quad (\nabla\lambda^{(4)} \cdot r^{(4)})_* > 0 \quad \Pi(0) < \Pi(0)_{thres}$

In the following, we analyze the discontinuity propagation in a constant state, starting from the experimental data shown in section (6.1.2)(see Table 6.1, 6.2 and 6.3).

	Debris Flow
α_{xx}	7.25
γ	0.4
φ_*	0.61
$\lambda_*^{(4)}$	1.7
m	2.65
v_T	0.1
h	2
$(\nabla\lambda^{(4)} \cdot r^{(4)})_*$	6.5
ν_*	-138.94
η	$e^{(-138.94\sigma)}$
ϕ	$-0.13 + 1.13\ e^{(-138.94\sigma)}$
Π_{thres}	-21
$\Pi(0)$	-24
σ_{cr}	0.016

Table 6.1: Numerical data and numerical results for Debris Flows (Yake Dake).

	Pyroclastic Flow
α_{xx}	7.25
γ	0.0007
φ_*	0.29
$\lambda_*^{(4)}$	1.41
m	2.65
v_T	0.1
h	1
$(\nabla\lambda^{(4)} \cdot r^{(4)})_*$	8.8
ν_*	-70356.43
η	$e^{(-70356.42\sigma)}$
ϕ	$-0.00062 + e^{(-70356.42\sigma)}$
Π_{thres}	-7995
$\Pi(0)$	-8000
σ_{cr}	0.00011

Table 6.2: Numerical data and numerical results for Pyroclastic Flows (Mount St.Helens).

	Avalanche
α_{xx}	7.25
γ	0.0008
φ_*	0.29
$\lambda_*^{(4)}$	4.4
m	2.65
v_T	0.1
h	10
$(\nabla\lambda^{(4)} \cdot r^{(4)})_*$	8.8
ν_*	-61603.1
η	$e^{(-61603.1\sigma)}$
ϕ	$-0.00066 + e^{(-61603.1\sigma)}$
Π_{thres}	-7000
$\Pi(0)$	-7005
σ_{cr}	0.00012

Table 6.3: Numerical data and numerical results for Avalanches (Elm Rock).

In figures 6.5, 6.6, 6.7 and 6.8 we have shown the evolution of weak discontinuities with respect to σ, concerned with the previous geophysical mass flows. In the first three figures it is easy to ascertain that the value of the discontinuity amplitude becomes unbounded in a finite critical time σ_{cr}. In the figure 6.8 (obtained in the case of Pyroclastic Flows, Mount St.Helens) we show a case where the discontinuity amplitude vanishes in the time.

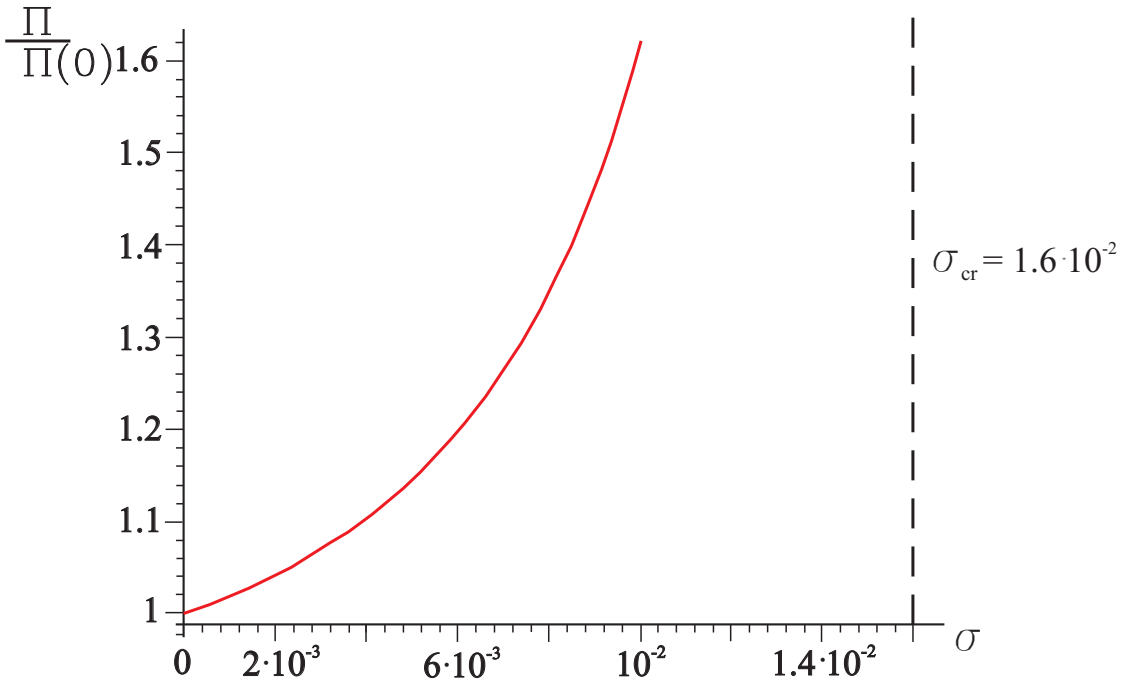

Fig. 6.5: The evolution of discontinuity amplitude in a Debris Flows (Yake Dake).

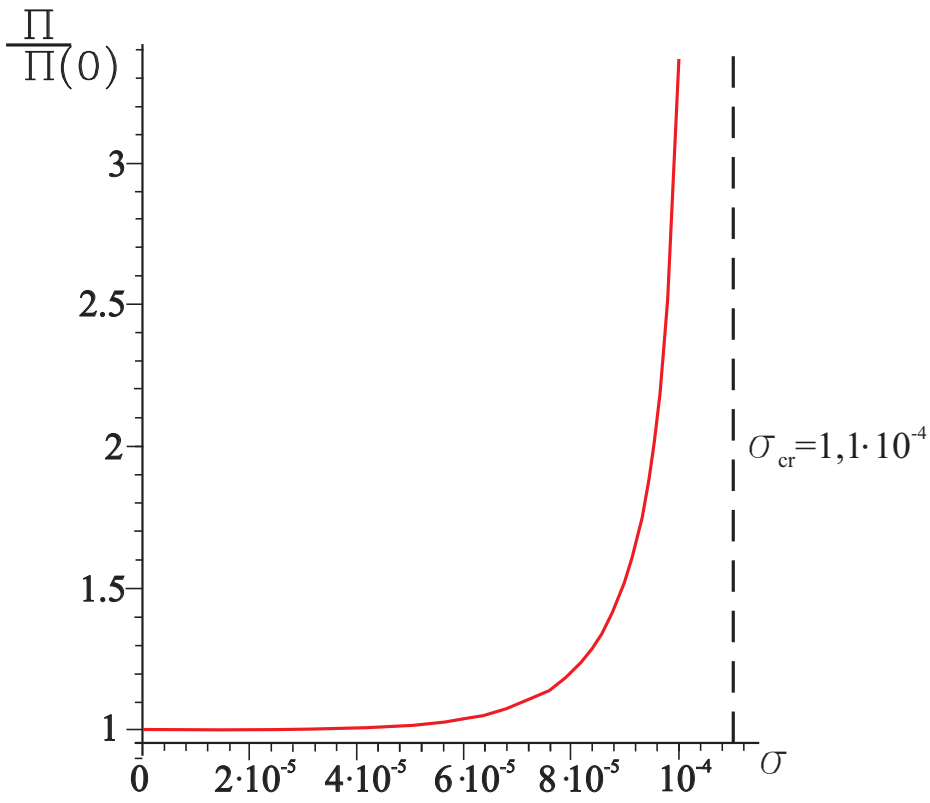

Fig. 6.6: The evolution of discontinuity amplitude in a Pyroclastic Flows (Mount St.Helens)

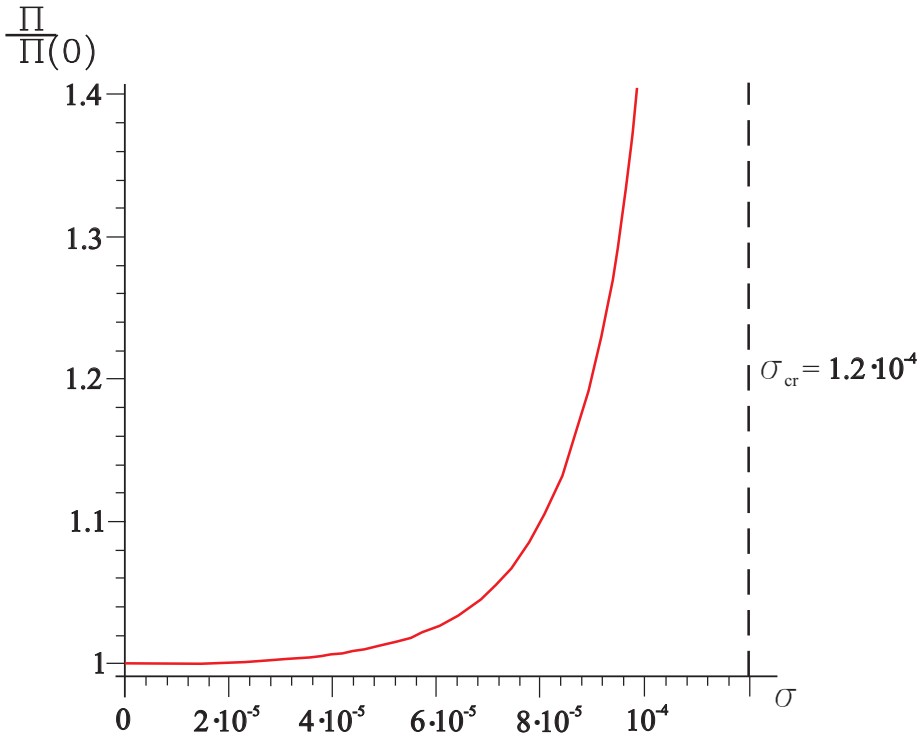

Fig. 6.7: The evolution of discontinuity amplitude in Avalanches(Elm Rock).

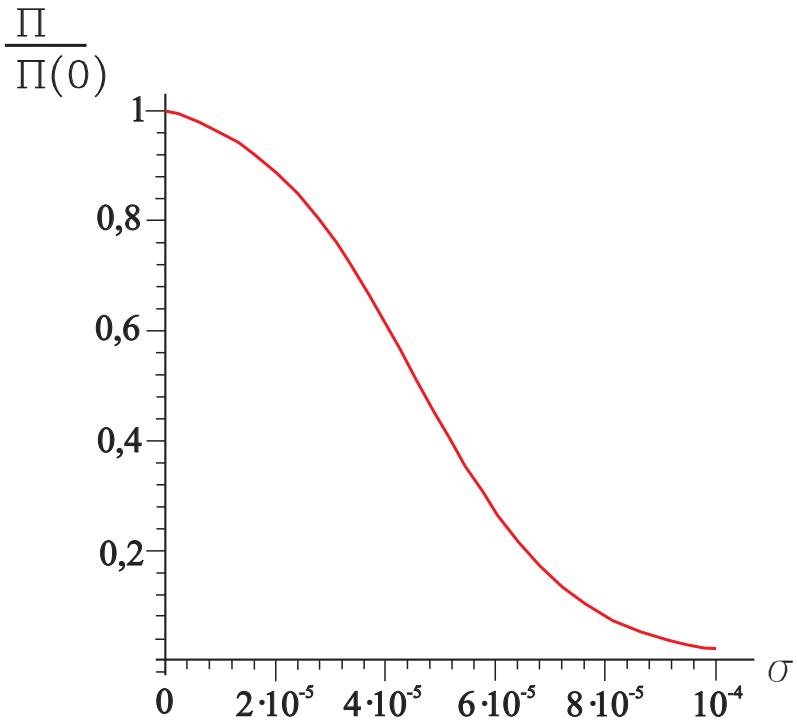

Fig. 6.8: The evolution of discontinuity amplitude in a Pyroclastic Flows (Mount St.Helens). In this case the discontinuity amplitude asymptotically vanishes and does not exist a critical time.

In figures 6.9, 6.10 and 6.11 we show the feature of the curves $\sigma_{cr} = \sigma_{cr}(\Pi(0))$, in the case of the geophysical mass flows previously considered. We observe that σ_{cr} is defined starting from the values of $\Pi(0) < \Pi_{thres}$ and is increasing with respect to $\Pi(0)$.

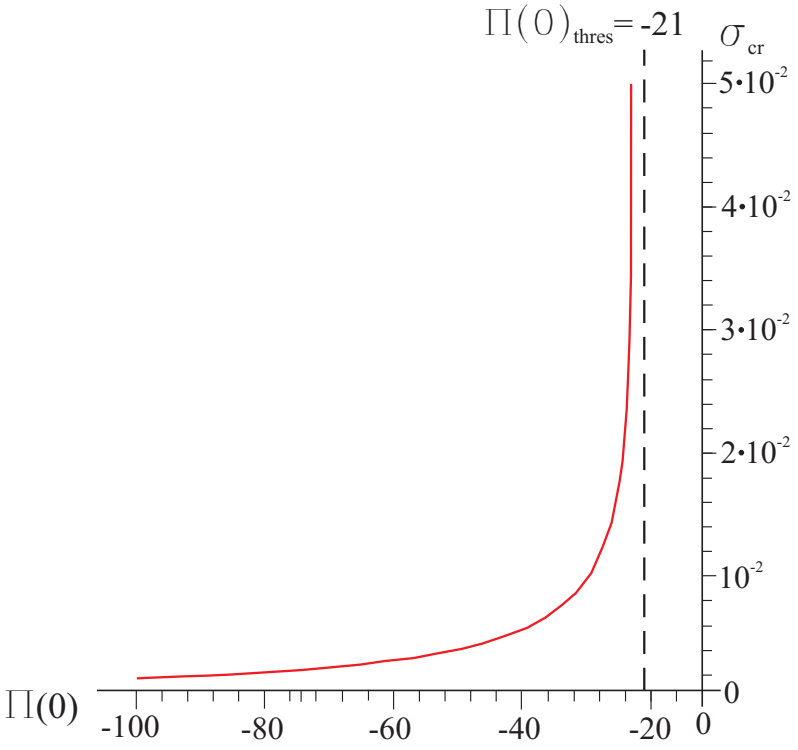

Fig. 6.9: The curve $\sigma_{cr} = \sigma_{cr}(\Pi(0))$ for Debris Flows (Yake Dake).

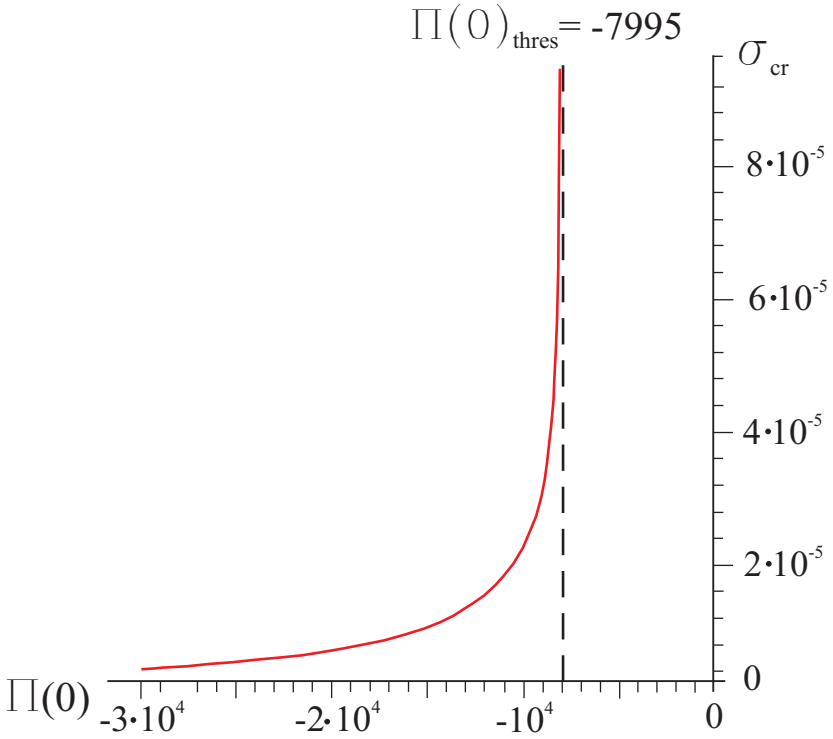

Fig. 6.10: The curve $\sigma_{cr} = \sigma_{cr}(\Pi(0))$ for Pyroclastic Flows (Mount St.Helens).

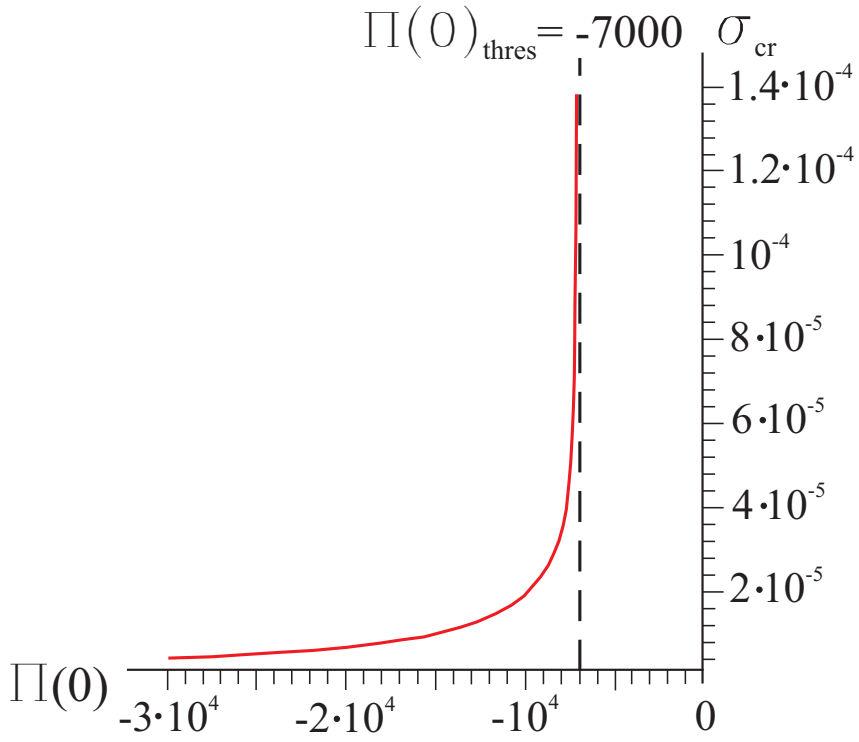

Fig. 6.11: The curve $\sigma_{cr} = \sigma_{cr}(\Pi(0))$ for Avalanches (Elm Rock).

Conclusion

In this thesis the study of the complex phenomena of geophysical mass flows have been approached by starting from the analysis of their specific characteristics and by inserting them in the framework of the different phenomena of surface erosion.

By analyzing the various classifications of gravitational phenomena, it was possible to highlight the type of motion in relation to the different physical properties of the materials involved and to the mechanisms of initiation, propagation and arrest.

The main goal of this thesis has been the study of the complete mechanisms of propagation of the geophysical mass flows through the use of mathematical models that allow for the landslide event simulation along its path.

We have considered some interesting mathematical models used in the engineering practice. The first was the pioneering modeling of Savage and Hutter. They started from the mass and momentum balance laws based on a Coulomb constitutive description of dry granular material and developed a "thin layer" model for granular flows down inclines.

The successive models of Iverson and Iverson-Denlinger argue that the presence of interstitial fluid alters the behavior of flows and should be included in the constitutive behavior of the flowing material. They took in consideration the mixture theory equations and through a careful examination of experiments, developed a system of mass and momentum balance laws for the flow considered as a solid-fluid mixture.

Moreover, we have considered a simple model for a debris flow surges, that offers a simple analysis of the steady-state, where it is assumed that the surge heads act as a rigid body shifted with resistance at the base of Coulomb type and pushed back by a mass completely liquefied. This analysis allows us to make quantitative predictions of the behavior of geophysical mass flows, and to better understand more elaborate models.

On the basis of the models described so far, we have written a mathematical model, which includes as special cases the model of Savage and Hutter or at the model of Iverson. We analyzed for these models the wave propagation

features and the growth of discontinuities. Moreover, after having found the critical time we applied these results to some geophysical mass flows and we got numerical results.

In the final part of the thesis the Pitman-Le two fluid model is considered and the region of the field where the model is hyperbolic is characterized. By taking into account some real geophysical mass flows, we have shown a procedure to evaluate the approximate roots of the characteristic equation. Finally, we have written the evolution equation for the weak discontinuity amplitude in a constant state. We have discussed about the possibility to exist a critical time when discontinuity amplitude goes to infinite and show some numerical results.

For the "two flows classes model" and for the Pitman-Le model we found a threshold value of initial discontinuity that separates the values that bring to zero the discontinuity amplitude and from the values that bring the discontinuity amplitude to infinite in a finite critical time.

In addition as a future research we planned to study the shock waves for both types of models and to look for exact and numerical solutions.

Bibliography

[1] R. I. Tiling (ed.) Volcanic hazards: short course in geology, vol. 1. American Geophysical Union. Washington, D.C. (1989).

[2] National Research Council 1991 The eruption of Nevado del Ruiz Volcano, Colombia, South America, November 13, 1985. (1991). Washington, DC: The Committee on Natural Disasters.

[3] National Research Council 1994 Mount Rainier: active cascade volcano. Washington, DC: The US Geodynamics Committee.

[4] S. D. Ellen and R. W. Fleming, *Mobilization of debris flows from soil slips, San Francisco Bay region, California, in Debris Flows/Avalanches: Process, Recognition, and Mitigation*, Rev. Eng. Geol., voI. 7, edited by J. E. Costa and G. F. Wieczorek, pp. 31-40, Geol. Soc. of Am., Boulder, Colo., (1987).

[5] L. H. Fairchild and M. Wigmosta, *Dynamic and volumetric characteristics of the 18 May 1980 lahars on the Toutle River, Washington* in Proceedings of the Symposium on Erosion Control in Volcanic Areas Tech. Mem. 1908, pp. 131-153, Jpn. Public Works Res. Inst., Min. of Constr., Tokyo (1983).

[6] T. R. Howard, J. E. Baldwin and H. F. Donley, *U.S. Geol. Surv. Prof Pap.*, **1434**, 163-184 (1988).

[7] G. Plafker and G. E. Ericksen, *Natural Phenomena*, **1**, 277-314 (1978).

[8] J. K. Mitchell, *Fundamentals of Soil Behavior*, 422 pp., John Wiley, New York (1976).

[9] T. Takahashi, *I. Hydraul. Div. Am. Soc. Civ. Eng.*, **104**, 1153-1169 (1978).

[10] K. M. Scott, J. W. Vallance and P. T. Pringle, *US. Geol. Surv. Prof. Pap.*, **1547**, 56 pp., (1995).

[11] R.P.Sharp, and L.H.Nobles, *Geol. Soc. Am. Bull.*, **64**, 547-560 (1953).

[12] H. Suwa, *Trans. Jpn. Geomorphol. Union*, **9**, 151-178 (1988).

[13] G. F. Wieczorek, E. L. Harp, R. K. Mark and A. K. Hhattacharyya, *Us. Geol. Surv. Prof. Pap.*, **1434**, 133-162 (1988).

[14] H. M. Jaeger and S. R. Nagel, *Science*, **255**, 1523-1531 (1992).

[15] S. B. Savage, *Mechanics of debris flows, in Hydraulic Engineering '93.* In: Proceedings of the 1993 Conference of the Hydraulics Division of the American Society of Civil Engineers), vol. 2, 1402-1407, Am. Soc. of Civ. Eng., New York (1993).

[16] S. B. Savage, *Adv. Appl. Mech.*, **24**, 289-366 (1984).

[17] K. Sassa, *The mechanism of debris flow.* In Proceedings of the Eleventh International Conference on Soil Mechanics and Foundation Engineering, pp. 1173-1176, A. A. Balkema, Rotterdam, Netherlands (1985).

[18] N. Sitar, S. A. Anderson and K. A. Johnson, Conditions for initiation of rainfall-induced debris flows, in Stability and Performance of Slopes and Embankments Il Proceedings, pp. 834-849 Geotech. Eng. Div., Am. Soc. of Civ. Eng., New York (1992).

[19] L. Siebert, *J. Volcanol. Geotherm. Res.*, **22**, 163-197 (1984).

[20] A. E. Scheidegger, *Rock Mech.*, **5**, 231-236 (1973).

[21] T. C. Pierson, *Earth Surf. Processes*, **5**, 227-247 (1980).

[22] T. C. Pierson, *Sedimentology*, **28**, 49-60 (1981).

[23] T. C. Pierson, *Geol. Soc. Am. Bull.*, **96**, 1056-1069 (1985).

[24] T. C. Pierson, *Flow behavior of channelized debris flows, Mount St. Helens, Washington, in Hillslope Processes*, edited by A. D. Abrahams, pp. 269-296, Allen and Un-win, Winchester, Mass., 1986.

[25] T. C. Pierson, *J. Volcanol. Geotherm. Res.*, **66**, 283-294 (1995).

[26] T. C. Pierson and J. E.Costa, *Geol. Soc. of Am., Boulder, Colo.*, **7**,1-12 (1987).

[27] T. C. Pierson and K. M. Scott, *Water Resour. Res.*, **21**, 1511-1524 (1985).

[28] T. C. Pierson, R. J. Janda, J. C. Thouret and C. A. Borrero, *J. Volcanol. Geotherm. Res.*, **41**, 17-66 (1990).

[29] S. B. Savage and K. Hutter, *J. Fluid Mech.*, **199**, 177-215 (1989).

[30] A. J. C. de Saint-Venant, *C. R. Acad. Sc. Paris* **73**, 147-154 (1871).

[31] K. Hutter, M. Siegel, S. B. Savage and Y. Nohguchi, *Theory. Acta Mech.*, **100**, 37-68 (1993).

[32] F. Bouchut and M. Westdickenberg, *Comm. Math. Sci.* **2**, 359-389 (2004).

[33] R. P. Denlinger and R. M. Iverson, *J. Geophys. Res.* **109** (2004) F01014, doi:10.1029/2003JF000085.

[34] J. M. N. T. Gray, M. Wieland and K. Hutter, *Proc. R. Soc. Lond. A* **455**, 1841-1874 (1999).

[35] R. M. Iverson, and R. P. Denlinger, *Journal of Geophysical Research*, **106**, 553-566 (2001).

[36] A. K. Patra, A. C. Bauer, C. C. Nichita, E. B. Pitman, M. F. Sheridan, M. Bursik, B. Rupp, A. Webber, A. J. Stinton, L. M. Namikawa and C. S. Renschler, *J. Volcanology Geotherm. Res.*, **139**, 1-21 (2005).

[37] S. P. Pudasaini and K. Hutter, *J. Fluid Mech.*, **495**, 193-208 (2003).

[38] S. P. Pudasaini, Y. Wang and K. Hutter, *Natural Hazards and Earth System Sciences*, **5**, 799-819 (2005) .

[39] S. P. Pudasaini, *Dynamics of flow avalanches over curved and twisted channels: theory, numerics and experimental validation.* Dissertation, Fachbereich Mechanik, Technische Universitat Darmstadt. Available at: http://elib.tu-darmstadt.de/diss/000393.

[40] S. P. Pudasaini and K. Hutter, *Granular avalanche model in arbitrarily curved and twisted mountain terrain: a basis for the extension to debris flow.* In: Debris-Flow Hazards Mit- igation: Mechanics, Predictions and Assessment (Eds. D. Rickenmann and C.-L. Chen). **1**, 491-502, Millpress.

[41] K. Hutter, *Debris and mudflows: are we asking the correct questions? What are the deficits?*In: Mitteilungen der Versuchsanstalt fur Wasserbau Hydrologie und Glaziologie an der Eidgenössischen Technischen Hochschule Zurich **190**, 91-105 (2005).

[42] R. M. Iverson, *Rev. Geophys*, **35**, 245-296 (1997).

[43] R. M. Iverson, and R. P. Denlinger *Journal of Geophysical Research*, **106**, 537-552 (2001).

[44] C. Mineo and M. Torrisi, *Waves in a model for two flow classes.* Submitted for publication (2010)

[45] G. Boillat, *La Propagation des Ondes*, Gauthier-Villars, Paris, (1965).

[46] C. Mineo and M. Torrisi, *On the hyperbolicity of a two-fluid model for debris flows.* In: IUTAM-ISIMM Symposium on Mathematical Modeling and Physical Instances of Granular Flows. Reggio Calabria (Italy), September 14-18, 2009, Melville, New York: AIP Conference Proceedings, **1227**, 72-78 (2010)

[47] C. Mineo and M. Torrisi, *Discontinuity waves in a two fluid model for debris flows avalanches.* Submitted for publication (2010).

[48] D. J. Varnes, *Slope movement types and processes, in Landslides-Analysis and Control*, edited by R. L. Schuster and R. J. Krizek, Spec. Rep. Natl. Res. Counc. Transp. Res. Board, 176, pp. 11-33, Natl. Acad. of Sci., Washington, D.C. (1978).

[49] J. N. Hutchinson and R. K. Bandhari, *Geotechnique*, **21**, 353-358 (1971).

[50] J. N. Hutchinson, *Can. Geotech.*, **23**, 115-126 (1986).

[51] J. N. Hutchinson, *Morphological and geotechnical parameters of landslides in relation to geology and hydrogeology (General Report)*, Proc. Of the V Int. Symp. on Landslides, Lausanne, Balkema, Rotterdam, 1-12 (1988).

[52] P. Coussot and J. M. Piau, *Rheol. Acta*, **33**, 175-184 (1994).

[53] P. Coussot and S. Proust, *J Geophys. Res.*, **25**, 217-25 (1996).

[54] A. Daido, *On the occurrence of mud-debris flow*, Bull. Disaster Prev. Res. Inst. Kyoto Univ., Part 2, 21 (187), 109-135 (1971).

[55] J. H. Fink, M. C. Malin, R. E. D'Alli and R. Greeley, *Geophys. Res. Lett.*, **8**, 43-46 (1981).

[56] M. A. Hampton, H. J. Lee and J. Locat, *Rev. Geophys.*, **34**, 33-59 (1996).

[57] J. N. Hayashi and S. Self, *J. Geophys. Res.*, **97 (B6)**, 9063-9071 (1992).

[58] K. J. Hsu, *Geol. Soc. Am. Bull.*, **86**, 129-140 (1975).

[59] R. H. Jahns, *Desert floods*, Contrib. 499, pp. 10-15, Calif. Inst. of Technol., Pasadena, (1949).

[60] J. Li and J. Yuan, *Z. Geo-morphol.*, **27**, 326-341 (1983).

[61] K. Miyamoto and S. Egashira, *J. Hydrosci. Hydraul. Eng. Jpn. Soc. Civ. Eng.*, **SI-2**, 1-19 (1993).

[62] D. M. Morton and R. H. Campbell, *Eng. Geol.*, **7**, 377-384 (1974).

[63] A. Musso, *Analisi delle colate rapide*, Corso di aggiornamento DESEG AGI, Udine (1994).

[64] J W. Vallance and K. M. Scott, *Geol. Soc. Am. Bull.*, **109(2)**, 143-163 (1997).

[65] G. Seminara and M. Tubino, *Debris Flows: Meccanica, Controllo e Previsione*. Gruppo Nazionale per la Difesa dalle Catastrofi Idrogeologiche. Roma, CNR, Presidenza del Consiglio del Ministri, Dipartimento della Protezione Civile, 1993. p.iii, 3-8, 11-21, 24-30, 207-208, 238-239.

[66] J. Melosh, *Acta Mech.*, **64**, 89-99 (1986).

[67] S. B. Savage and K. Hutter, *Analysis, Acta Mech.*, **86**, 201-223 (1991).

[68] R. J. Atkin and R. E. Craine, *Q. J. Mech. Appl. Math.* **29**, 209-244 (1976).

[69] J. Bear, *Dynamics of Fluids in Porous Media*, Dover, Mineola, N. Y., 764 pp. (1972).

[70] R. M. Iverson, *Math. Geol.*, **23**, 1027-1048 (1993).

[71] P. F. Coleman, *Spring Meet. Suppl.*, **154**, 74(16) (1993).

[72] K. X. Whipple, *Debris-flow fans: Process and form, Ph.D. dissertation*, Univ. of Washington, Seattle, 205 pp. (1994).

[73] J. J. Major, *Experimental studies of deposition by debris flows: Process, characteristics of deposits and effects of pore-fluid pressure, Ph.D. dissertation*, Univ. of Wash., Seattle, 341 pp. (1976).

[74] R. M. Iverson, *Geotechnique*, **40**, 139-143 (1990).

[75] R. M. Iverson, *Sensitivity of stability analyses to groundwater data, in Landslides* In: Proceedings of the Sixth International Symposium on Landslides, 1, edited by D. H. Bell, 451-457, (1992).

[76] B. Hunt, *J. Hydraul. Eng.*, **120**, 1350-1363, (1994).

[77] M. Abramowitz and I. A. Stegun, *Handbook of Mathematical Functions with Formulas, Graphs, and Mathematical Tables*, U.S. Dept. of Commer., Natl. Inst. of Stand. and Technol., Gaithersburg, Md., (1964).

[78] C. B. Vreugdenhil, *Numerical Methods for Shallow-Water Flow*, Kluwer Acad., Norwell, Mass., 261 pp., (1994).

[79] W. J. M. Rankine, *Philos. Trans. R. Soc. London*, **147**, 9-27 (1857).

[80] T. W. Lambe and R. V. Whitman, *Soil Mechanics*, John Wiley, New York, 553 (1979).

[81] M. K. Hubbert and W. W. Rubey, *Geol. Soc. Am. Bull.*, **70**, 115-166, (1959).

[82] K. Terzaghi, *The shearing resistance of saturated soils and the angle between planes of shear.* In: First International Conference on Soil Mechanics, 54-56 (1936).

[83] R. M. Iverson and R. G. LaHusen, *Science*, **246**, 769-799, (1989).

[84] R. B. Bird, W. E. Stewart and E. N. Lightfoot, *Transport Phenomena*, 780 pp., John Wiley, New York, (1960).

[85] H. Schlichting, *Boundary-Layer Theory*, 7th ed., 814 pp., McGraw-Hill, New York, (1979).

[86] R. M. Iverson, M. E. Reid and R. G. LaHusen, *Ann. Rev. Earth Planet. Sci.*, **25**, 85-138 (1987).

[87] M. E. Reid, R. G. LaHusen and R. M. Iverson, *Debris-flow initiation experiments using diverse hydrologic triggers*, in Debris Flow Hazards Mitigation: Mechanics Prediction and Assessment, edited by C. L. Chen, pp. 1-11, Am. Soc. of Civ. Eng., Reston, Va., (1997).

[88] J. Hadamard, *Lecons sur la propagation des Ondes*, Hermann, Paris, (1903).

[89] A. Jeffrey, *Quasilinear Hyperbolic Systems and Waves*, In Research Notes in Mathematics vol. 5 Pitman, London (1976).

[90] E. B. Pitman and L. Le, *Phil. Trans. R. Soc. A*, **363**, 1573-1601 (2005).

[91] T. B. Anderson and R. Jackson, *Ind. Eng. Chem. Fundamen.*, **6**, 527-539 (1967).

[92] J. F. Richardson, and W. N. Zaki, *Trans. Inst. Chem. Engrs* , **32**, 35-53 (1954).

[93] GDR MiDi, *Eur. Phys. J. E*, **14**, 341-365 (2004).

[94] F. da Cruz, S. Emam, M. Prochnow, J. N. Roux, and F. Chevoir, *Phys. Rev. E*, **72**, 021309 (2005).

[95] D.Berzi and J.T.Jenkins, *J. Fluid Mech.*, **608**, 393-410, (2008).

[96] J. Jena and V. D. Sharma, *J. Eng. Math*, **60**, 43-53 (2008).

[97] T. Raja Sekhar and V.D. Sharma, *Applied Mathematics Letters*, **23**, 327-330 (2010).